AD A014192

BRL CR 250

# BRL

AD

CONTRACT REPORT NO. 250

# A NEW, GENERAL THEORY OF PLASTICITY FOR STRUCTURAL METAL ALLOYS

Prepared by

The John Hopkins University
34th and Charles Streets
Baltimore, Maryland 21218

DDC
RECEIVED
AUG 26 1975
B

July 1975

Approved for public release; distribution unlimited.

USA BALLISTIC RESEARCH LABORATORIES
ABERDEEN PROVING GROUND, MARYLAND

Destroy this report when it is no longer needed.
Do not return it to the originator.

Secondary distribution of this report by originating or sponsoring activity is prohibited.

Additional copies of this report may be obtained from the National Technical Information Service, U.S. Department of Commerce, Springfield, Virginia 22151.

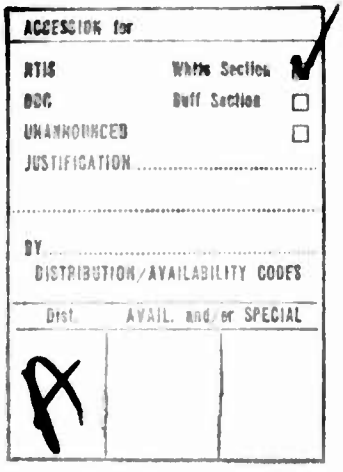


The findings in this report are not to be construed as an official Department of the Army position, unless so designated by other authorized documents.

UNCLASSIFIED

SECURITY CLASSIFICATION OF THIS PAGE (When Data Entered)

(12) 111 p.

## REPORT DOCUMENTATION PAGE

READ INSTRUCTIONS BEFORE COMPLETING FORM

| | |
|---|---|
| 1. REPORT NUMBER: BRL Contract Report No. 250 | 2. GOVT ACCESSION NO. |
| 3. RECIPIENT'S CATALOG NUMBER | |
| 4. TITLE (and Subtitle): A New, General Theory of Plasticity for Structural Metal Alloys, | 5. TYPE OF REPORT & PERIOD COVERED: Final Report, 14 Oct 69 to 17 Jul 74 |
| | 6. PERFORMING ORG. REPORT NUMBER |
| 7. AUTHOR(s): James F. Bell | 8. CONTRACT OR GRANT NUMBER(s): DAAD05-70-C-0054 |
| 9. PERFORMING ORGANIZATION NAME AND ADDRESS: The Johns Hopkins University, 34th and Charles Streets, Baltimore, Maryland 21218 | 10. PROGRAM ELEMENT, PROJECT, TASK AREA & WORK UNIT NUMBERS: 61102A, 1T161102A33E-06-052AJ |
| 11. CONTROLLING OFFICE NAME AND ADDRESS: US Army Ballistic Research Laboratories, Aberdeen Proving Ground, Maryland 21005 | 12. REPORT DATE: July 1975 |
| | 13. NUMBER OF PAGES: 111 |
| 14. MONITORING AGENCY NAME & ADDRESS (if different from Controlling Office): 1A-1T-161102-A-33-E | 15. SECURITY CLASS. (of this report): UNCLASSIFIED |
| | 15a. DECLASSIFICATION/DOWNGRADING SCHEDULE |

16. DISTRIBUTION STATEMENT (of this Report)

Approved for public release; distribution unlimited

17. 1-T-161102-A-33-E-06

17. DISTRIBUTION STATEMENT (of the abstract entered in Block 20, if different from Report)

18. SUPPLEMENTARY NOTES

19. KEY WORDS (Continue on reverse side if necessary and identify by block number)

| | |
|---|---|
| plasticity | plastic flow |
| equations of state | stress strain diagrams |
| impact loading | torsion tests |
| deformation | tension tests |
| failure | wave propagation |

20. ABSTRACT (Continue on reverse side if necessary and identify by block number)

A new, general theory of plasticity for structural metal alloys of steel, aluminum, and copper is presented. Based in experiment, general constitutive equations are provided in the two-dimensional domain for any arbitrary loading path, whether proportional or non-proportional. Two regions of large deformation have been found, an intermediate elastic-plastic region and a totally plastic region, the former bounded by an inner and outer yield surface. The functional relation between the generalized stress

DD FORM 1 JAN 73 1473 EDITION OF 1 NOV 65 IS OBSOLETE

UNCLASSIFIED

191 750

and strain is parabolic, with detailed constitutive relations given for each region of deformation. A new phenomenon of "eruptive" plastic deformation has been found when impact velocities are sufficiently high for the strain to reach the outer yield surface bounding the regions of plasticity. At this critical velocity the maximum strain increases from three to eight times, depending on the alloy, over that immediately below the critical value. A new material parameter for the metal alloys is found to characterize the large deformation of rods, tubes, and plates of maraging steel, 1095 steel, 1020 steel; 7075-T6 aluminum, 2024-T3 aluminum, 6061-T6 aluminum, 5083-H131, 2014-T4, 1100-H14, 1100-H18 aluminum; hard copper; and hard alpha brass. Detailed response is given for these metals from zero stress to the onset of failure.

## Contents


Preface ..... i

Introduction ..... 1

Theory of Plasticity for Structural Metal Alloys ..... 17

Experimental Data ..... 27

Torsion ..... 40

Proportional Loading ..... 53

Non-Proportional Loading ..... 59

Dynamic Plasticity ..... 74

Summary ..... 96

References ..... 99

Distribution List ..... 102

TABLE I.....12

TABLE II.....24

# A NEW, GENERAL THEORY OF PLASTICITY FOR STRUCTURAL METAL ALLOYS

James F. Bell
Professor of Solid Mechanics
The Johns Hopkins University

## Preface

During the five-year interval of this final report, a very large amount of research in theory and experiment was performed which culminated in the discovery, presented in the report which follows, that the years of research on the large dynamic and quasi-static deformation of twenty-seven different fully annealed metals served as the fundamental basis for the derivation of the general plasticity of the important structural metal alloys.

Because of the importance of the final result and the fact that much of the work of the first years of this contract were contributory to its achievement, I have decided here to summarize the important aspects of the research on the fully annealed metals in the introduction and devote the major portion of the work to their extension to the description of the structural metal alloys. For completeness, however, I shall list some of these individual areas of research, the results of which are appearing in journal publications or have appeared in my Handbuch der Physik treatise of 1973. They include my own research and that of my doctoral students.

1. Further study of incremental waves with dynamic pre-stress.
2. H. Moon's experimental and theoretical study of annealed aluminum for non-proportional loading below the first critical strain.
3. Further detailed study of the unloading waves.
4. The study of annealed aluminum and copper for proportional and non-proportional loading paths which provided the base for the alloy research.
5. Further studies of dynamic plasticity in the vicinity of the melting point in annealed aluminum.
6. Elastic wave reflection experiments by Professor W. Hartman.
7. An extensive experimental study of reflections of plastic waves at an elastic boundary.



PRECEDING PAGE BLANK-NOT FILMED

8. An experimental and theoretical study of annealed aluminum undergoing double compression.
9. A detailed study of the inhomogeneous deformation of the grains of aluminum multicrystals undergoing statistically parabolic large deformation.
10. An experimental study of the effects of varying the prior annealing and deformation of aluminum as affecting the parabolic generalization on subsequent reloading.
11. Experiments chosen to further explore the second-order transition phenomena in large deformation.

All of the studies above were carried to completion during the interval of this contract. They have indeed provided the background for the continuing research on the structural metal alloys described here.

Although it is certainly true that much remains to be done in extending the general theory of plasticity to a more extensive list of alloys, in comprehending some of the details, and in further studying the wave propagation, interaction, reflection, etc. in these "as-received" hardened metals, it is thought that the historic problem of determining general constitutive equations for structural metal alloys subject to arbitrary loading has been resolved. The major problems now lie in applied mechanics and design.

Acknowledgements

The labors in this research of Faith Hoeckel and James Randall, research assistants, and Rajendra Khanwalkar, graduate student, as well as those of earlier participants in the work are much appreciated.

# A NEW, GENERAL THEORY OF PLASTICITY FOR STRUCTURAL METAL ALLOYS

James F. Bell
Professor of Solid Mechanics
The Johns Hopkins University

## Introduction

The theory of plasticity for structural metal alloys to be presented here is one which came entirely from the study of the patterns revealed in hundreds of experiments of a great many types. It is my opinion that experiments in three dimensions, when available, will correlate with the completely generalized theory. In fact, evidence is available from my earlier three-dimensional studies of the development of plastic waves close to impact surfaces, that the present theory indeed does correlate with observation.

The main body of experiment from which the present theory for structural metal alloys was developed is two dimensional. Therefore, I shall present the new developments within the bounds of the experimental situations considered up to this point in time. This means, that for all experiments, including the 2500 from my laboratory, at least one normal stress component is zero. Whether in microseconds during wave propagation after high velocity impact or in quasi-static experiments lasting three or more weeks, five physical situations have been studied.

The five physical situations studied are;

1. The axial loading of solid cylinders, which includes the symmetrical impact of identical specimens in free flight to study finite amplitude wave propagation by means of diffraction gratings; the quasi-static loading of polycrystalline specimens; and the axial loading of single crystals with known initial orientations to determine the resolved shear stress, resolved shear strain response function.

2. The loading of thin-walled tubes in any combination of

axial stress and torsional shear, with simultaneous internal pressure to produce a tangential stress component. Such thin-walled cylinders also have been submitted to tensile and compressive impact to study the propagation of finite amplitude waves.

3. Two-dimensional compression, sometimes called double compression, in which an axial load is applied on a cubic specimen on one pair of cube faces, a second load is applied perpendicularly on a second pair of cube faces of just the proper amount to maintain zero strain in that direction, and a third pair of cube faces is free of stress but permitted to deform.

4. Tension and compression tests performed on specimens removed from rolled plates at a variety of angles from the rolling direction, including that perpendicular to the plate.

5. Relatively thin cantilever beams subjected to large deflection.

The maximum number of stress components simultaneously considered in any of those physical situations was three; at least one normal stress component was zero. Within the framework of these measurements, however; (a) ambient temperatures have been varied over nearly the entire temperature scale, to 0.95 $T_m$; (b) maximum strains were from infinitesimal elastic values to 60%; (c) strain rates have ranged from $10^{-9}$ to $10^{4}$, i.e., a range of a million million; (d) specimen purities have varied from alloys to metals of 99.999% purity; (e) polycrystals with five different crystal structures and cubic single crystals with initial orientations over the entire stereographic triangle were studied; (f) impact velocities included values from infinitesimal elastic to 25000 cm/sec; (g) investigations were made of many different prior deformation, thermal, and chemical histories; (h) specimens were of various grain sizes, diameters, and lengths; (i) many different boundary conditions were chosen to explore in plastic waves the problems of initiation, growth, propagation, reflection, interaction, etc.

As indicated above, the only truly three-dimensional

problems in plasticity which I have studied are the initiation and growth of plastic waves in the first diameter of an impacted cylinder. In a number of papers I described this process in great detail.[1,2,3,4,5] Those results are not part of the development given here.

In the work described below, $\sigma_x$, $\sigma_y$, and $S = \sigma_{xy}$ are defined in experiment as, respectively, the axial stress, the direction of which is maintained throughout the experiment; the tangential stress which remains perpendicular to the axial component throughout the test; and the torsional shear stress in the twisting of thin-walled tubes. In every instance, no matter how large the strain, these stresses are defined with respect to the undeformed configuration; i.e., they are nominal or engineering stresses.

The extensional strains, $\epsilon_x$, $\epsilon_y$, $\epsilon_z$, and the torsional shear strain $\Delta = \frac{\epsilon_{xy}}{2}$ are directionally coincident with the corresponding stresses. These strains also are defined with respect to the undeformed configuration.

For the hollow tube, where $r_m$ is the mean radius and $r_o$ and $r_i$ are the outer and inner radii, $\ell_o$ is the initial length, $\theta$ is the measured angle of twist, and P is the applied torque around the specimen axis, we have Eq. (1)

$$S = \frac{P}{2\pi r_m^2 (r_o - r_i)} \quad , \quad \Delta = \frac{r_m \theta}{\ell_o} \qquad (1)$$

The choice of stress definition and strain measure, of course, is arbitrary. The advantage here of choosing engineering stress and strain components is that it has revealed a great simplification, which has been discovered both for theory and for experiment. Incompressibility is not assumed since, as these experiments amply have demonstrated,

$$\epsilon_x + \epsilon_y + \epsilon_z = 0 \qquad (2)$$

For internal pressure - tension in hollow tubes, the ratios of $\sigma_y/\sigma_x$ from 0 to 1 have been considered. For the double compression of cubes, $\sigma_y/\sigma_x = 1$. For combined axial - torsion loading with $\sigma_z = \sigma_y = 0$, combinations of stress ratios from simple tension or simple compression to simple torsion have been studied for proportional and for non-proportional loading.

The choice of a generalized stress and generalized strain for large deformation must be commensurate with all loading paths considered, including simple axial loading and simple torsion. To the experimentists, a satisfactory generalized stress is given in Eq. (3).

$$\Gamma = \sqrt{\frac{2}{3}} \sqrt{\sigma_x^2 + \sigma_y^2 - \sigma_x\sigma_y + 3S^2} \qquad (3)$$

As will be shown below, the study of non-proportional loading paths for fully annealed pure metals and for structural metal alloys has shown that the generalized strain must be determined from integration along the strain path,(*) as given in Eq. (4).

$$\Gamma = \int \sqrt{(d\epsilon_x)^2 + (d\epsilon_y)^2 + (d\epsilon_z)^2 + \left(\frac{d\phi}{2}\right)^2} \qquad (4)$$

For proportional loading, Eq. (4) may be integrated to provide Eq. (5).

$$\Gamma = \sqrt{\epsilon_x^2 + \epsilon_y^2 + \epsilon_z^2 + \frac{\phi^2}{2}} \qquad (5)$$

---

(*) A single exception was discovered by H. Moon[6] for very small plastic strains in fully annealed aluminum. Moon found that the integrated form of Eq. (5) was applicable during non-proportional loading. His constitutive equations for non-proportional loading are incremental, with the incremental strain vector not perpendicular to the loading surface. However, for strains above the order of 1% in this solid, Eq. (4) must be integrated along the strain path, as in all other known situations.

From the statement from experiment of Eq. (2), this may be written

$$\Gamma = \sqrt{2}\sqrt{\epsilon_x^2 + \epsilon_y^2 + \epsilon_x\epsilon_y + \frac{\sigma^2}{4}}$$

Unless specifically designated, in experiments considering either dynamic or quasi-static unloading, all the results here are for monotonically increasing or non-decreasing generalized stress, $dT \geq 0$. The range of strain for quasi-static loading has been, from 0 to 0.60 for axial loading in tension and in compression, 0 to 0.30 for the simple torsion of thin-walled tubes, 0.15 in double compression, and simultaneous maxima of 0.14 in tension and 0.24 in torsion for combined tension-torsion loading. The maximum measured compression strain in my studies of plastic wave propagation has been 0.25, corresponding in annealed aluminum to a projectile velocity of 25000 cm/sec. The maximum strain rates have been 25000/sec measured in the vicinity of the impact face.

This study of the large deformation of structural metal alloys, including a number of high-strength steel and aluminum alloys, has shown that there exist two distinct, well-defined regions of plasticity, separated by an equally well-defined boundary. There are thus two yield surfaces: an inner yield surface at the end of linear elasticity, and an outer yield surface at the end of the intermediate elastic-plastic region. This discovery is analogous to but different from the earlier discovery of two yield surfaces first observed by H. Moon[6] in his doctoral research in this laboratory in 1973. Moon's observations were made during the reloading after unloading of a fully annealed metal, whereas the outer yield surface for the metal alloy is a fixed determinable boundary, not related to a previous unloading or loading.

The first plastic region, bounded by the inner yield surface or the end of linearity and by the outer yield surface or the beginning of total plasticity, I have found is an elastic-plastic region which I have chosen to designate as the intermediate plastic region. This name is chosen to be historically just to Henri Tresca, and to James Guest who, in the 1870's and 1900, respectively, protested that the developing theories in ideal plasticity denied its existence.

The second plastic region, which I have designated as

the totally plastic region, is bounded by the outer yield surface and the ultimate stress. It is important to point out that much of the controversy surrounding the interpretation of yield surfaces, including the normality to the yield surface of the strain increment vector, has arisen because the properties of the inner and outer yield surfaces are markedly different. Since preparation of specimens can alter the location of these yield surfaces, contrasting earlier experimental results are easily understood. Fig. 1 is a schematic diagram of these concepts in axial loading.

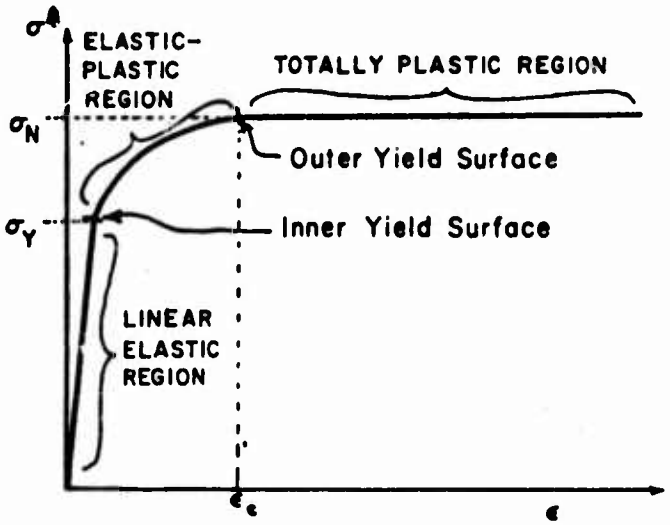


Fig 1

To develop a general statement from experiment for the response function for the "as-received" structural metal alloy, it is essential to trace briefly my previously established results in theory and experiment for the fully annealed polycrystal. The new theory of plasticity for the metal alloys is derived directly from those results in terms of the dominant component of the metal alloy. This brief statement regarding those earlier studies is fully supported in experiment and has been described in numerous

papers, in a monograph in 1968 for the Springer Tracts in Natural Philosophy entitled The Physics of Large Deformation of Crystalline Solids[7], and in a treatise in 1973 in Springer-Verlag's Handbuch der Physik, Vol. VIa/1, entitled "The Experimental Foundations of Solid Mechanics."[8] The Handbuch volume includes a bibliography of my earlier papers and those of my former doctoral students.

To state that it is possible to predict in detail the entire response function from zero strain to the ultimate stress of, say, 1095 quenched and tempered tool steel or 7075-T6 aluminum in the as-received condition, from measurement of the resolved shear stress, resolved shear strain response function of single crystals of the dominant component, requires the delineation of more than a little experimental development. Experiment does bear out that such indeed is the fact.

We therefore begin with the parabolic response function, of the stage III deformation of the cubic single crystal, Eq. (6),

$$\uparrow = \beta_s (\gamma - \gamma_b)^{1/2} \tag{6}$$

or, in incremental form, Eq. (7).

$$d\gamma = \frac{2 \uparrow d \uparrow}{\beta_s^2} \tag{7}$$

A decade and a half of the study of the properties of the parabola coefficients $\beta_s$ in Eq. (6) has been described fully in the monograph and treatise referred to above.[7,8] From many hundreds of experiments, those in the general literature and those performed in this laboratory, we see:

$$\beta_s = \left(\frac{2}{3}\right)^{1/2} \mu(0)\, B_o\, (1 - T/T_m) \tag{8}$$

where $B_o = 0.0052$ is a dimensionless universal constant shown by

experiment to be common to over 30 crystalline solids; $\mu(0)$ is the measured shear modulus of the isotropic solid at the zero point; $r = 1, 2, 3, \ldots$ is the integral index of a discrete distribution of deformation modes of crystalline solids; $T$ is the ambient temperature and $T_m$ is the melting point, both in degrees Kelvin.

The comparison of several hundred measured response functions for polycrystalline solids with an equal number of stage III resolved shear response functions for cubic single crystals revealed that when all stresses and strains are referred to the undeformed configuration, the aggregate ratios of Eq. (9) characterize the entire group of cubic solids studied.

$$\frac{\tau}{\uparrow} = \bar{K} = \frac{d\gamma}{d\Gamma} \qquad \text{where } \bar{K} = 2.50 \qquad (9)$$

From Eq. (7) we obtain for the fully annealed polycrystal the incremental parabolic form of Eq. (10).

$$d\Gamma = \frac{2\tau\, d\tau}{\bar{K}^3 \beta_s^2} \qquad (10)$$

For the fully annealed polycrystal, the integrated form may be written simply as Eq. (11).

$$\tau = \bar{K}^{3/2} \beta_s \left(\Gamma - \Gamma_b\right)^{1/2} \qquad (11)$$

where $\Gamma_b$ is the intercept of the parabola on the strain abscissa, with $\Gamma_b = 0$ for all dynamic tests in the fully annealed metal, and $\Gamma_b \approx 0$ for the initial parabola for quasi-static testing. To observe parabolicity in experimental data it is necessary to note only that in the $\tau^2$ vs $\Gamma$ plot of Eq.(12),

$$\tau^2 = \bar{K}^3 \beta_s^2 \left(\Gamma - \Gamma_b\right) \qquad (12)$$

the response function will appear as a straight line whose slope is $\bar{K}^3 \beta_s^2$ .. Illustrations of this behavior are shown in Figs. 2, 3, 4, and 5.

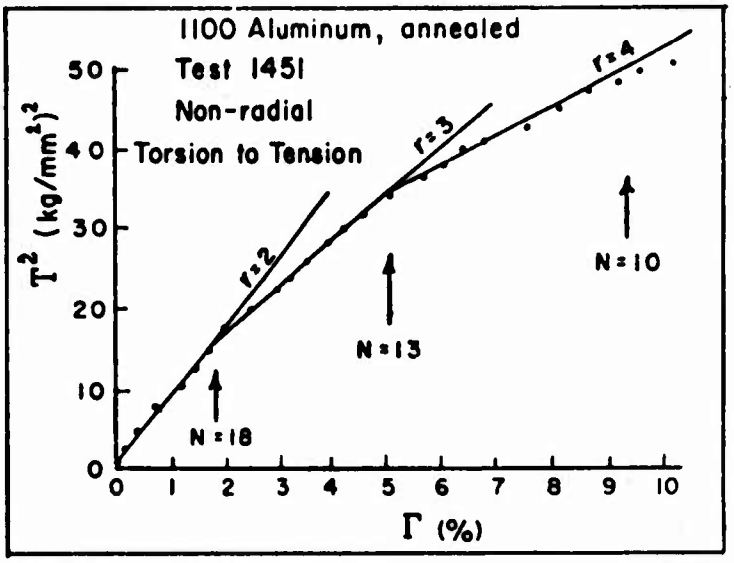


Fig. 2

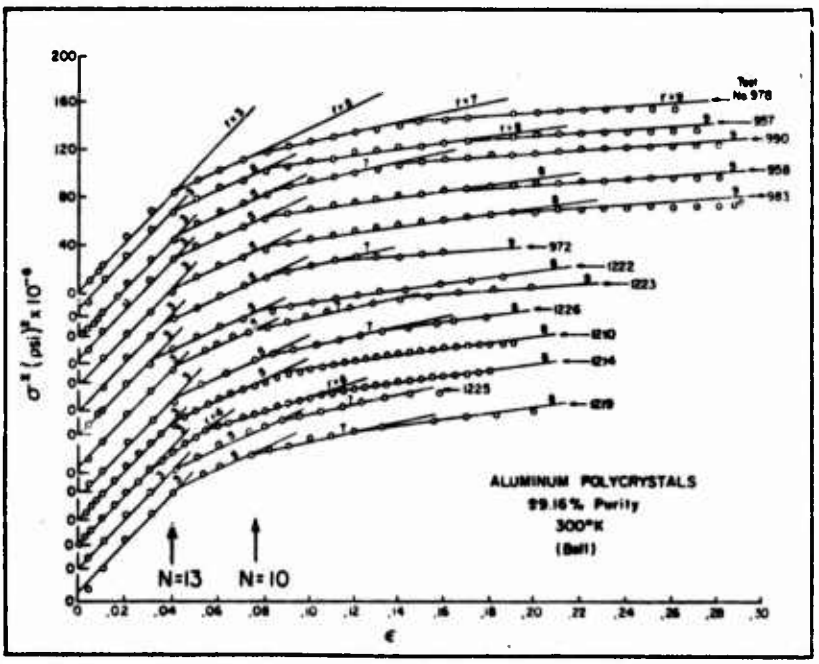


Fig. 3

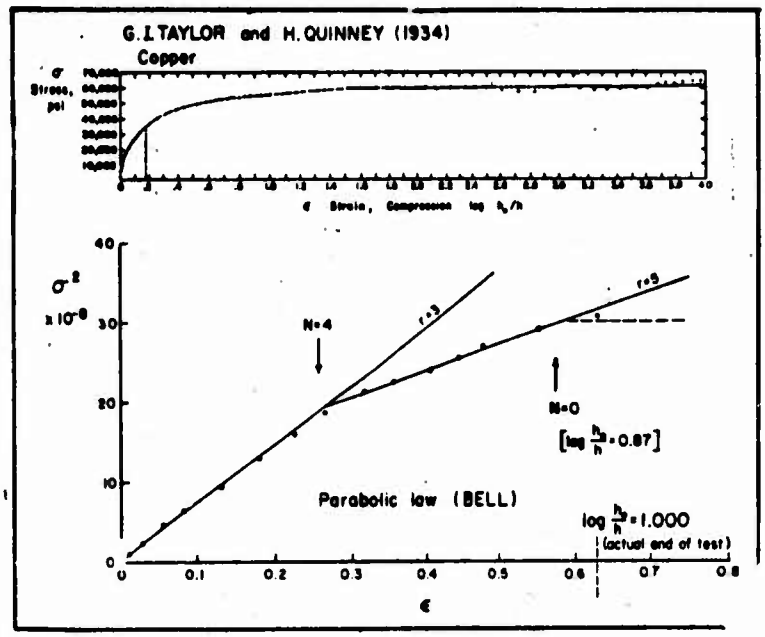
G. I. TAYLOR and H. QUINNEY (1934)
Copper
σ
Stress, psi
ε Strain, Compression log h₀/h
σ²
x10⁻⁸
N=4
r=3
r=5
N=0
[log h₀/h = 0.87]
Parabolic law (BELL)
log h₀/h = 1.000
(actual end of test)
ε

Fig 4

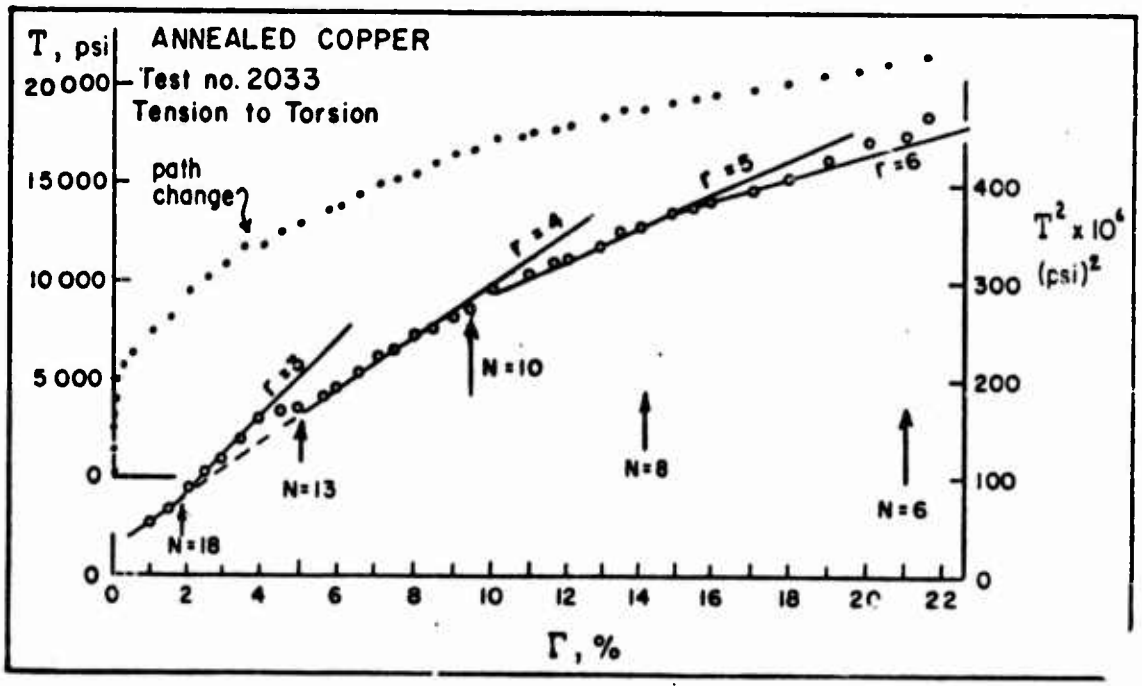
T, psi
ANNEALED COPPER
Test no. 2033
Tension to Torsion
path change
r=3
r=4
r=5
r=6
N=18
N=13
N=10
N=8
N=6
T², psi²
Γ, %

Fig. 5

In all these tests we note the presence of second-order transitions which I first discovered in impact tests in 1959-60, intensively studied during the next eight years, and first described in detail in the 1968 monograph[7] referred to above. These are second-order transitions, or discontinuities in the slope. Over two thousand experiments performed in this laboratory since 1960 have shown in detail that the slopes of the individual members of this sequence involve a change of the mode index, r , of Eq. (8).

As with Bridgman who in the 1930's and 1940's first found second-order transitions in the hydrostatic compression of several solids including nickel, rubber, etc., the second-order transitions which I have discovered in large distortional deformation also occur at fixed strains. When second-order transitions are found, they occur in a well defined sequence of eight critical strains or shear angles.

From the statistical study of the results of hundreds of tests which provided from thirty to over sixty determinations of each critical strain for both single and polycrystals over the whole range of proportional and non-proportional loading paths, I found that these critical strains occur in the form given in Eq. (13).

$$\Gamma_N = \frac{1}{\sqrt{2}} \left( \frac{2}{3} \right)^{N/2} \tag{13}$$

where N = 0, 2, 4, 6, 8, 10, 13, 18.

In Table I the values determined for the generalized strain $\Gamma_N$ are tabulated and may be compared with a few illustrations given in Figs. 2, 3, 4, and 5.

TABLE I.

| N | TRANSITION STRAINS | | | |
|---|---|---|---|---|
| | $\Delta_N$ | $\epsilon_N$ | $\Gamma_N$ | $\gamma_N$ |
| 0 | 1.000 | 0.577 | 0.707 | 1.766 |
| 2 | 0.667 | 0.385 | 0.471 | 1.178 |
| 4 | 0.444 | 0.257 | 0.314 | 0.786 |
| 6 | 0.296 | 0.171 | 0.209 | 0.523 |
| 8 | 0.198 | 0.114 | 0.140 | 0.349 |
| 10 | 0.132 | 0.076 | 0.093 | 0.233 |
| 13 | 0.072 | 0.041 | 0.051 | 0.125 |
| 18 | 0.026 | 0.015 | 0.018 | 0.046 |

Setting $\sigma_y = S = 0$, the series of critical strains for axial loading $\epsilon_N$ may be determined from a knowledge of $\Gamma_N$. The values for this special case are included in Table I. Similarly for $\sigma_x = \sigma_y = 0$, the sequence of critical strains $\Delta_N$ for simple torsion may be obtained. We note that the largest value for $N = 0$ corresponds to a shear angle of $45^\circ$, a fact of no small significance in understanding the structure of this critical strain.

Finally, from the aggregate ratio, since $\gamma_N$ may be determined from $\Gamma_N$, i.e., $\gamma_N = \bar{K}\Gamma_N$, we may calculate the critical values $\gamma_N$ for the single crystal resolved shear strain. These also are included in Table I.

In Bologna, Italy in the fall of 1970, while contrasting experimental results in the large deformation of fully annealed metals from this laboratory with those of several other investigators, in particular while "de-true-ing" the measurements of Evan A. Davis[9,10] on copper and steel tubes in 1943-45, I discovered constitutive equations in the two-dimensional domain for nominal stress and nominal strain.

In the original form, these constitutive equations were limited to proportional loading save for a few non-proportional loading tests in fully annealed aluminum. The deformation of the latter paths, as is now known and as will be shown below, is approximated closely by deformation type response functions applicable to proportional loading.

In the past several years a large number of experiments have been performed in fully annealed metals with many different loading paths chosen to ascertain whether incremental type or deformation type constitutive equations are applicable. The results for the fully annealed metals are decisive.

In general, the constitutive equations are incremental, but of course they may be readily integrated to provide deformation type response functions for proportional loading. It should be noted that for engineering purposes, for a large class of non-proportional loading paths, the use of deformation type constitutive equations will closely approximate observation. This is perhaps one of the reasons for the previous controversy over different experimental results.

Whether the generalized strain is obtained by integrating along the strain path for completely general loading paths or by the direct use of $\Gamma$ in Eq. (5) for proportional loading, the aggregate ratios for Eq. (9) and the parabolic response for the generalized stress and strain of Eq. (10) are unchanged. For general loading paths in the fully annealed metals in the two-dimensional domain for which $\sigma_z = 0$, we have Eqs. (14). The corresponding integrated form for proportional loading is given in Eqs. (15) where $\sigma_b$, etc., designates the intercept on the strain abscissa for the particular domain of strain considered.

| GENERAL LOADING PATHS | PROPORTIONAL LOADING PATHS |
|---|---|
| $d\epsilon_x = \frac{4\sigma_x - 2\sigma_y}{3\bar{k}^3\beta_s^2}\, dT$ | $\epsilon_x = \frac{2\sigma_x - \sigma_y}{3\bar{k}^3\beta_s^2}\, T + \epsilon_{xb}$ |
| $d\epsilon_y = \frac{4\sigma_y - 2\sigma_x}{3\bar{k}^3\beta_s^2}\, dT$ | $\epsilon_y = \frac{2\sigma_y - \sigma_x}{3\bar{k}^3\beta_s^2}\, T + \epsilon_{yb}$ |
| (14) | (15) |
| $d\epsilon_z = -\frac{2(\sigma_x + \sigma_y)}{3\bar{k}^3\beta_s^2}\, dT$ | $\epsilon_z = -\frac{\sigma_x + \sigma_y}{3\bar{k}^3\beta_s^2}\, T + \epsilon_{zb}$ |
| $d\Delta = \frac{4S\, dT}{\bar{k}^3\beta_s^2}$ | $\Delta = \frac{2S\,T}{\bar{k}^3\beta_s^2} + \Delta_b$ |

For $\sigma_y = 0$ we have the situation for the simultaneous tension–torsion of a thin-walled tube for which the second and third of the incremental equations (14) merely state that $d\epsilon_y = d\epsilon_z = -\frac{d\epsilon_x}{2}$. For this situation for any loading path, the incremental strain vector $d\epsilon_x/d\Delta$ becomes Eq. (16).

$$\frac{d\epsilon_x}{d\Delta} = \frac{\sigma_x}{3S} \tag{16}$$

We thus expect for the fully annealed solid that the normality condition will hold. A single exception for very small plastic strain in fully annealed aluminum has been observed by H. Moon, as is footnoted on page 4 above.

For the comparison of the fully annealed polycrystalline response function with the resolved shear response function of the single crystal, the most important situation is that for which

$\sigma_y = S = 0$ , for which the aggregate ratio of Eq. (9) becomes that of Eq. (17).

$$\frac{\sigma_x}{\uparrow} = \bar{m} = \frac{d\gamma}{d\epsilon_x} \qquad \text{where } \bar{m} = \sqrt{\tfrac{3}{2}}\,\bar{k} = 3.06 \quad (17)$$

The value of $\bar{m} = 3.06$ is numerically equivalent to that obtained by G. I. Taylor[11-14] in 1938 and by Bishop and Hill[15,16] in their reconsideration of his theory in 1951. These theories, however, do not provide the observed $\bar{k}$ of Eq. (9) for more general loading states. T. Dawson[17] in his doctoral research in this laboratory several years ago, reexamined the Taylor theory to include not only continuity but also stress equilibrium; he obtained aggregate ratios which differed from experiment in all instances, including the ratio for the value of $\bar{m}$ .

It is my opinion that the past difficulty in correlating experiment and theory lies primarily in the implicit assumption of homogeneous strain always heretofore made. Measurements referred to in the preface of this report show that this assumption is seriously in error, but, nevertheless, for axial loading, the value is indeed $\bar{m} = 3.06$ for every one of the large number of crystalline solids for which such comparisons have been made.

In recent research, not included in this report, I have succeeded in formulating a new theory of the aggregate for which inhomogeneous deformation is permitted, and in which individual crystallite stresses and strains and their sum may be determined from a single resolved shear response function which applies to the bounded crystal. In the present report, in my earlier work,[18-21] and in the theories of Taylor, Bishop and Hill, and Dawson, the comparison is between the aggregate and the free, unbounded single crystal.

Introducing Eq. (6) and Eq. (7) for the unbounded single crystal into Eq. (17) provides for the axial loading of the polycrystal, Eqs. (18) and (19).

$$d\epsilon_x = \frac{2\sigma_x \, d\sigma_x}{\bar{m}^{3} \beta_s^{2}} \tag{18}$$

$$\sigma_x = \bar{m}^{3/2} \beta_s \left(\epsilon_x - \epsilon_{xb}\right)^{1/2} \tag{19}$$

The strain $\epsilon_{xb}$ is the intercept on the strain abscissa. For all dynamic tests, $\epsilon_{xb} = 0$. For fully annealed metals, $\epsilon_{xb}$, which easily may be determined from measurement, is exceedingly small.

The resolved shear stress, resolved shear strain for the shear deformation of the single crystal of Eq. (6) is calculated from axial tension or compression in a specimen whose initial crystallographic orientations are known from x-ray measurement. This is the response function for the free single crystal. The key to the main discovery reported upon here for the structural metal alloys is that when for simple axial testing the resolved shear response function of Eq. (6) is compared in terms of the aggregate ratios of Eq. (17), the value of $\bar{m}$ is increased, compared to the value obtained for the fully annealed metal. Designating this new ratio as $M$, we have Eq. (20),

$$M = \lambda_N \bar{m} \tag{20}$$

where $\lambda_N = 1 + \epsilon_N$.

With each of the many metal alloys which have been studied, the value of $\lambda_N$ in Eq. (20) is a material constant independent of the type of test, independent of the shape of the specimen, whether it be a bar, a tube, or a plate, and independent of whether or not the loading paths are proportional or non-proportional.

## Theory of Plasticity for Structural Metal Alloys

During the last year of the five-year contract for which this is the final report, I began a systematic effort to consider whether or not a general theory of plasticity for the fully annealed solid, briefly outlined above, was in any way extendible to structural metal alloys such as 1095 tool steel, HF-1 steel, mild steel, or aluminum alloys such as 7075-T6 and 6061-T6, and copper alloys such as hardened alpha-brass, etc. All these metals were tested in the "as-received" condition except for 1095 tool steel and HF-1 steel which had to be annealed in order to machine specimens, but subsequent quenching and tempering produced the original metal.

The experiments performed were many and of many types. They included diffraction grating measurements of wave profiles during propagation of plastic waves, measurements of the time of contact and coefficient of restitution in a symmetrical free-flight impact, and quasi-static measurements in thin-walled tubes for many different types of proportional and non-proportional loading paths. The results of this work far exceeded the original expectation, for in every instance, without exception, the theory and concepts which I had developed in nearly 25 years of research with B. R. L., the Army Research Office, and the Air Force Office of Scientific Research have been shown to be essential for the understanding of the large deformation of the structural metal alloy. The deformation from zero strain to ultimate stress for any arbitrarily chosen loading path now can be completely defined.

As the experimental data accumulated, it became obvious that there were two regions of plastic deformation. In the discussion above it was pointed out that the intermediate region of elastic-plastic deformation is bounded by an inner yield surface and an outer yield surface and that the second totally plastic region is bounded by the outer yield surface and the ultimate stress.

Denoting $T_Y$ and $\Gamma_Y$ as the generalized stress and strain at the inner yield surface or the end of linearity in small deformation,

and $T_N$ and $\Gamma_C$ as the generalized stress and measured strain at the outer yield surface or the boundary between the intermediate elastic-plastic region and the totally plastic region, we find from experiment for both proportional and non-proportional loading paths that in the intermediate elastic-plastic region for the structural metal alloy the aggregate ratio of Eq. (9) for the fully annealed metal becomes Eq. (21),

$$\frac{T - T_Y}{\uparrow} = \lambda_N \bar{K} = \frac{d\gamma}{d\Gamma} \tag{21}$$

where $\lambda_N = 1 + \epsilon_N$ is the parameter introduced in Eq. (20).

For the totally plastic region in generalized stress and strain, experiment has shown that the aggregate ratios of Eq. (9) become Eq. (22).

$$\frac{T}{\uparrow} = \lambda_N \bar{K} = \frac{d\gamma}{d\Gamma} \tag{22}$$

A comparison of the incremental form of Eq. (7) provides for the intermediate region, Eq. (23),

$$d\Gamma = \frac{2(T - T_Y)\,dT}{\lambda_N^3 \bar{K}^3 \beta_s^2} \tag{23}$$

and for the totally plastic region, Eq. (24).

$$d\Gamma = \frac{2T\,dT}{\lambda_N^3 \bar{K}^3 \beta_s^2} \tag{24}$$

These equations may be integrated in their respective regions of strain providing, from Eq. (23), Eq. (25) for the intermediate region,

$$T = T_Y + \lambda_N^{3/2} \bar{K}^{3/2} \beta_s (\Gamma - \Gamma_Y)^{1/2} \qquad \Gamma_Y \leq \Gamma \leq \Gamma_C \tag{25}$$

and Eq. (26) for the totally plastic region,

$$T = \lambda_N^{3/2} \bar{K}^{3/2} \beta_s \left( \Gamma - \Gamma_c + \frac{\Gamma_N}{\lambda_N} \right)^{1/2} \qquad \Gamma \geq \Gamma_c \tag{26}$$

where $\Gamma_N = \sqrt{3/2}\, \epsilon_N$.

$T_N$ at the c ter yield surface which bounds the second plastic region at $\Gamma = \Gamma_c$ is given, from Eq. (26), as Eq. (27).

$$T_N = \lambda_N \bar{K}^{3/2} \beta_s \Gamma_N^{1/2} \tag{27}$$

Letting $\beta = \bar{K}^{3/2} \beta_s$, the parabola coefficient for the fully annealed metal, and designating $\beta_a$ as the parabola coefficient in Eqs. (25) and (26) for the metal alloy, we have Eq. (28).

$$\beta_a = \lambda_N^{3/2} \beta \tag{28}$$

When the experimental values of T and $\Gamma$ have been determined for an arbitrary loading path, they may be plotted in two ways: in a $(T - T_Y)^2$ vs $\Gamma$ plot from which the observed constant slope will provide the value of $\beta_a$ for the intermediate region; and in a $T^2$ vs $\Gamma$ plot from which the observed constant slope of the straight line will provide the value of $\beta_a$ for the totally plastic region. In general, these two measured parabola coefficients are identical.

From the original parabola coefficients, $\beta_s$, for the single crystal, Eq. (8), we find that knowing the ambient temperature, the melting point, and $\mu(0)$, a sequence of parabola coefficients for the integral indices r provides from the fully annealed metal a value for $\beta$ for the dominant component of the metal alloy. Again, it is solely from experiment that the following result is obtained.

With $\beta$ known, the measurement of $T_N$ as the beginning of parabolicity in the totally plastic region in a $T^2$ vs $\Gamma$ plot, or as the end of parabolicity in a $(T - T_Y)^2$ vs $\Gamma$ plot for the intermediate region, provides a value of $\lambda_N$ from experiment [Eq. (27)]. The value so determined must be compatible with the

observed value of $\beta_a$, i.e., the slope of the measured straight line portion of the stress squared vs strain plot. When these values are compatible, as they have been in every instance in over one hundred experiments performed to determine $\lambda_N$ for 16 structural metal alloys, then the value of $\lambda_N$ may be determined for the general statements of Eqs. (25) and (26).

Before examining the data which reveal that a precise value of $\lambda_N$ is indeed associated with each metal, irrespective of the type of test or loading path, it is worth while to look a little more closely at the nature of this calculation of $\lambda_N$.

In the $T^2$ vs $\Gamma$ plot, the intermediate region is clearly not a straight line. However, from the differentiation of Eq. (25) one may obtain the slope of such a plot at any value of $T$ including that at the boundary between the two regions, $T_N$, as is given in Eq. (29).

$$\left(\frac{d\,T^2}{d\,\Gamma}\right)_N = \frac{T_N\,\beta_a}{(\Gamma_c - \Gamma_y)^{1/2}} \tag{29}$$

A comparison of the slope on one side of the outer yield surface and $\beta_a^2$ for the totally plastic region will reveal the sharp discontinuity at which parabolicity begins in the totally plastic region. One of the important values of $\lambda_N$, as will be shown immediately below, is that which characterizes 6061-T6 aluminum, 5083-H131 aluminum, hardened alpha-brass, and hardened copper, for example, and which has the value $\lambda_N = 1.385$. In Fig. 6 we see that for uniaxial loading, where $\sigma_y = S = 0$, where for the mode index $r = 1$, $\beta$ of fully annealed aluminum is given as $\beta = 6.86 \times 10^4$ psi; for $r = 2$, $\beta = 5.6 \times 10^4$ psi; and for $r = 3$, $\beta = 4.57 \times 10^4$ psi, we have from Eqs. (27) and (28), the three calculated curves shown in the $\sigma^2$ vs $\epsilon$ plot.

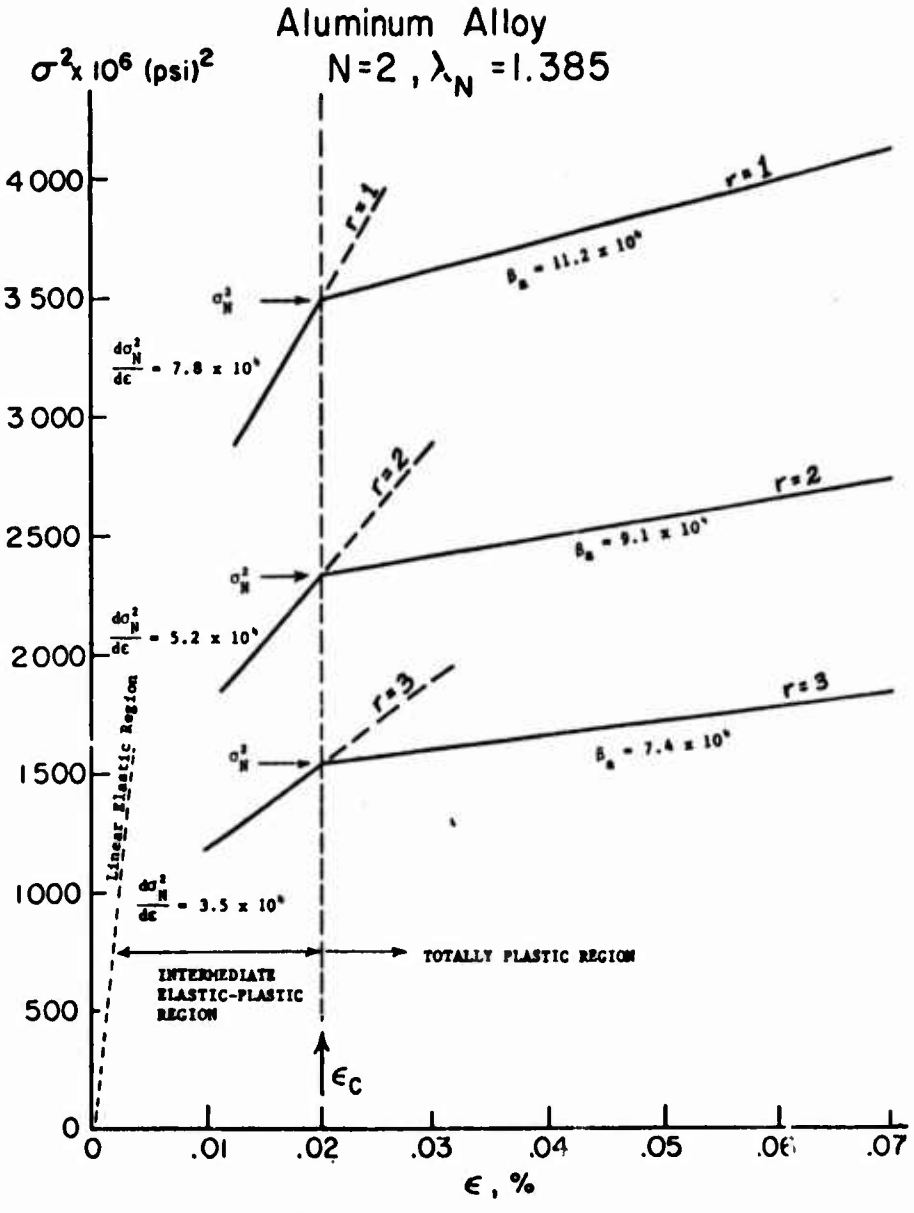


Fig. 6

The calculated values of $\sigma_N^2$ at the outer yield surface are shown. Also shown is the slope in a $\sigma^2$ vs $\epsilon$ plot from the intermediate region, i.e., Eq. (29) for only $\sigma_x \neq 0$.

First, we note that these slopes are markedly different at the boundary which, as will be shown in the experimental data below, may be specified with precision. Second, we note that the values of $\sigma_N^2$ differ by such a magnitude when the mode index r is changed by unity that there is no possibility of confusion in these determinations. And, finally, we observe that with such large differences present in these determinations, the compatibility

between values of $\lambda_N$, simultaneously determined from Eqs. (27) and (28), establishes the applicability of the concept of the plastic deformation of metal alloys discovered from this research.

On the following pages, I shall provide many illustrations of different loading paths, etc., for each of the 16 metal alloys thus far studied. At this point, however, I shall summarize the results to facilitate the overview of the data.

The first and most important fact, as indicated above, is that the value of $\lambda_N$ or correspondingly $\epsilon_N$ is a fixed material constant for each metal alloy. The second important fact is that when the $\lambda_N$'s are determined from Eqs. (27) and (28), the calculated values of $\epsilon_N$ fall with great precision into the sequence of critical strains $\epsilon_N$ shown in Table I. What is remarkable about this recent discovery is that the $\epsilon_N$'s are stable values defining the state of a given metal alloy, and they are identical with the critical strains observed in the fully annealed solid, i.e., the strains at which second-order transitions occur for the monotonically increasing large deformation of the fully annealed metal and the single crystal. Thus it becomes obvious that it is essential to comprehend this quantized phase and second-order transition structure before developing any general theory of plasticity purporting to deal with the physical facts.

For example, the second-order transition structure for the fully annealed metal, as well as the raising of the elastic limit $T_Y$ for the metal alloy, can give rise to an apparent viscosity in the sense of an increase of stress, when the underlying response function in fact is non-viscous, and the observed increase is due solely to the presence or non-presence of a second-order transition at a critical strain.

In Fig. 7 is shown a plot of the experimentally determined values of $\epsilon_N$ for all the metal alloys thus far examined. For clarity, I have plotted the experimentally determined ratio

$$\frac{\epsilon_N}{\lambda_N} = \sqrt{\frac{2}{3}}\, T_N^2/\theta_2^2 \qquad (\text{since } \Gamma_N = \sqrt{\tfrac{2}{3}}\,\epsilon_N) \text{ against } \epsilon_N .$$

The arrows in Fig. 7 show the location of the critical strains $\epsilon_N$ from Table I. My discovery of this distribution, which in fact came just after the termination of this contract, in research under a subsequent B. R. L. contract, occurred only after a large amount of data had been accumulated in the different metals.

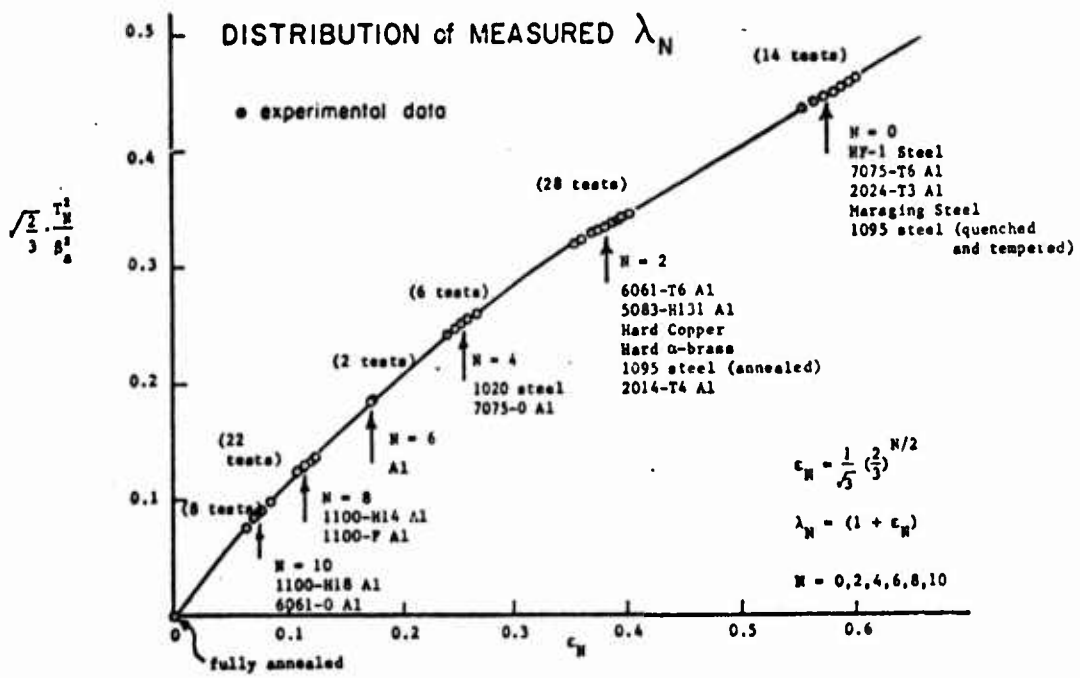


Fig. 7

A summary of the values of N and the mode index r for the different metal alloys is given in Table II. These are the results of nearly 100 individual tests in tension, compression, torsion, and combined tension-torsion, in proportional or non-proportional loading paths. In the final column of Table II, I have compared

the average value of all the measured values of $\lambda_N$ for all of the metal alloys in each class designated by N . As may be seen, the correlation of these values with predicted $\lambda_N$ and with the predicted values of critical strains from Table I is indeed precise.

TABLE II

| | | | |
|---|---|---|---|
| Maraging Steel | N-0 | r-1 | Avg. Exp. $\lambda_N$ - 1.575 |
| HF-1 Steel, quenched & tempered | N-0 | r-3 | |
| HF-1 Steel, isothermal | N-0 | r-4 | |
| 1095 Steel, quenched & tempered | N-0 | r-4 | Predicted $\lambda_N$ - 1.577 |
| 7075-T6 Aluminum | N-0 | r-1 | |
| 2024-T3 Aluminum | N-0 | r-2 | |
| 5083-H131 Aluminum | N-2 | r-1 | |
| 6061-T6 Aluminum | N-2 | r-2 | Avg. Exp. $\lambda_N$ - 1.373 |
| 2014-T4 Aluminum | N-2 | r-2 | |
| 1095 Steel, annealed | N-2 | r-6 | Predicted $\lambda_N$ - 1.385 |
| Hard Copper | N-2 | r-4 | |
| Hard Alpha-brass (70-30) | N-2 | r-4 | |
| Hard Alpha-brass (70-30) | N-2 | r-5 | |
| 1020 Steel | N-4 | r-4 | Exp. - 1.254 |
| 7075-0 Aluminum | N-4 | r-1 | Pred. - 1.257 |
| 1100-H14 Aluminum | N-8 | r-2 | Exp. - 1.1144 |
| 1100-F Aluminum | N-8 | r-2 | Pred. - 1.1140 |
| 1100-H18 Aluminum | N-10 | r-1 | Exp. - 1.075 |
| 6061-0 Aluminum | N-10 | r-2 | Pred. - 1.076 |

From an inspection of Table II, we note that the value of N is dependent upon the prior thermal, mechanical, and chemical histories, i.e., the metallurgical recipe which produced the stable structural metal alloy. Thus, for 7075-T6 aluminum, $N = 0$, $r = 1$ ; for 7075-0 aluminum, however, this solid is defined for $N = 4$, $r = 1$ . Similarly, for 6061-T6 aluminum, we have $N = 2$, $r = 2$ ; whereas for 6061-0 aluminum, $N = 10$, $r = 2$ . From a series of experiments involving a very large number of tests on "as-received" 1100 aluminum, the material state $N = 8$, $r = 2$ is firmly established. If this solid

is annealed at 90% of the melting point, i.e., at 1100°F, one obtains the fully annealed solid for which $\lambda_N = 1.000$. If, on the other hand, the annealing temperature is successively altered, then values of $N = 10$, $r = 2$; $N = 13$, $r = 2$; $N = 18$, $r = 2$; and $N = 18$, $r = 1$ are obtained as the annealing temperature is raised.

With the values of $\lambda_N$ known for a given metal alloy, it becomes possible to provide constitutive statements for the two-dimensional domain similar to those for Eqs. (14) and (15) for the fully annealed solid. There is one difference, however. For the fully annealed solid, the intermediate elastic-plastic region either is non-existent or is so small that it can be ignored; whereas for the metal alloy, it is necessary to define the response functions in each of two domains.

For the intermediate region, where $\Gamma_Y < \Gamma \leq \Gamma_c$ we have the incremental equations for general loading paths, Eqs. (30), and the integrated form for proportional loading, Eqs. (31).

$$\left.\begin{aligned} d\varepsilon_x &= \frac{4(\sigma_x - \sigma_{xY}) - 2(\sigma_y - \sigma_{yY})}{3\,\lambda_N^3\,\bar{k}^3\beta_s^2}\,dT \\ d\varepsilon_y &= \frac{4(\sigma_y - \sigma_{yY}) - 2(\sigma_x - \sigma_{xY})}{3\,\lambda_N^3\,\bar{k}^3\beta_s^2}\,dT \\ d\varepsilon_z &= -\frac{2(\sigma_x - \sigma_{xY}) + 2(\sigma_y - \sigma_{yY})}{3\,\lambda_N^3\,\bar{k}^3\beta_s^2}\,dT \\ d\delta &= \frac{4(S - S_Y)}{\lambda_N^3\,\bar{k}^3\,\beta_s^2}\,dT \end{aligned}\right\} \qquad (30)$$

$$\left.\begin{aligned} \varepsilon_x &= \frac{2(\sigma_x - \sigma_{xY}) - (\sigma_y - \sigma_{yY})}{3\,\lambda_N^3\,\bar{k}^3\,\beta_s^2}\,(T - T_Y) + \varepsilon_{xY} \\ \varepsilon_y &= \frac{2(\sigma_y - \sigma_{yY}) - (\sigma_x - \sigma_{xY})}{3\,\lambda_N^3\,\bar{k}^3\,\beta_s^2}\,(T - T_Y) + \varepsilon_{yY} \\ \varepsilon_z &= -\frac{(\sigma_x - \sigma_{xY}) + (\sigma_y - \sigma_{yY})}{3\,\lambda_N^3\,\bar{k}^3\,\beta_s^2}\,(T - T_Y) + \varepsilon_{zY} \\ \delta &= \frac{2(S - S_Y)}{\lambda_N^3\,\bar{k}^3\,\beta_s^2}\,(T - T_Y) + \delta_Y \end{aligned}\right\} \qquad (31)$$

Correspondingly, for the totally plastic region, for $\Gamma \geq \Gamma_s$, we have Eqs. (32) for general loading paths, and Eqs. (33) for proportional loading.

$$\left.\begin{aligned} d\varepsilon_x &= \frac{4\sigma_x - 2\sigma_y}{3\lambda_N^3 \bar{k}^3 \beta_s^2}\, dT \\ d\varepsilon_y &= \frac{4\sigma_y - 2\sigma_x}{3\lambda_N \bar{k}^3 \beta_s^2}\, dT \\ d\varepsilon_z &= -\frac{2(\sigma_x + \sigma_y)}{3\lambda_N^3 \bar{k}^3 \beta_s^2}\, dT \\ d\delta &= \frac{4S}{\lambda_N^3 \bar{k}^3 \beta_s^2}\, dT \end{aligned}\right\} \quad (32)$$

$$\left.\begin{aligned} \varepsilon_x &= \frac{2\sigma_x - \sigma_y}{3\lambda_N^3 \bar{k}^3 \beta_s^2}\, T + \varepsilon_{xc} - \frac{\varepsilon_{xN}}{\lambda_N} \\ \varepsilon_y &= \frac{2\sigma_y - \sigma_x}{3\lambda^3 \bar{k}^3 \beta_s^2}\, T + \varepsilon_{yc} - \frac{\varepsilon_{yN}}{\lambda_N} \\ \varepsilon_z &= -\frac{\sigma_x + \sigma_y}{3\lambda_N^3 \bar{k}^3 \beta_s^2}\, T + \varepsilon_{zc} - \frac{\varepsilon_{zN}}{\lambda_N} \\ \delta &= \frac{2S}{\lambda_N^3 \bar{k}^3 \beta_s^2}\, T + \delta_c - \frac{\delta_N}{\lambda_N} \end{aligned}\right\} \quad (33)$$

Limiting the discussion to the combined tension-torsion of thin-walled hollow tubes for which $\sigma_y = \sigma_z = 0$, we note that the incremental strain vector $d\epsilon_x/ds$ in the intermediate region has the form of Eq. (34),

$$\frac{d\epsilon_x}{ds} = \frac{\sigma_x - \sigma_{xY}}{3(S - S_Y)} \quad (34)$$

whereas from Eqs. (32) and (33), the incremental strain vector has the form of Eq. (35) in the totally plastic region.

$$\frac{d\epsilon_x}{ds} = \frac{\sigma_x}{3S} \quad (35)$$

From experiment in non-proportional loading paths, as will be shown below, the direction of the incremental strain vector in the intermediate region is found to depend upon the memory of the individual components $\sigma_{xY}$ and $S_Y$ when the loading path has passed through the inner yield surface. Thus, for simple torsion followed by constant torsion plus increasing tension, $\sigma_{xY} = 0$ and $S_Y \neq 0$. If the corner occurs in the intermediate region, then during increasing tension at constant torsion, we have $d\epsilon/ds = \sigma_x / 3(S_o - S_Y)$ where $S_o$ = constant. On the other hand, for simple tension followed by constant tension plus increasing torsion, where $\sigma_{xY} \neq 0$, and $S_Y = 0$, we have, after turning a corner in the intermediate region, $d\epsilon/ds = (\sigma_x - \sigma_{xY}) / 3S$.

The fact just stated provides a very interesting experimental check upon the value of $\lambda_N$ calculated from Eqs. (27) and (28) for a given metal alloy. A plot of strain components in $\epsilon_x$ vs $s$ space reveals that at the boundary of the outer yield surface, between the intermediate elastic-plastic region and the totally plastic region, the incremental strain vector undergoes an abrupt change. For initial torsion, for the situation considered above, the slope change will be from $d\epsilon_x/ds = \sigma_x/3S - \sigma_{xY}/3S$ in the intermediate region to $d\epsilon_x/ds = \sigma_x/3S$ in the totally plastic region.

Choosing a metal alloy for which $\sigma_N$ is not too much greater than $\sigma_Y$, abrupt angular changes are indeed visible, as will be shown below from experimental data. In fact, from such a measurement it is possible to determine the value of $\lambda_N$ independent of the usual procedure given in its calculation from Eqs. (27) and (28).

Experimental Data

The statements of loading surfaces and constitutive equations just given for the metal alloy when compared with the earlier equivalent statements for the fully annealed metal reveals that what is presented here is a unified theory for the total class of metals, since for the fully annealed metal $\lambda_N = 1.000$ or $\epsilon_N = 0$. For this situation $\Gamma_e = 0$, and the intermediate elastic-plastic region either disappears or becomes so small as to be negligible.

Hence, in providing at this point the experimental base from which the above statements were derived, it is pertinent to present experimental data for both the metal alloys and the fully annealed metal, since the phenomena observed in one are anticipated in the other.

The introduction of the material constant $\Gamma_N / \lambda_N$ in Eq. (26) corresponds to a statement of the origin of the parabola for the totally plastic region in the present reference configuration. Introducing the experimental results for the metal alloys first, it is convenient to begin with simple loading situations. For axial loading in tension or compression, $\sigma_x \neq 0$, $\sigma_z = \sigma_y = S = 0$, Eq. (25) for the intermediate region becomes Eq. (36),

$$\sigma = \sigma_Y + \lambda_N^{3/2} \bar{m}^{3/2} \beta_s (\epsilon - \epsilon_Y)^{1/2} \qquad \epsilon_Y \leq \epsilon \leq \epsilon_c \tag{36}$$

and Eq. (26) for the totally plastic region becomes Eq. (37),

$$\sigma = \lambda_N^{3/2} \bar{m}^{3/2} \beta_s \left(\epsilon - \epsilon_c + \frac{\epsilon_N}{\lambda_N}\right)^{1/2} \qquad \epsilon \geq \epsilon_c \tag{37}$$

where $\bar{m} = \sqrt{\frac{3}{2}}\, \bar{k}$

The stress at the boundary of the outer yield surface, between the two plastic regions of Eq. (27), becomes Eq. (38).

$$\sigma_N = \lambda_N \bar{m}^{3/2} \beta_s \epsilon_N^{1/2} \tag{38}$$

As of this writing, approximately one hundred quasi-static measurements for the several different metal alloys and approximately the same number of wave propagation experiments have been performed. For the former, many different loading paths have been considered, while for the latter, all data have been obtained from the symmetrical free-flight impact of identical metal alloy cylinders.

In Fig. 8a is shown a tensile test in 1095 tool steel, quenched and tempered at 950°F. Fig. 8b is a $\sigma^2$ vs $\epsilon$ plot of

these data from which the observed beginning of plasticity for the totally plastic region is seen to occur at $\sigma_N^2 = 26{,}200 \times 10^6$, at an $\epsilon_o$ of 0.061 . The corresponding value of $\sigma_N$ is 162,000 psi.

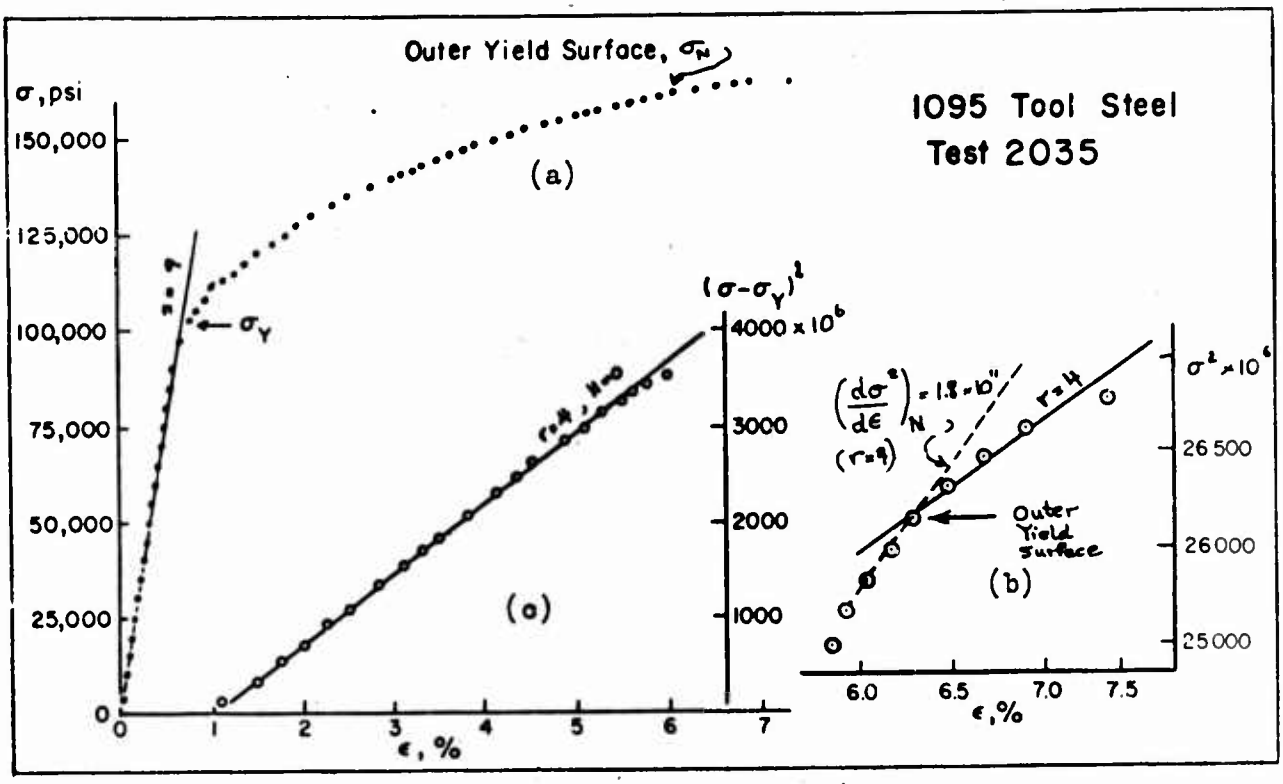


Fig. 8 a,b,c

For the known parabola coefficient, r = 4 , for the fully annealed metal, $\bar{m}^{1/2}\beta_s = 12.6 \times 10^4$ psi. The calculated value of $\lambda_N$ from Eq. (38) is $\lambda_N = 1.625$ which for this test is $\lambda_N = 1.577$, 3% above the average value for N = 0 from Table II. For this value of $\lambda_N$ the $\beta_a$ predicted from Eq. (28) is $26.0 \times 10^4$ psi. The solid line in Fig. 8b corresponds to a square of this predicted parabola coefficient. The dashed line in Fig. 8b is the slope for the intermediate region at $\sigma_N$ determined from Eq. (29) which, for axial loading, becomes Eq. (39).

$$\left(\frac{d\sigma^2}{d\epsilon}\right)_N = \frac{\sigma_N \beta_a}{(\epsilon_c - \epsilon_Y)^{1/2}} \qquad (39)$$

Introducing $\beta_a = 26.0 \times 10^4$ from the previous calculation and observing from Fig. 8a that the value of $\epsilon_c - \epsilon_Y = 0.054$, we have for the predicted slope of the intermediate region, upon reaching $\sigma_N$, $d\sigma_N^2/d\epsilon = 1.80 \times 10^{11}$, which indeed correlates with the observed experimental results. As was indicated earlier, a sharp change in such a plot from a slope of $1.80 \times 10^{11}$ to $0.68 \times 10^{11}$, i.e., $\beta_a^2$, makes the outer yield surface readily discernible.

Finally, in Fig. 8c we see a plot of $(\sigma - \sigma_Y)^2$ vs $\epsilon$ for the intermediate region. From squaring Eq. (36) there should be a slope $\beta_a^2$ for the mode index r, identical with that in the totally plastic region, i.e., r = 4. That this indeed is the situation is seen in Fig. 8c, where the solid line corresponds to the slope of $\beta_a^2$ for $r = 4$, $\lambda_N = 1.625$, i.e., $N = 0$.

We thus see that when we know the values of N and r which describe a stable material structure, then we may obtain the response function for tension from zero strain to the ultimate stress.

As a second example, Figs. 9a,b,c provide a similar correlation with Eqs. (36), (37), (38), and (39) for 5083-H131 aluminum metal alloy. The measured value of $\sigma_N^2$ from Fig. 9b, $\sigma_N^2 = 3489.5 \times 10^6$, provides $\sigma_N = 59{,}072$ psi. The value of $\lambda_N$ calculated for $N = 2$, $r = 1$ which characterizes this alloy provides $\lambda_N = 1.386$. From Table II this is seen to be precisely the predicted critical value for $N = 2$. For this value of $\lambda_N$ the parabola coefficient $\beta_a$ from Eq. (28) is $11.2 \times 10^4$, which is seen as the slope of the solid line. Correspondingly, at the end of the intermediate region at a strain $\epsilon_c$ of 0.051, the slope at $\sigma_N$ from Eq. (39) is $d\sigma^2/d\epsilon = 2.94 \times 10^8$.

The $(\sigma - \sigma_Y)^2$ vs $\epsilon$ plot in the intermediate region of Fig. 9c, the slope (solid line) of which is the square of this parabola coefficient $\beta_a = 11.2 \times 10^4$, is clearly in close correlation with the response function of Eq. (36).

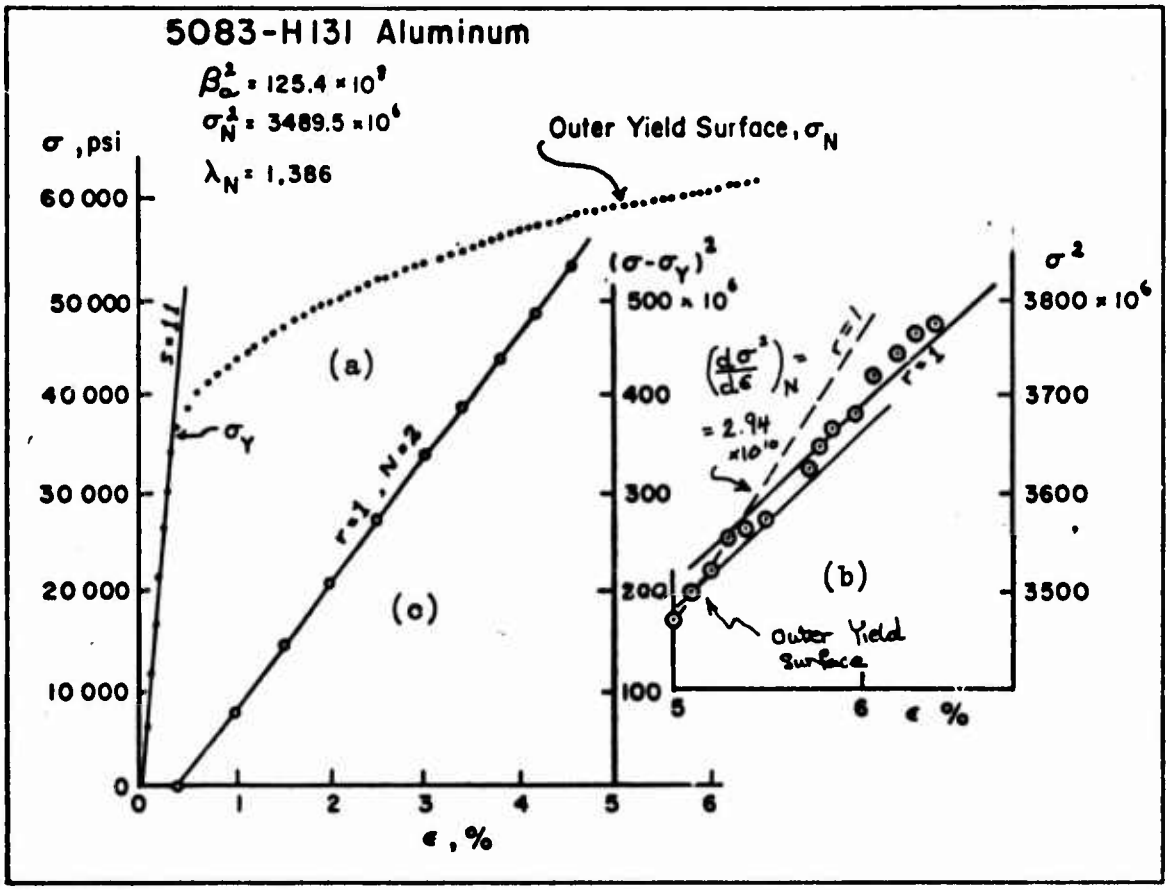


Fig. 9 a, b, c.

In Figs. 10a,b,c, 11a,b,c, and 12 a,b,c, similar results are shown for tensile tests for 6061-T6 aluminum alloy, 2024-T3 aluminum, and 1100, H-14 aluminum for which the measured values of $\lambda_N$ are 1.365, 1.590, and 1.120. These differ by 2.5%, 0.8%, and 0.5% from the predicted values of $\lambda_N$ for N = 0, N = 2, and N = 8, respectively (see Table II). Again, in each instance, at the end of the intermediate region the predicted slope (dashed line) from Eq. (39) is in close agreement, as are the slopes $\beta_a$ calculated from Eq. (28).

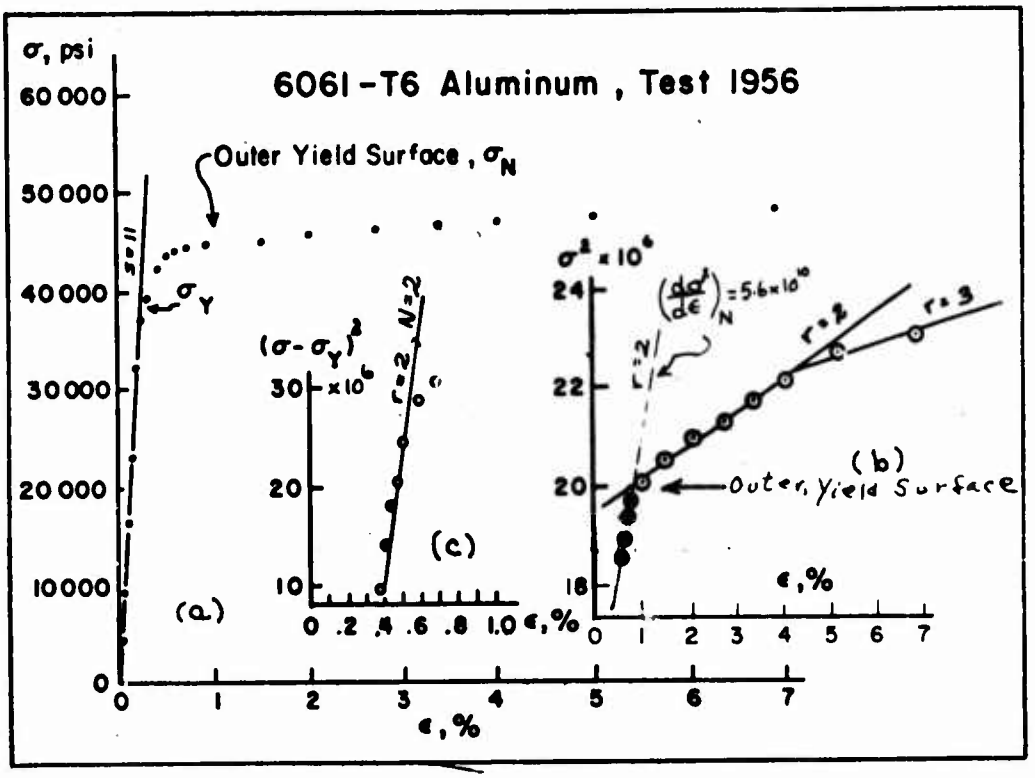


Fig. 10

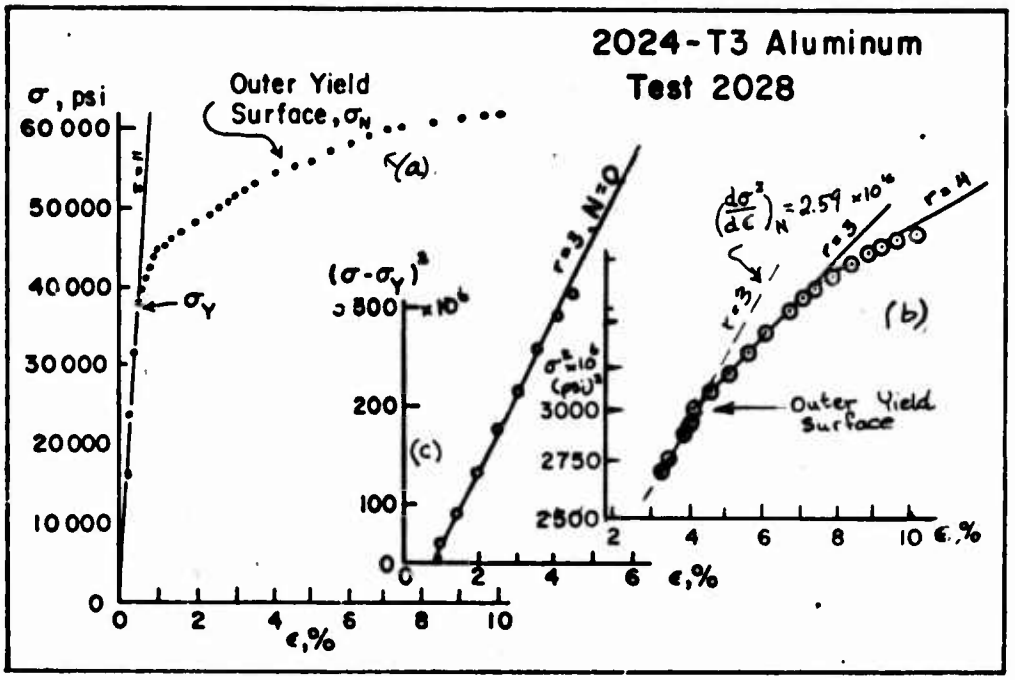
2024-T3 Aluminum
Test 2028
σ, psi
Outer Yield Surface, σN
(a)
σY
r=∞
60 000
50000
40 000
30000
20000
10 000
0
0 2 4 6 8 10
ε,%
(σ-σY)²
3 800
200
100
0
(c)
r=3, N=0
σ²×10⁶ (psi)²
3000
2750
2500
2 4 6
ε,%
(dσ²/dε)N = 2.59 ×10⁶
r=3
r=∞
(b)
Outer Yield Surface
2 4 6 8 10 ε,%

Fig. 11

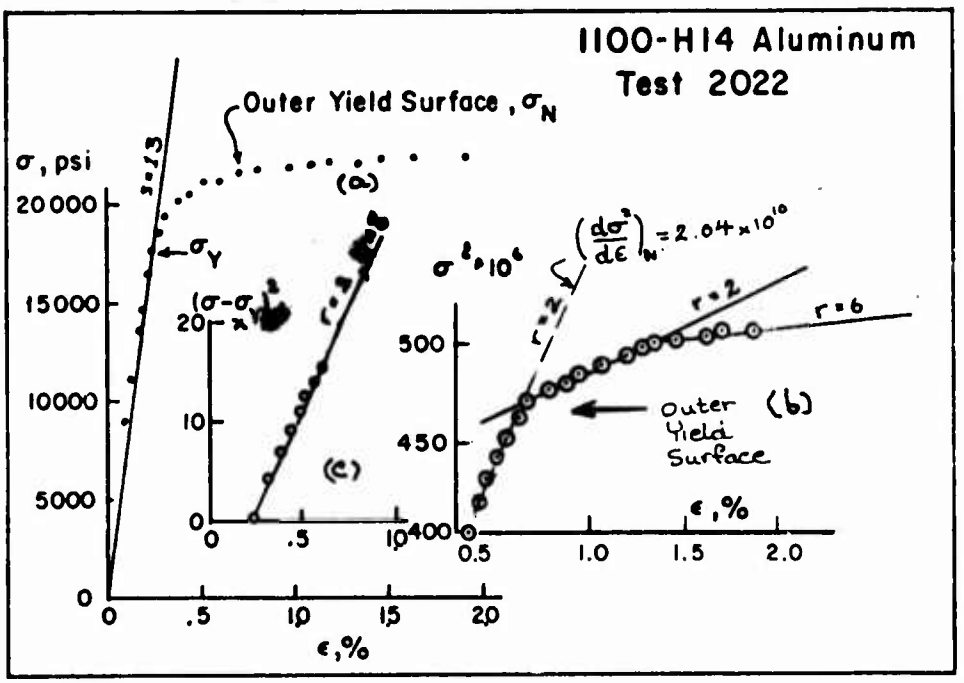
1100-H14 Aluminum
Test 2022
Outer Yield Surface, σN
σ, psi
r=1/3
(a)
σY
20000
15000
10000
5000
0
0 .5 1.0 1.5 2.0
ε,%
(σ-σY)²
20
10
0
(c)
r=3
0 .5 1.0
σ²×10⁶
500
450
400
(dσ²/dε)N = 2.04×10¹⁰
r=2
r=6
(b)
Outer Yield Surface
0.5 1.0 1.5 2.0
ε,%

Fig. 12

The test #2028 in 2024-T3 aluminum is included to point out that whereas the most common value of $r$ for this solid is $r = 2$ when $N = 0$, the preparation of the alloy can differ sufficiently to lower the initial parabola from $r = 2$ to $r = 3$. This is a common observation in the fully annealed metals where differences in the annealing procedure also can produce a shift in the mode index $r$. In the approximately 100 measurements considered here, however, this is an uncommon occurrence. The value of $r$ and the value of $N$ are, in general, material constants for the stable state.

In the studies of the fully annealed metal described in my monograph of 1968 on The Physics of Large Deformation of Crystalline Solids,[7] I stated, and acted upon, my strong conviction that for single crystals and for polycrystals any new generalization should be compared with the previous experiments in the literature. Accordingly, I include here, in Figs 13A and 13B $\sigma^2$ vs $\epsilon$ plots of two axial tests of Holt, Babcock, Green, and Maiden[22] from measurements in 1967 on 6061-T6 and 7075-T6 aluminum. For the former (Fig. 13A), the outer yield surface, readily seen at $\sigma_N^2 = 2410 \times 10^6$, provides a value of $\lambda_N = 1.395$ which differs by 0.7% from the predicted value of 1.385 shown in Table II. For the latter (Fig. 13B), $\lambda_N = 1.610$ for a mode index $r = 1$, which differs by 2% from the predicted value of $\lambda_N = 1.577$. The $\beta_a$ of $9.23 \times 10^4$ calculated from Eq. (28) for this value of $\lambda_N$ is shown to be in good agreement with the experimental data, as is the slope from Eq. (39) at the end of the intermediate region, i.e., at the outer yield surface.

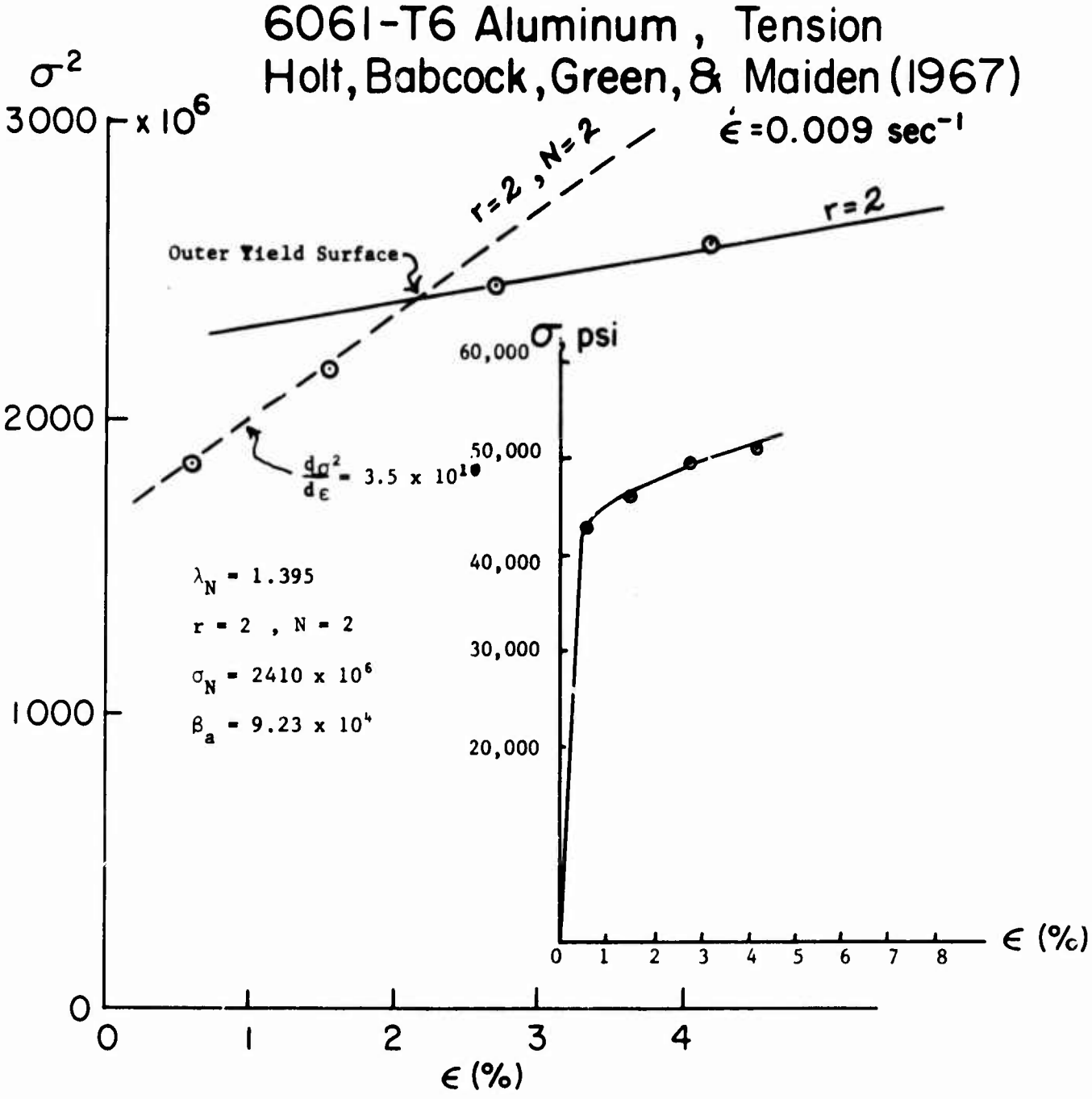
6061-T6 Aluminum, Tension
Holt, Babcock, Green, & Maiden (1967)
$\dot{\epsilon}$ = 0.009 sec$^{-1}$
$\sigma^2$
3000
x 10$^6$
2000
1000
0
r=2, N=2
r=2
Outer Yield Surface
$\frac{d\sigma^2}{d\epsilon}$ = 3.5 x 10$^{10}$
$\lambda_N$ = 1.395
r = 2 , N = 2
$\sigma_N$ = 2410 x 10$^6$
$\beta_a$ = 9.23 x 10$^4$
0 1 2 3 4
$\epsilon$ (%)
$\sigma$, psi
60,000
50,000
40,000
30,000
20,000
0 1 2 3 4 5 6 7 8
$\epsilon$ (%)

Fig. 13A

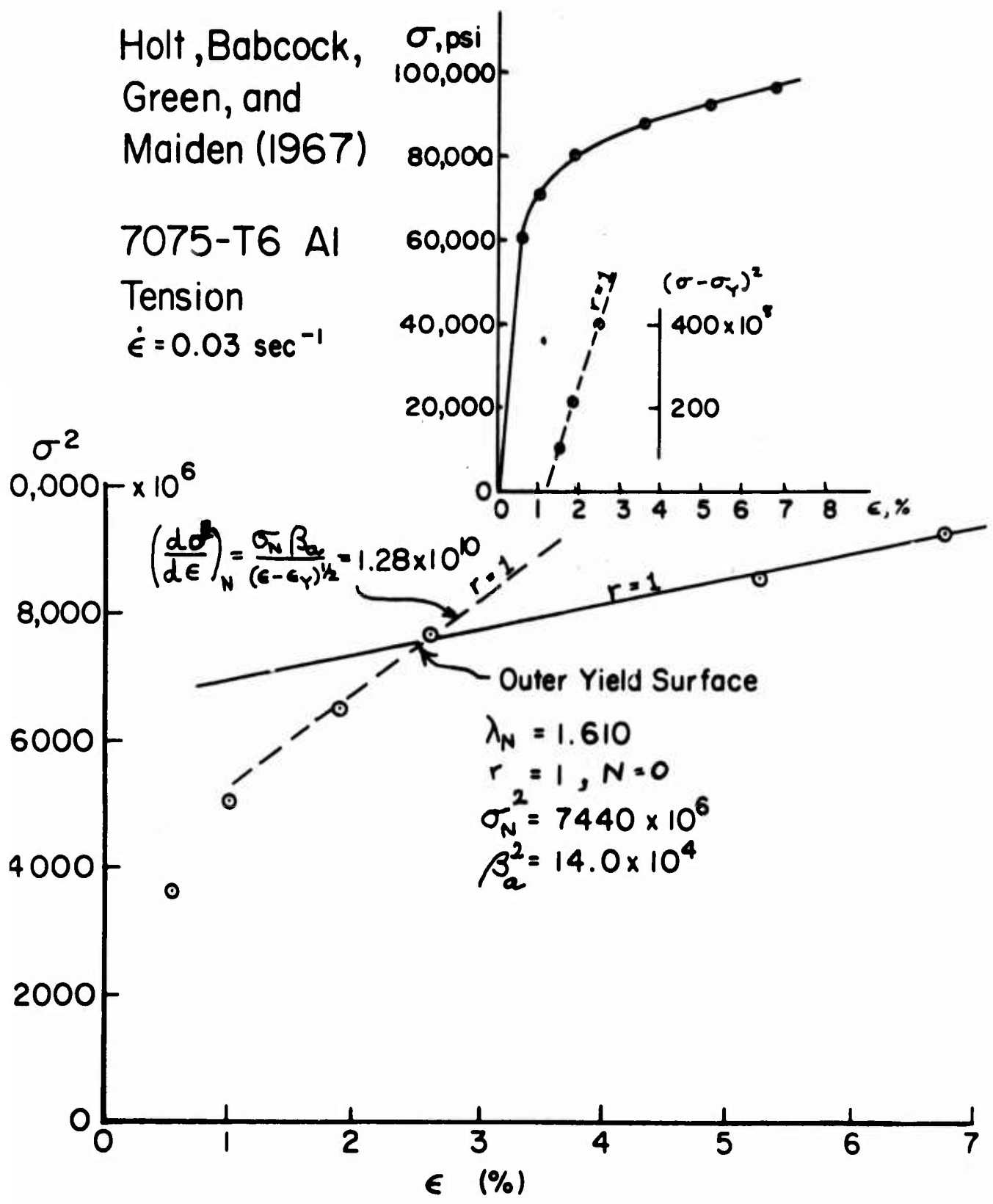
Holt, Babcock, Green, and Maiden (1967)
7075-T6 Al
Tension
$\dot{\epsilon} = 0.03\ sec^{-1}$
$\sigma$, psi
100,000
80,000
60,000
40,000
20,000
0
0 1 2 3 4 5 6 7 8 $\epsilon$, %
$(\sigma - \sigma_Y)^2$
$400 \times 10^6$
200
$\sigma^2$
0,000
$\times 10^6$
$\left(\frac{d\sigma^2}{d\epsilon}\right)_N = \frac{\sigma_N \beta_\alpha}{(\epsilon - \epsilon_Y)^{1/2}} = 1.28 \times 10^{10}$
r = 1
r = 1
8,000
6000
4000
2000
0
Outer Yield Surface
$\lambda_N = 1.610$
r = 1, N = 0
$\sigma_N^2 = 7440 \times 10^6$
$\beta_\alpha^2 = 14.0 \times 10^4$
0 1 2 3 4 5 6 7
$\epsilon$ (%)

Holt, et al. also provided tensile tests in 6061-O as well as 6061-T6 aluminum which I introduce here as Fig. 14a,b to illustrate that the value of N is indeed dependent upon the prior history of the specimen. In a $\sigma^2$ vs $\epsilon$ plot of their test in 6061-O aluminum a value of $r = 2$ is maintained, but from a measured $\sigma_N^2 = 276 \times 10^6$ the value of $\lambda_N$ is $\lambda_N = 1.076$ which is precisely the value from Table II for $N = 10$. Their test in 6061-T6, on the other hand, provided a value of $\sigma_N^2 = 2410 \times 10^6$ for $r = 2$, with the measured $\lambda_N = 1.395$ close to the predicted $\lambda_N = 1.385$ which is standard for the hardened alloy. Once again, the predicted and the measured slopes at the end of the intermediate region, as determined from Eq. (39), are in close agreement.

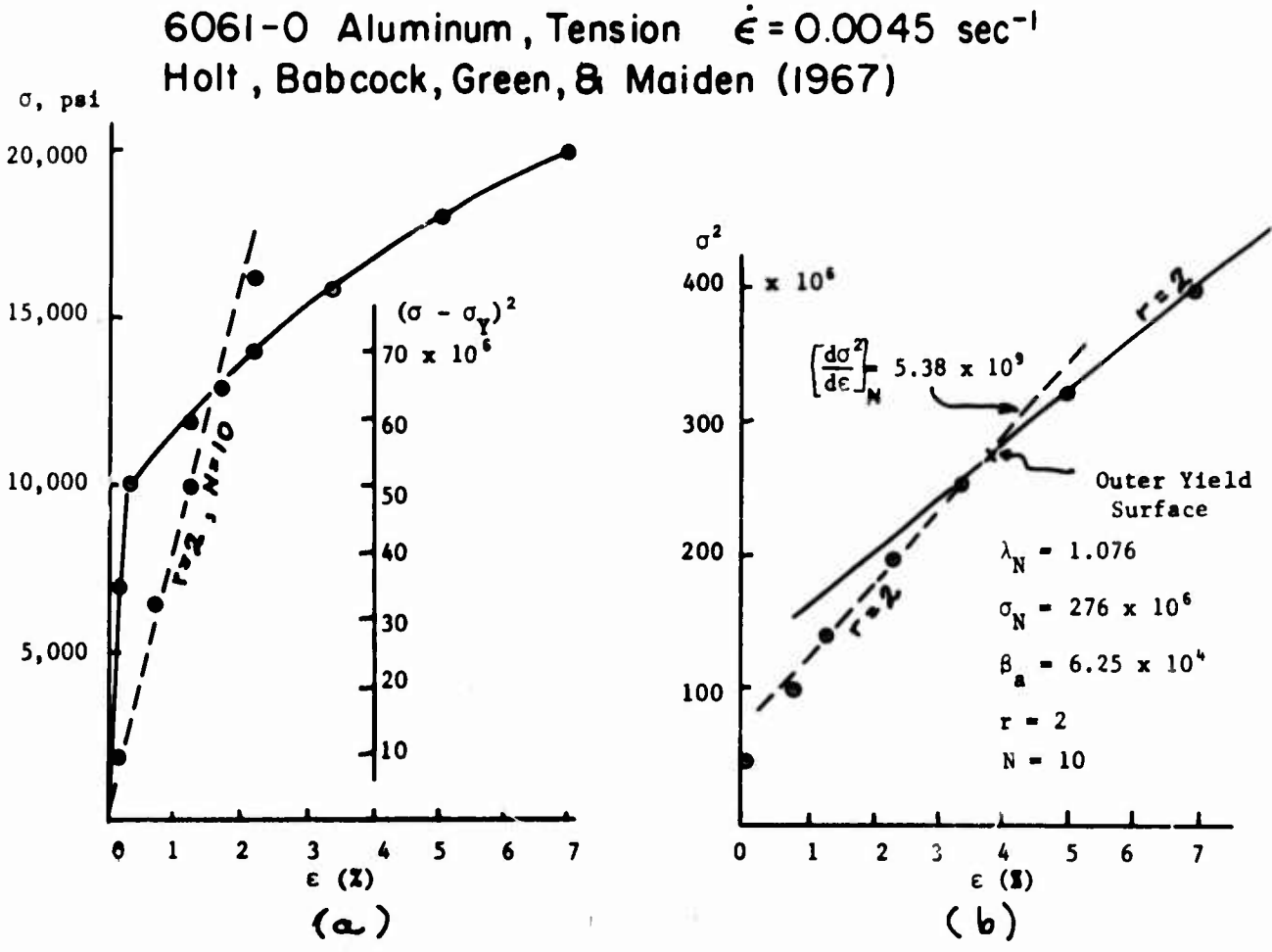


Fig. 14 a,b

For the stable material, an alternate example of this dependence of the critical strain upon the prior history of the specimen is shown in a test of mine in annealed 1095 steel, machined from the same rod as that of the quenched and tempered specimen shown in Fig. 8 above. From Fig. 15 one sees that the value of $N$ has changed from $N = 0$ to $N = 2$. The measured value of $\sigma_N^2 = 5214 \times 10^6$ provides $\lambda_N = 1.385$, which is precisely the value from Table II for $N = 2$. The mode index $r$ for 1095 steel in the annealed state has changed from $r = 4$ to $r = 6$. The same value of $r$ applies in both the intermediate region and the totally plastic region, as may be seen from the comparison of prediction and measurement from Eq. (39), i.e., $d\sigma^2/d\epsilon$, given as the dashed line in Fig. 15.

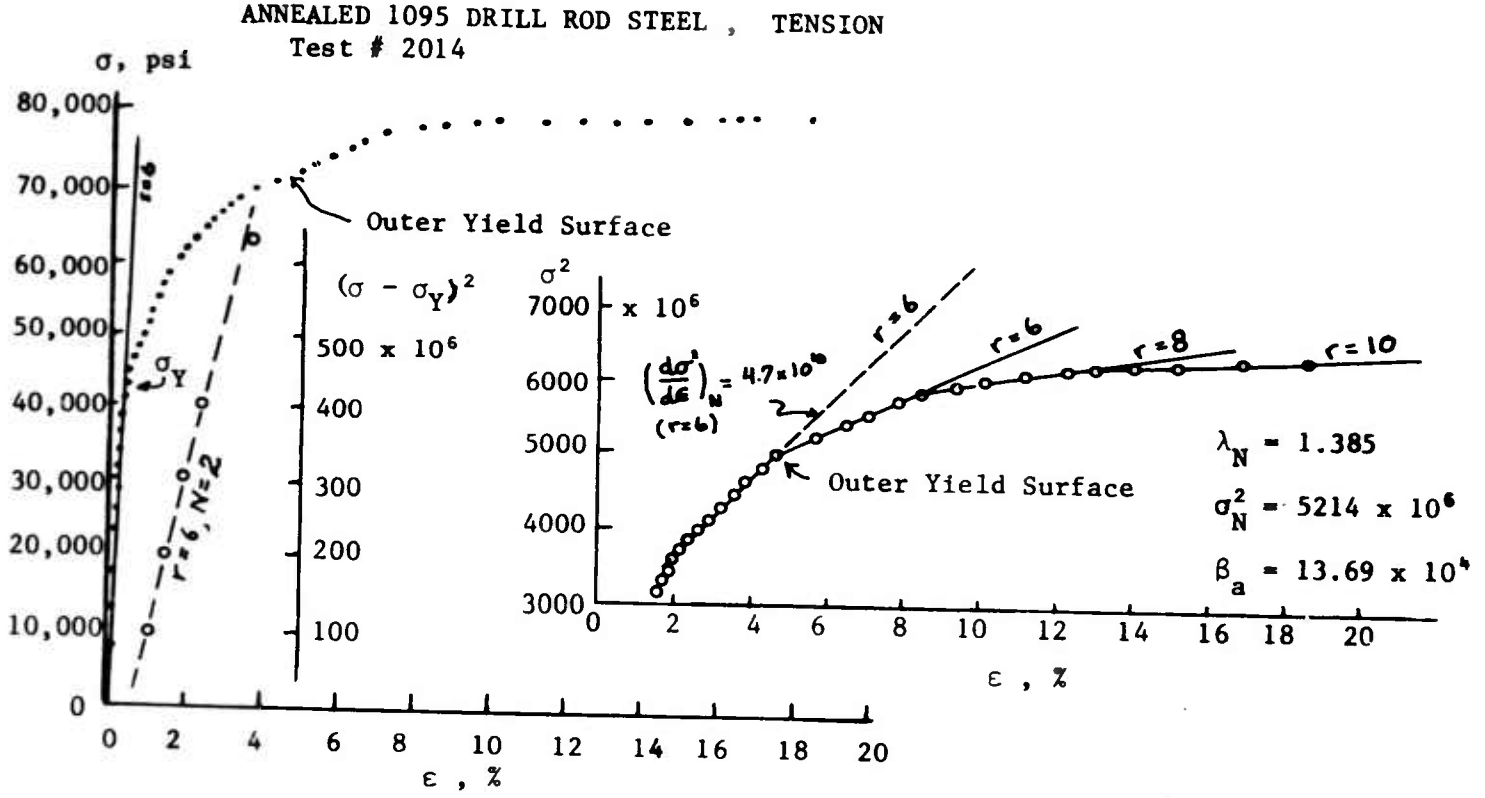
ANNEALED 1095 DRILL ROD STEEL , TENSION
Test # 2014
σ, psi
80,000
70,000
60,000
50,000
40,000
30,000
20,000
10,000
0
r=6
r=6, N=2
σY
Outer Yield Surface
(σ - σY)²
500 x 10⁶
400
300
200
100
0 2 4 6 8 10 12 14 16 18 20
ε , %
σ²
7000
x 10⁶
6000
5000
4000
3000
(dσ²/dε)N = 4.7x10⁶
(r=6)
r=6
r=6
r=8
r=10
Outer Yield Surface
λN = 1.385
σN² = 5214 x 10⁶
βa = 13.69 x 10⁴
0 2 4 6 8 10 12 14 16 18 20
ε , %

Fig. 15.

An experimental program is in progress to study these changes in the value of N associated with variations in the prior annealing history. For 1100F aluminum annealed at 1100°F and furnace cooled, the fully annealed aluminum which has been a standard in this laboratory for over 20 years, $\lambda_N = 1.000$. For 1100 H-14 aluminum, for which a great many measurements have been made in the as-received condition, $N = 8$, $r = 2$. By lowering the annealing temperature in successive stages, values of $N = 18$, $r = 2$; $N = 13$, $r = 2$; $N = 10$, $r = 1$; and $N = 10$, $r = 2$ have been obtained from the introduction of measured values into Eq. (38).

Torsion

Equations (25) through (29) provide for the simple torsion of thin-walled tubes for which $\sigma_z = \sigma_y = \sigma_x = 0$, $S \neq 0$, Equs. (40), (41), and (42).

$$S = S_Y + \lambda_N^{3/2} \bar{n}^{3/2} \beta_s (\sigma - \sigma_Y)^{1/2} \quad \text{where } \bar{n} = \frac{\bar{K}}{\sqrt{2}} \qquad (40)$$
$$S_Y \leq S \leq S_c$$

$$S = \lambda_N^{3/2} \bar{n}^{3/2} \beta_s \left(\sigma - \sigma_c + \frac{\sigma_N}{\lambda_N}\right)^{1/2} \quad \text{and} \quad \frac{\bar{m}}{\bar{n}} = \sqrt{3} \qquad (41)$$
$$\sigma \geq \sigma_c$$

$$S_N = \lambda_N \bar{n}^{3/2} \beta_s \sigma_N^{1/2} \qquad \sigma = \sigma_c \qquad (42)$$

Eq. (29) which gave in generalized stress and strain the slope at the end of the intermediate elastic-plastic region, i.e., at the outer yield surface, becomes for simple torsion, Eq. (43). The parabola coefficient $\beta_a$ for simple torsion is the same as that in Eq. (28) except that the value of $\beta$ becomes $\beta = (\bar{n})^{3/2} \beta_s$.

$$\left(\frac{dS^2}{d\sigma}\right)_N = \frac{S_N \beta_a}{(\sigma - \sigma_Y)^{1/2}} \qquad (43)$$

The apparatus for the experiments on the torsion of thin-walled tubes was designed to permit dead weight loading, in which the shear stress rate from zero strain to failure was constant during a given test.

In Fig. 16 a,b,c is shown a simple torsion test in 6061-T6 aluminum for which $\lambda_N$ calculated from measured $S_N$ and measured $\beta_a$ in Eqs. (28) and (42) has the value $\lambda_N = 1.374$. This value is very close to prediction, i.e., 1.385, as given in Table II. It is, of course, the same value of $\lambda_N$ obtained for this material in the tension tests: $N = 2$, $r = 2$.

Fig. 16 a,b,c

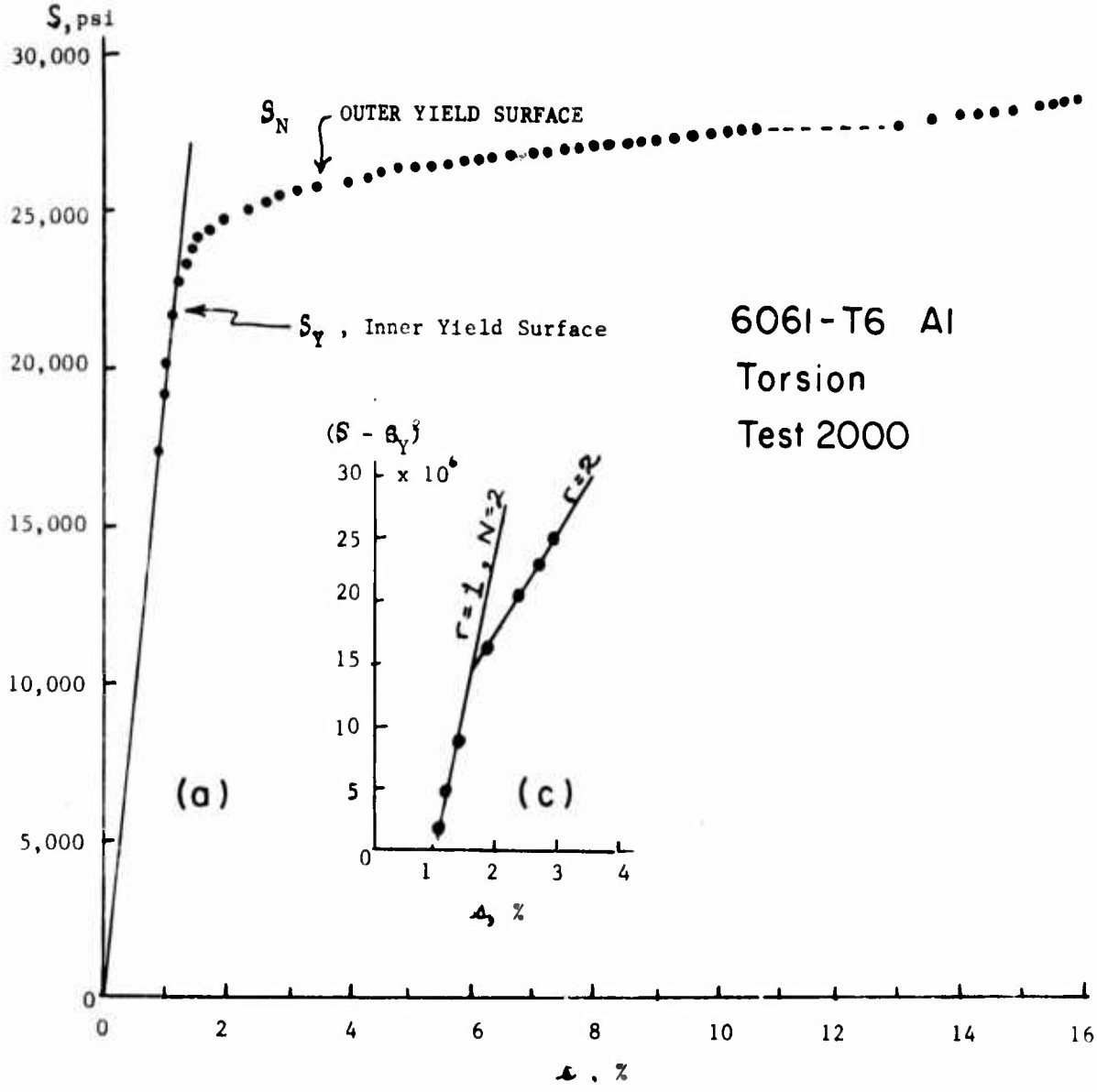
S, psi
30,000
25,000
20,000
15,000
10,000
5,000
0
$S_N$
OUTER YIELD SURFACE
$S_Y$ , Inner Yield Surface
6061-T6 Al
Torsion
Test 2000
(a)
$(S - S_Y)^2$
x $10^6$
r=1, N=2
r=2
(c)
$\epsilon_p$ %
0 2 4 6 8 10 12 14 16
$\epsilon$ , %

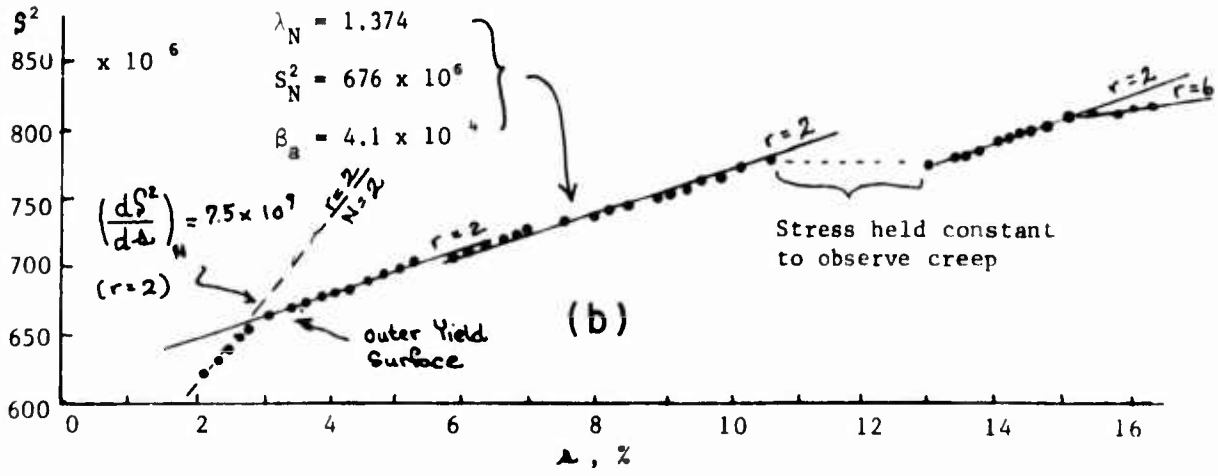
$S^2$
x $10^6$
850
800
750
700
650
600
$\lambda_N$ = 1.374
$S_N^2$ = 676 x $10^6$
$\beta_a$ = 4.1 x $10^4$
$\left(\frac{dS^2}{d\epsilon}\right)_N$ = 7.5 x $10^7$
(r=2)
r=2
r=6
Stress held constant
to observe creep
outer Yield
Surface
(b)
0 2 4 6 8 10 12 14 16
$\epsilon$ , %

In the $S^2$ vs $\Delta$ plot of Fig. 16b we see not only that there is a correlation with the straight line of the predicted parabola, but also that the slope (dashed line) at the end of the intermediate elastic-plastic region is in close agreement with prediction from Eq. (43), with $r = 2$ .

Fig. 16c is an $(S - S_Y)^2$ vs $\Delta$ plot in which the solid line shown is the predicted parabola from Eq. (40) for $\lambda_N = 1.374$ and $r = 2$ .

The test of Fig. 17 a,b,c, is included to show a not uncommon occurrence in such tests when a failure either in rupture or buckling occurs as the loading path reaches the outer yield surface. The predicted value of $\lambda_N$ for 2024-T3 aluminum is $N = 0$, i.e., $\lambda_N = 1.577$ from Table II. Using the predicted value, one obtains a value of $S_N$ at the point of failure, but with a slope from Eq. (43) at the end of the elastic-plastic region. Here, too, there is a close correlation between prediction and measurement. However, as may be seen from the $(S - S_Y)^2$ vs s plot of Fig. 17c, in this instance the mode index also is $r = 2$ . This is the mode index which was used in Eq. (43) in the comparison of slopes in Fig. 17b.

Fig. 17 a,b,c

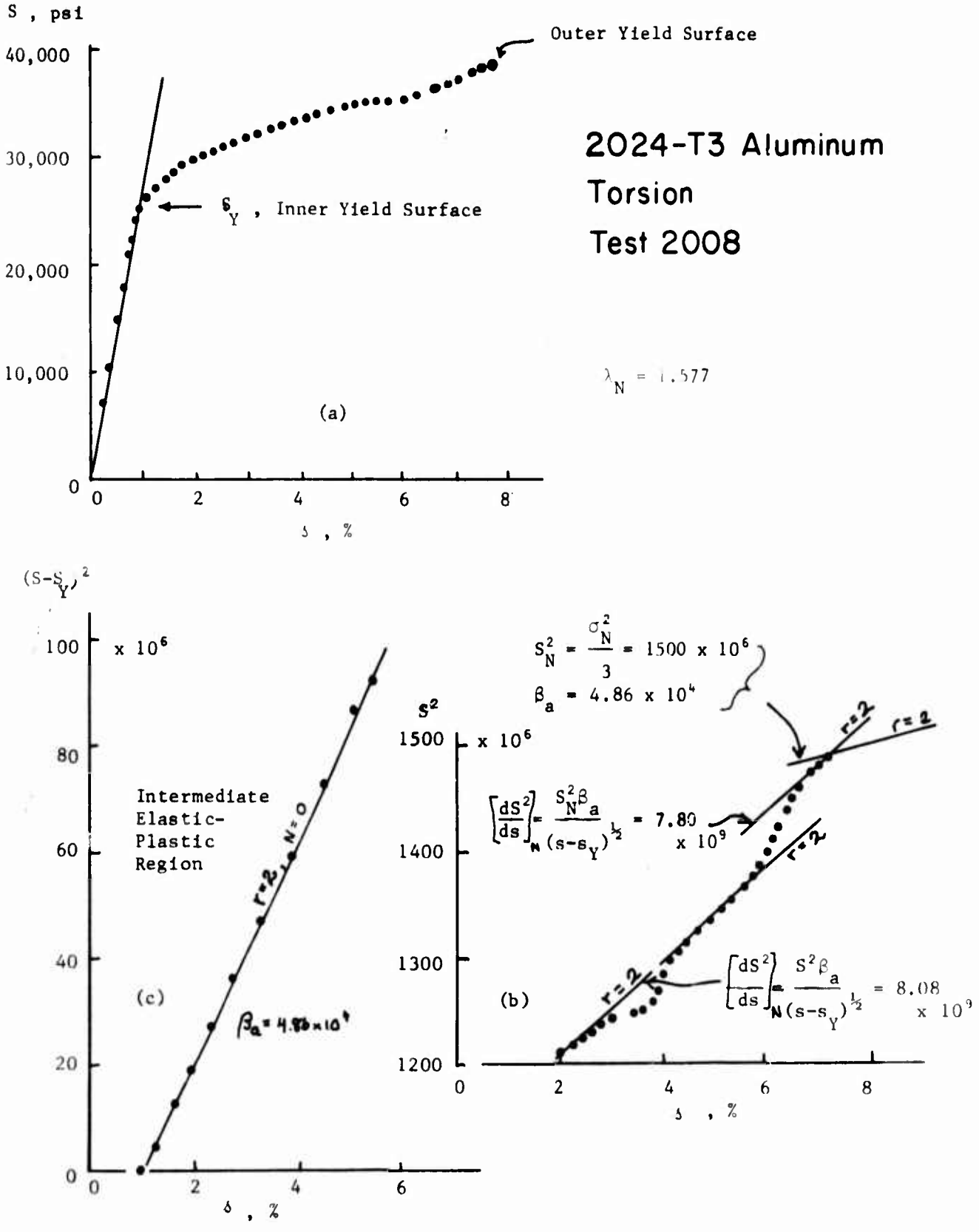
S , psi
40,000
30,000
20,000
10,000
0
Outer Yield Surface
$S_Y$ , Inner Yield Surface
(a)
0
2
4
6
8
δ , %
2024-T3 Aluminum
Torsion
Test 2008
$\lambda_N$ = 1.577
$(S-S_Y)^2$
100
x 10^6
80
60
40
20
0
Intermediate
Elastic-
Plastic
Region
r=2, N=0
(c)
$\beta_a$ = 4.86 x 10^4
0
2
4
6
δ , %
$S^2$
1500
x 10^6
1400
1300
1200
$S_N^2 = \frac{\sigma_N^2}{3}$ = 1500 x 10^6
$\beta_a$ = 4.86 x 10^4
r=2
r=2
$\left[\frac{dS^2}{ds}\right]_N = \frac{S_N^2 \beta_a}{(s-s_Y)^{1/2}}$ = 7.80 x 10^9
r=2
r=2
(b)
$\left[\frac{dS^2}{ds}\right]_N = \frac{S^2 \beta_a}{(s-s_Y)^{1/2}}$ = 8.08 x 10^9
0
2
4
6
8
δ , %

In Fig. 18 a,b,c, is shown a simple torsion test in 1100-H14 aluminum for which $\lambda_N = 1.105$, a little below the predicted value of $\lambda_{II} = 1.114$. Here, too, the torsion data provide the same N = 8, r = 2 as for the tension tests.

Like several of the tests shown above, we see here that when the strain in the totally plastic region proceeds sufficiently far, then second-order transitions occur, similar to those found in the fully annealed metal.

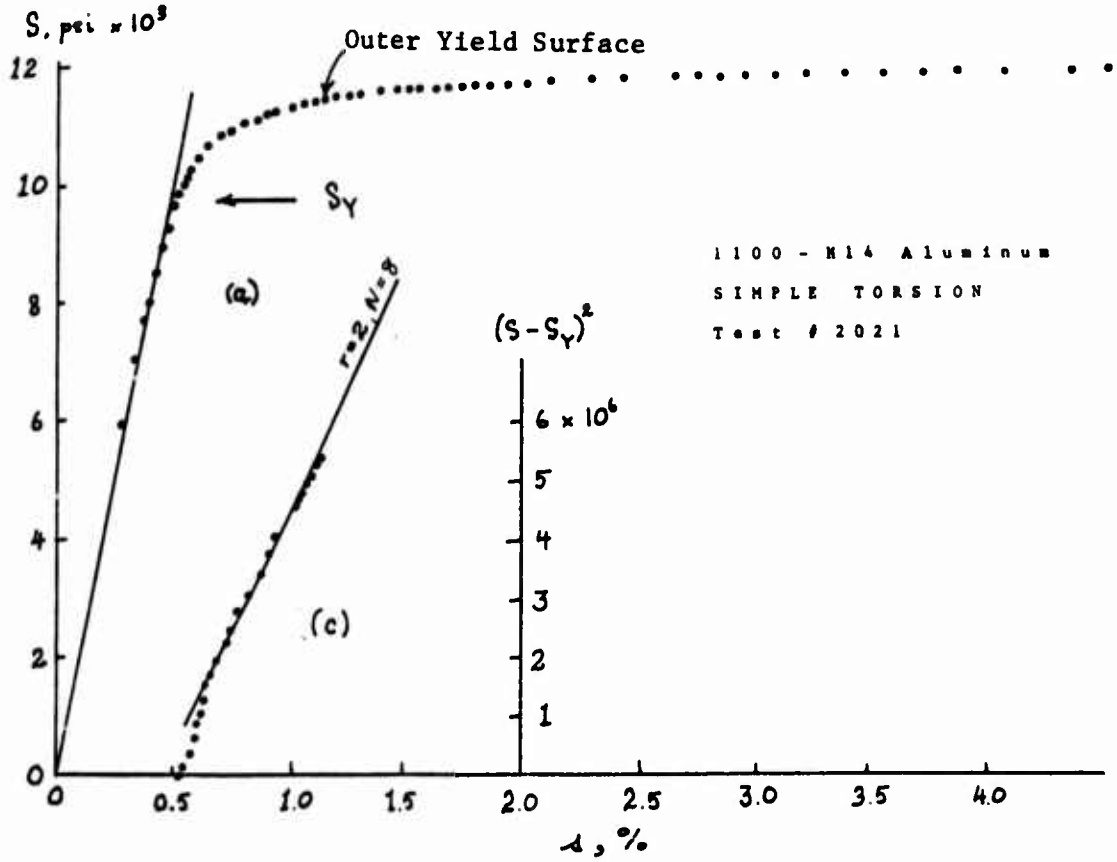


Fig. 18 (a) and (c)

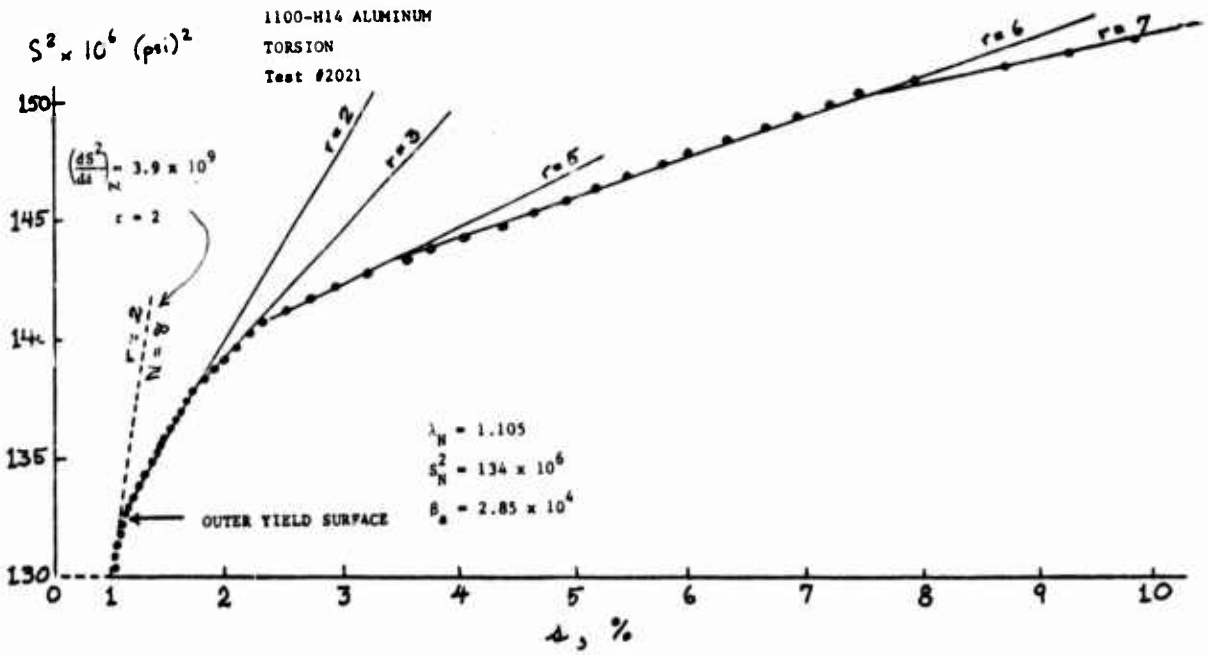
1100-H14 ALUMINUM
TORSION
Test #2021
$S^2 \times 10^6$ (psi)$^2$
150
145
140
135
130
0
1
2
3
4
5
6
7
8
9
10
$\varepsilon_3$ %
$\left(\frac{dS^2}{d\varepsilon}\right)_N = 3.9 \times 10^9$
r = 2
r=2
r=3
r=5
r=6
r=7
OUTER YIELD SURFACE
$\lambda_N = 1.105$
$S_N^2 = 134 \times 10^6$
$\beta_a = 2.85 \times 10^4$

Fig 18 (b)

Just as with the tensile data, I have included a torsion test of another investigator, namely Nicholas and Garey[23] who published data in 1969 on 7075-T6 aluminum. For 7075-T6, which is the highest strength aluminum alloy we have, $N = 0$, $r = 1$, as was indicated from the tensile data. That the same value is found in the torsion tests of yet another group of investigators is a further demonstration that these are indeed material parameters. The correlation with Eqs. (40), (41), (42), and (43) for a measured $\lambda_{II} = 1.555$ and $r = 1$ are shown in Fig. 19 a,b,c. The predicted value of $\lambda_{II}$ for $N = 0$ is 1.577.

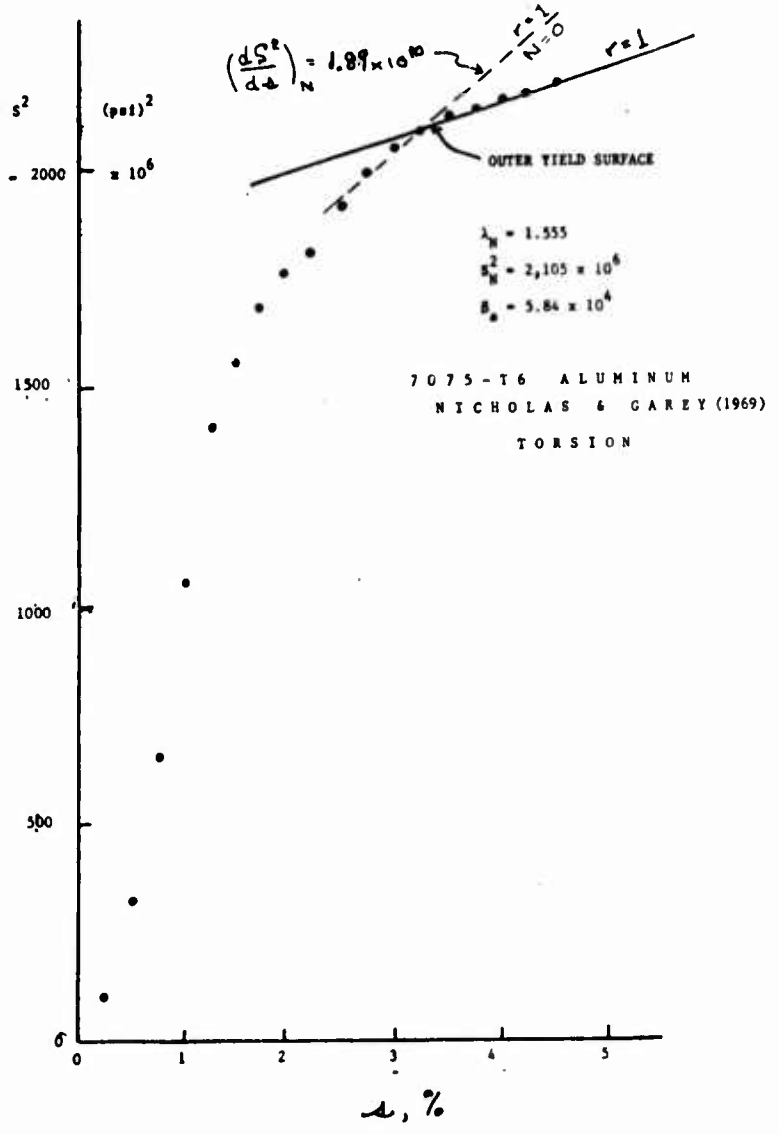


Fig. 19 (b)

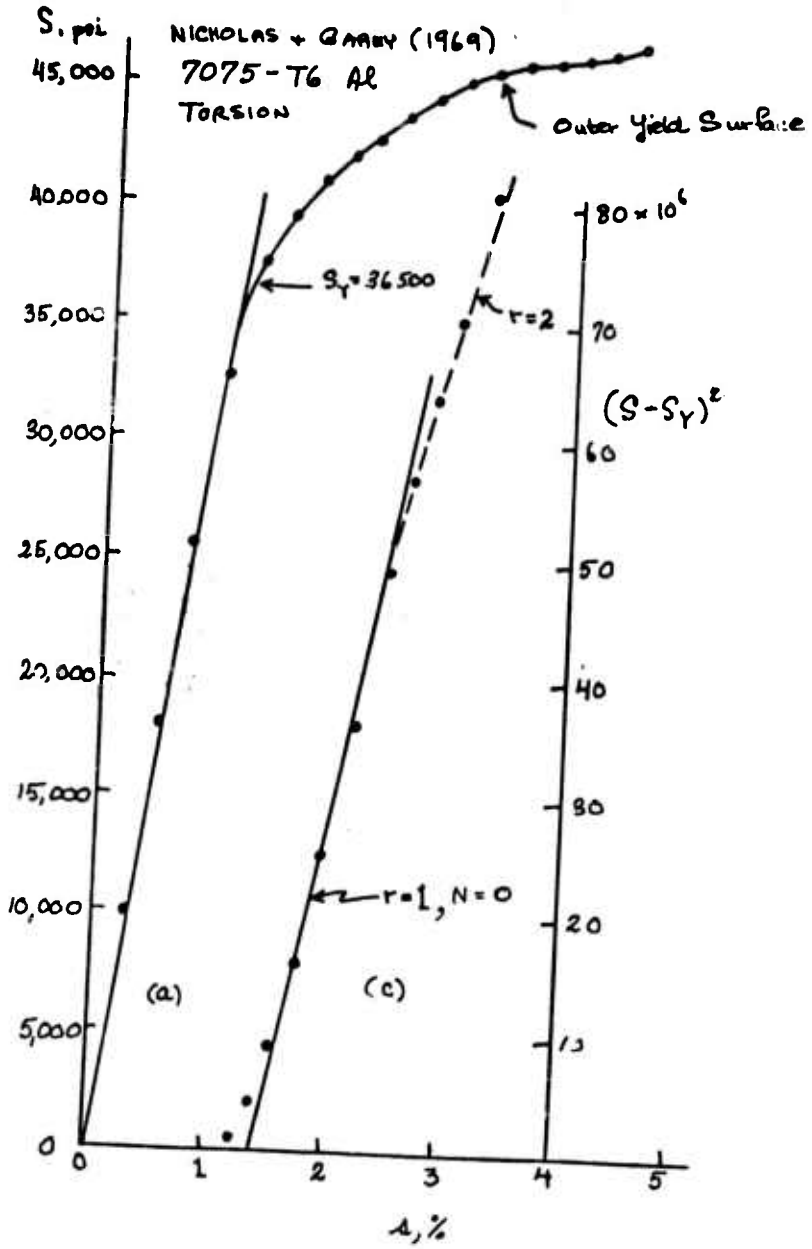
S, psi
NICHOLAS + GARNEY (1969)
7075-T6 Al
TORSION
Outer Yield Surface
45,000
40,000
35,000
30,000
25,000
20,000
15,000
10,000
5,000
0
$S_Y$ = 36,500
r=2
r=1, N=0
80 × 10^6
70
60
50
40
30
20
13
$(S-S_Y)^2$
(a)
(c)
0
1
2
3
4
5
Δ, %

Fig. 19 (a) and (c)

In Fig. 20 a,b,c is shown a test of T. Nicholas and J. D. Campbell[23] (1972) in HE15WP aluminum alloy, which in American nomenclature is 2014-T4 . For this torsion test, $\lambda_N = 1.400$ , which is slightly higher than the predicted value of 1.385 for $N = 2$ .

Despite the discontinuous deformation in both the intermediate and the totally plastic regions, this test, taken from the literature, demonstrates that still another structural metal alloy is in accord with the present generalization.

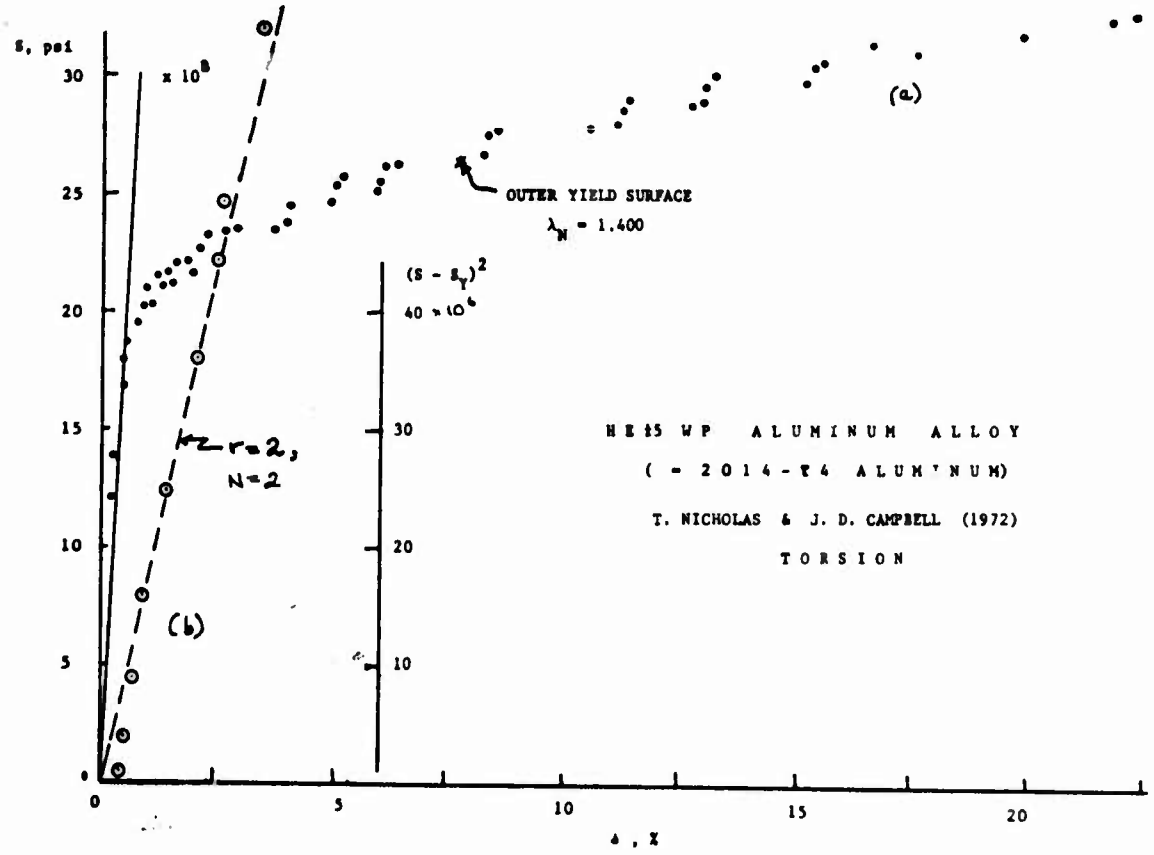


Fig 20 (a) and (c)

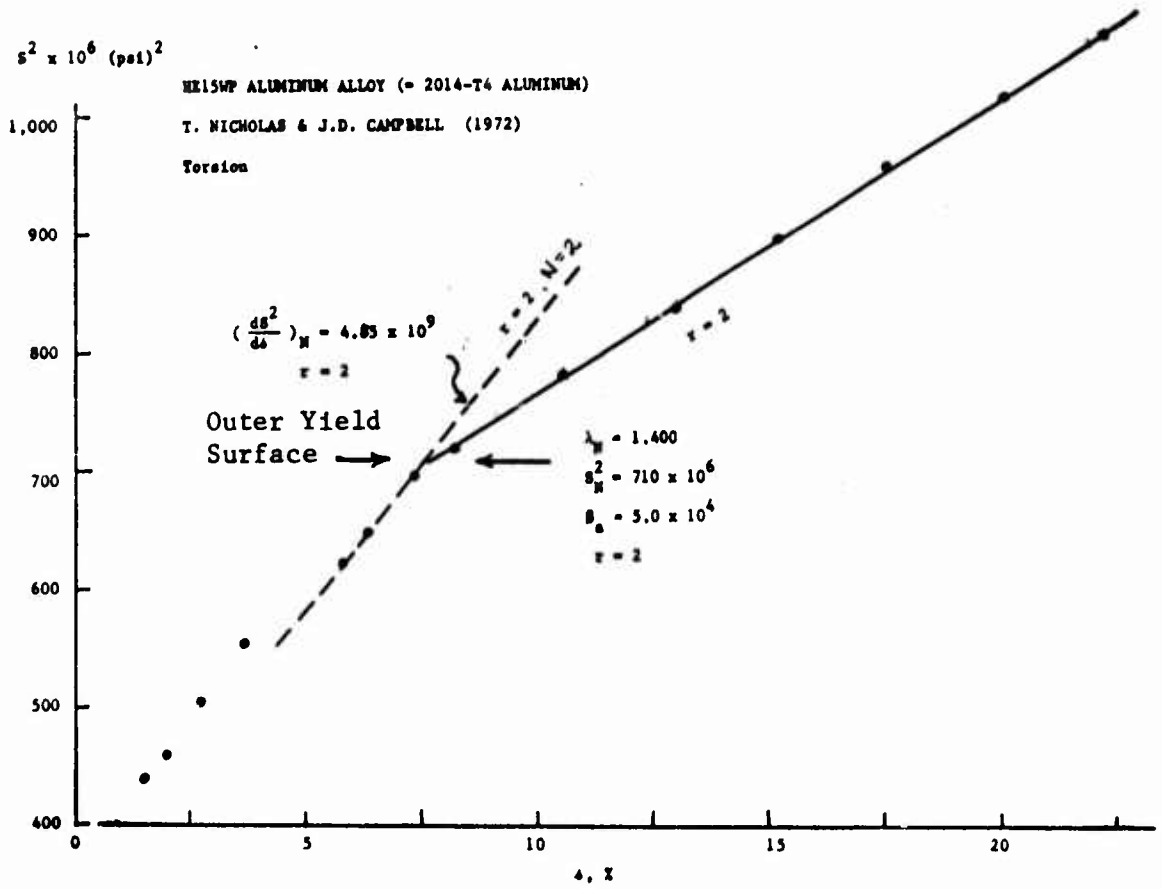
$s^2 \times 10^6$ (psi)$^2$
HE15WP ALUMINUM ALLOY (≈ 2014-T4 ALUMINUM)
T. NICHOLAS & J.D. CAMPBELL (1972)
Torsion
1,000
900
800
700
600
500
400
0
5
10
15
20
ε, %
$(\frac{ds^2}{d\epsilon})_M = 4.85 \times 10^9$
r = 2
r = 2 ; N=2
r = 2
Outer Yield Surface
$\lambda_M = 1.400$
$s^2_M = 710 \times 10^6$
$\epsilon_a = 5.0 \times 10^{-4}$
r = 2

Fig. 20 (b)

Fig. 21 a,b,c, shows a torsion test on a hard copper thin-walled tube for which the comparisons in each figure are similar to those given above, and for which a similar correlation between prediction and experiment is found. The calculated $\lambda_N = 1.382$ is almost precisely the predicted value of $N = 2$, $\lambda_N = 1.385$. In this test we also see second-order transitions occurring in the totally plastic region beyond the outer yield surface.

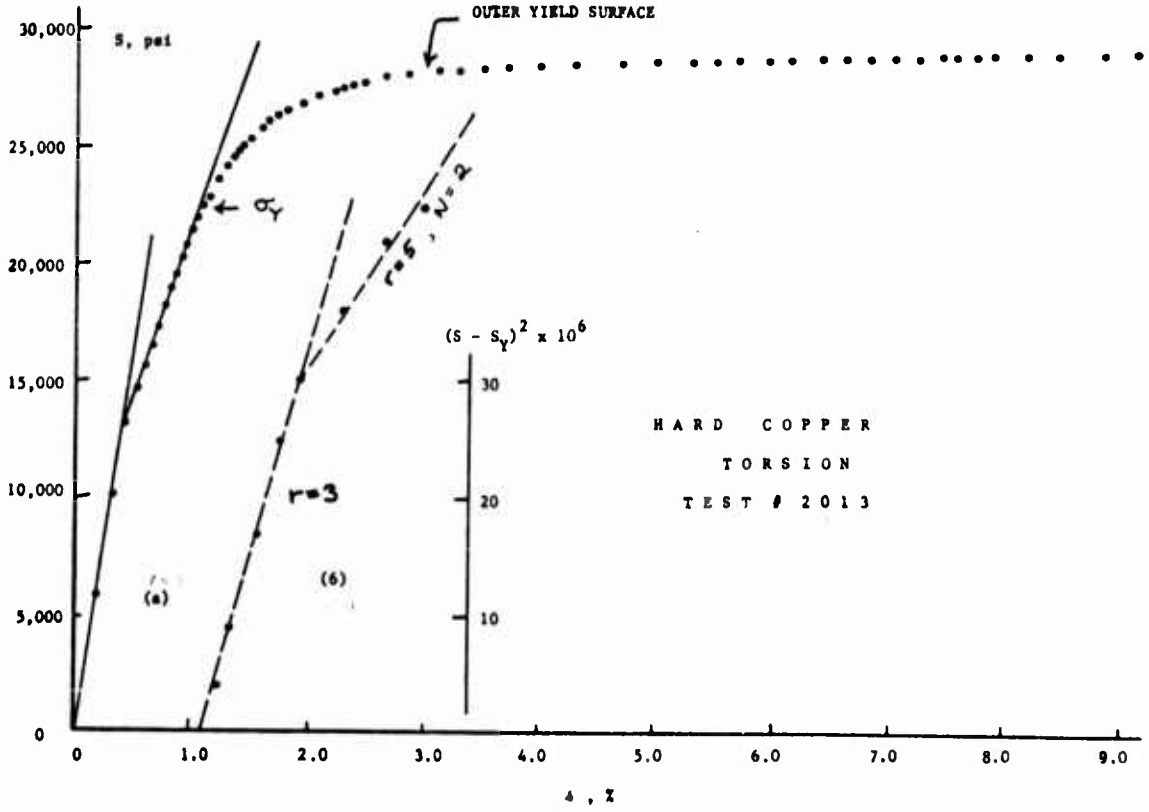


Fig 21 (a) and (c)

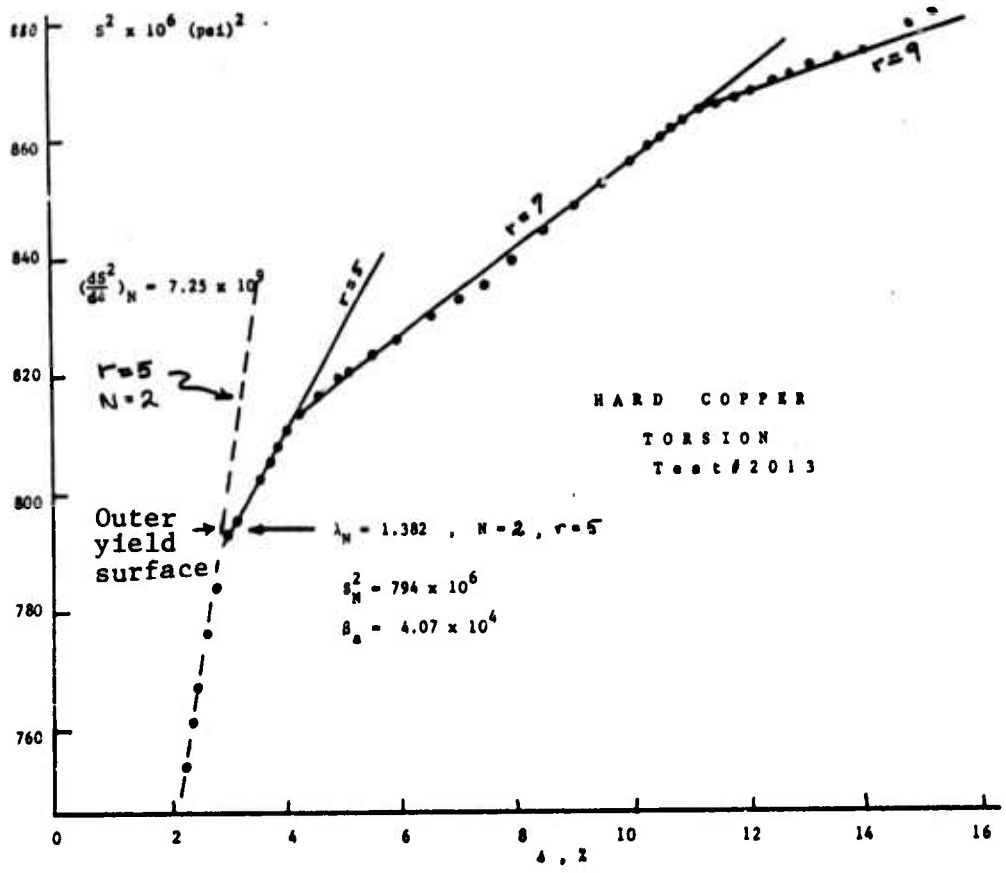
$s^2 \times 10^6$ (psi)$^2$
880
860
840
820
800
780
760
$(\frac{ds^2}{d\epsilon})_N = 7.25 \times 10^9$
r=5
N=2
r=7
r=9
HARD COPPER
TORSION
Test #2013
Outer yield surface
$\lambda_N = 1.382$ , N=2 , r=5
$s_N^2 = 794 \times 10^6$
$\beta_a = 4.07 \times 10^4$
0
2
4
6
8
10
12
14
16
$\epsilon$, %

Fig. 21 (b)

## Proportional Loading

A signal feature of the torsion-tension dead weight loading apparatus used in my laboratory is that the tension and torsion components are decoupled. In my Handbuch der Physik volume on "The Experimental Foundations of Solid Mechanics,"[8] I have fully delineated the advantages of dead weight testing machines in experimental studies of this type. One important reason for the superiority of a soft testing machine is that with the stress being specified and the strain being the measured quantity, the latter accommodates in terms of the discontinuous deformation, or steps, to wit, the Savart-Masson effect (usually labeled, with no historical justice, the "Portevin - le Chatelier effect").

In a combined loading test if one wishes to examine separately the different strain components of this stepped deformation, it is essential that the apparatus be decoupled, in the sense that when the specimen rotates in shear strain the tensile load is not required to rotate with it. Since in combined tension and torsion experiments, particularly for non-proportional loading, large amplitude steps are very commonly observed, as will be shown below, this decoupling is essential not only to obtain reproducibility but also to prohibit the limitations of the apparatus from altering the results obtained.

For combined loading in tension and torsion we refer to Eq. (25) for the intermediate elastic-plastic region; Eq. (26) for the totally plastic region; and Eqs. (27) and (28) to define the outer yield surface, i.e., to determine $\lambda_N$.

In contrast to simple loading, for which the equations for the loading surface and for the single response function coincide, in combined stress the generalized equations for the loading surface, Eqs. (25) and (26), must be considered simultaneously with the now separate constitutive equations, Eqs. (30) through (33).

To examine the applicability of these constitutive statements, either we may plot the individual stress components with respect to

their corresponding strain components, or we may consider the strain path in an $\epsilon$ vs $\sigma$ plot to compare with prediction in each of the two regions of deformation, in terms of Eqs. (30) through (34). A convenient method of measurement is to compare the direction of the strain increment vector, $d\epsilon/ds$, with prediction from Eq. (34) in the totally plastic region. For proportional loading, in which the strain increment vector has a constant slope, both Eqs. (34) and (35) are equivalent, and we may write Eq. (44).

$$\frac{\epsilon}{\sigma} = \frac{\sigma}{3S} \tag{44}$$

In Fig. 22 a,b,c, is shown a proportional loading test in 6061-T6 aluminum for which the ratio of the constant rate proportional loading was $\dot{\sigma}/\dot{S} = 2.931$. The plots are similar to those described above.

Fig. 22a shows a plot in generalized stress and strain. In Fig. 22b, for a $T^2$ vs $\Gamma$ plot we see the beginning of total plasticity at the outer yield surface, for a calculated value of $\lambda_{II} = 1.338$, 3% below the predicted value of 1.385. We note that the solid line for the predicted slope of $\rho_a$ for this value of $\lambda_{II}$ and $r = 2$, and the $T^2$ vs $\Gamma$ plot (dashed line) of the end of the intermediate elastic-plastic region, Eq. (29), are indeed in agreement with observation. In this instance, we add an additional figure, 22d, which is an $\epsilon$ vs $\sigma$ plot of the experimental data from zero strain to rupture.

As was anticipated, the slope is constant, and we see from the solid line that it is in almost precise agreement with the predicted strain increment vector from Eq. (44) from the known ratio of $\sigma/S$.

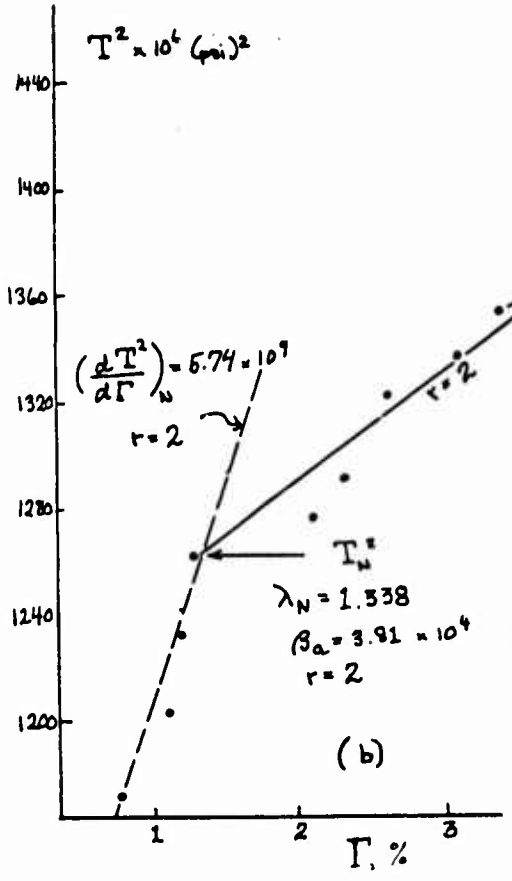


Fig 22 (b)

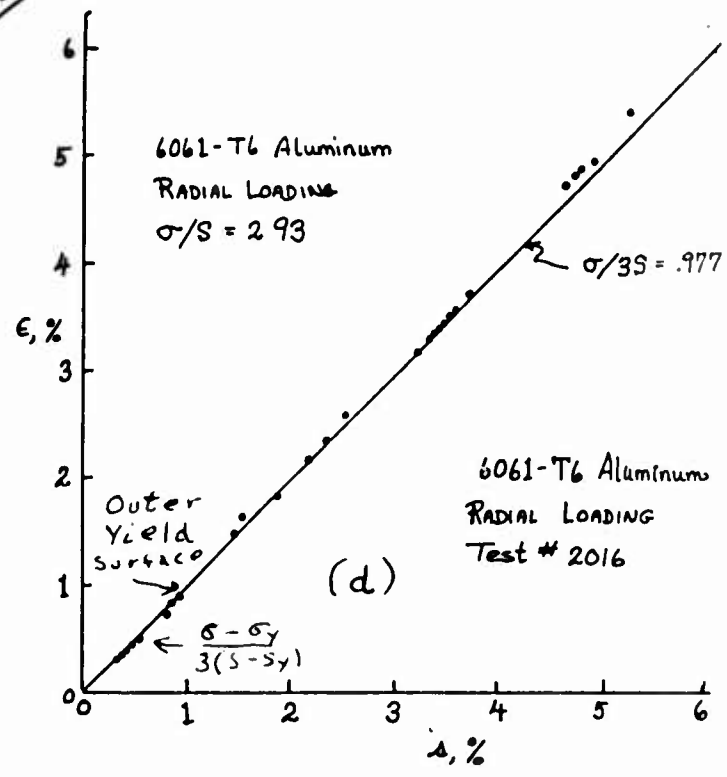


Fig 22(d) T

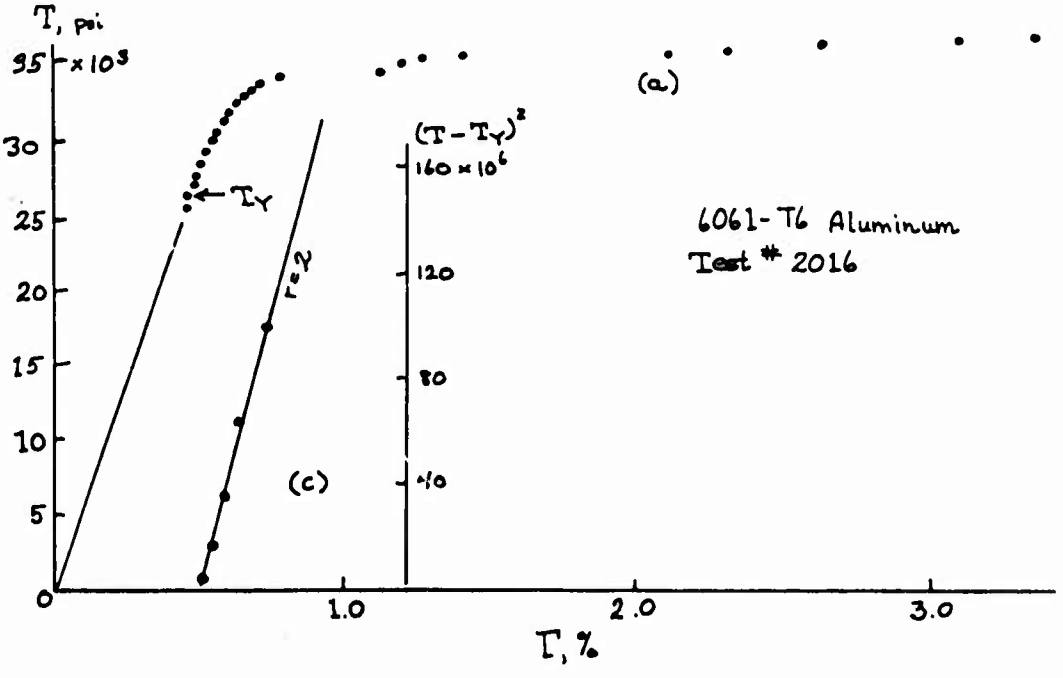




Fig 22 (a) and (c)

In Fig. 23 a,b,c, are shown the results for a proportional or radial test in 2024-T3 aluminum alloy for which the constant stress ratio $\dot{\sigma} / \dot{S} = 2.89$ or approximately the same as that of the 6061-T6 metal alloy of Fig. 22.

From the $T$ vs $\Gamma$ plot of Fig. 23a we see the appearance of steps in both the intermediate and the totally plastic region. This is even more evident in the $T^2$ vs $\Gamma$ plot of Fig. 23b.

We note that, as in the fully annealed metal, when steps do occur they depart from and return to the parabolic response function. We thus may determine a $T_N$ and a $\beta_a$ which in this instance provides a value of $\lambda_N = 1.531$, a little less than 3% below the predicted $\lambda_N = 1.577$. The solid line for the predicted value of $\beta_a$ is shown at the foot of the steps in the totally plastic region. Also in Fig. 23a is a $(T - T_Y)^2$ vs $\Gamma$ plot which provides an $r = 2$ response. The $(dT^2/d\Gamma)_N$ slope at the end of the intermediate region is also in agreement.

In Fig. 23c is an $\epsilon$ vs $s$ plot where, once again, the ratio of the measured strains are in close accord with the predicted slope (solid line) Eq. (44) for the known value of $\dot{\sigma} / \dot{S} = 2.892$.

In Fig. 24 a,b,c,d are shown a similar comparison for 1100-H14 aluminum alloy for which the measured value of $\lambda_N$ from the observed $T_N$ and $\beta_a$ is precisely the predicted value $\lambda_N = 1.114$.

In Fig. 24d we see that for a constant loading ratio of $\dot{\sigma} / \dot{S} = 2.73$, the predicted slope and the calculated slope in the $\epsilon$ vs $s$ plot are in close agreement both in the intermediate and in the totally plastic region, except for the initial linear elastic portion for which, of course, Eq. (44) does not apply.

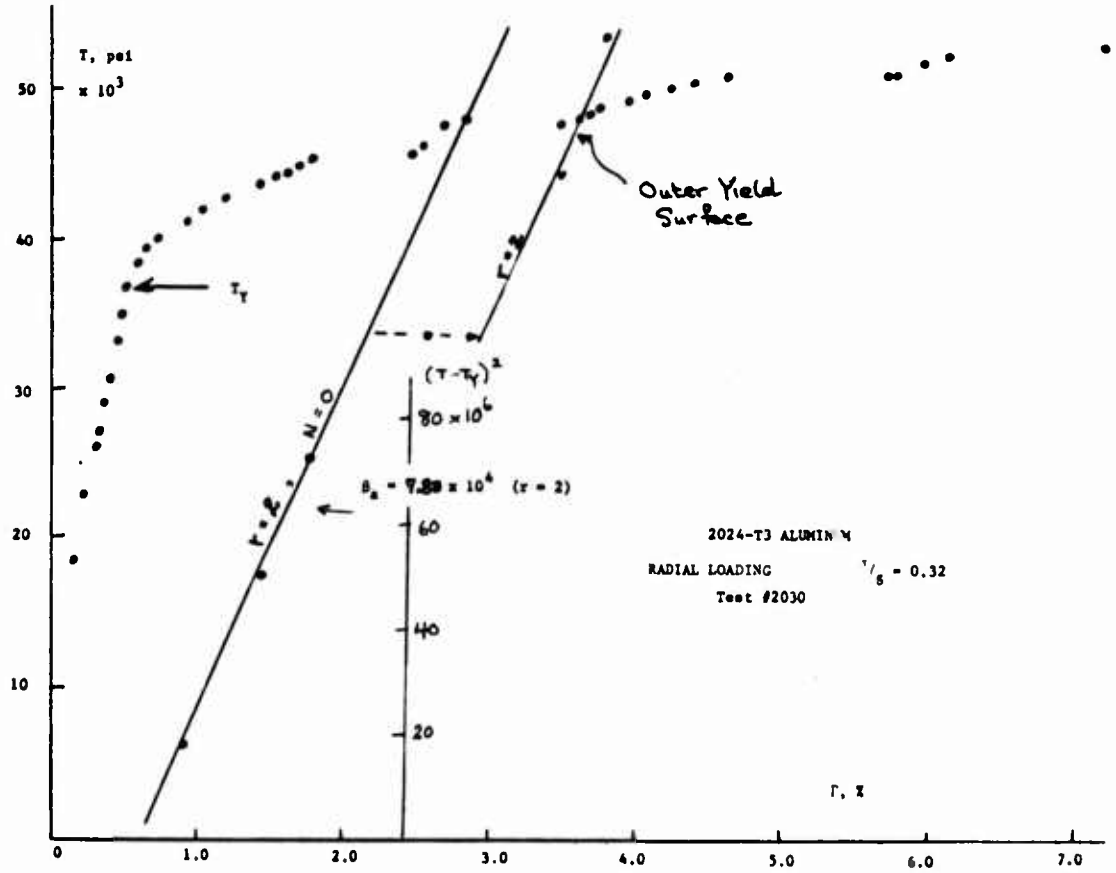


Fig 23 (a)

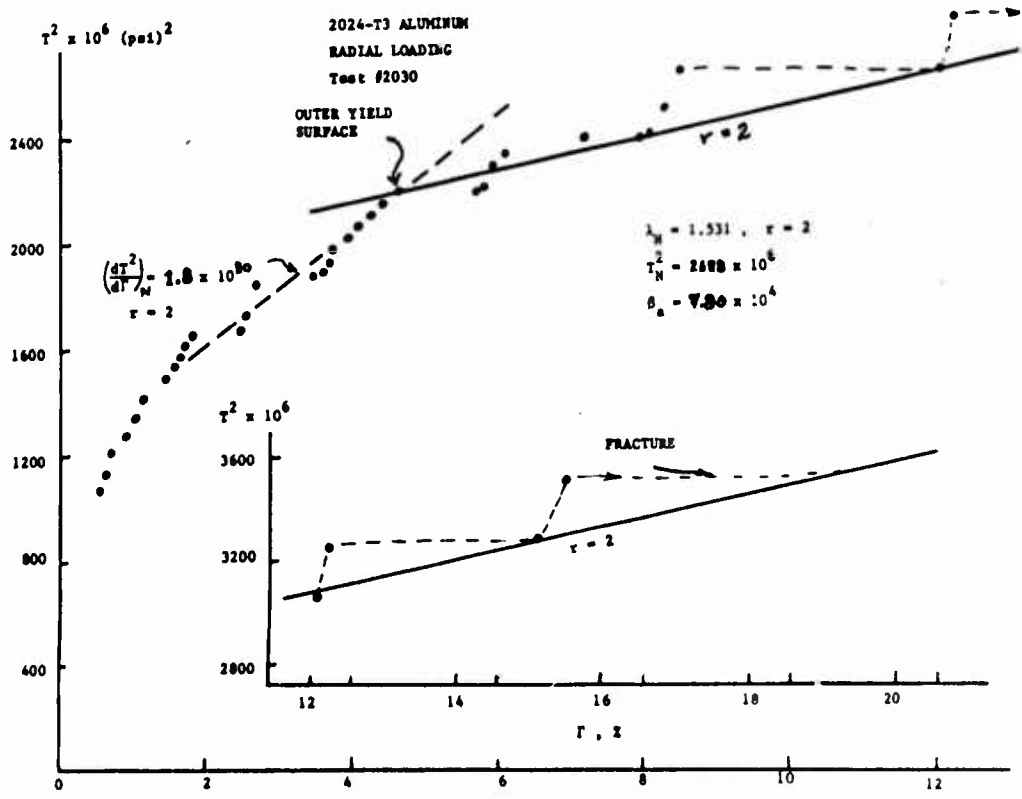




Fig 23 (b)

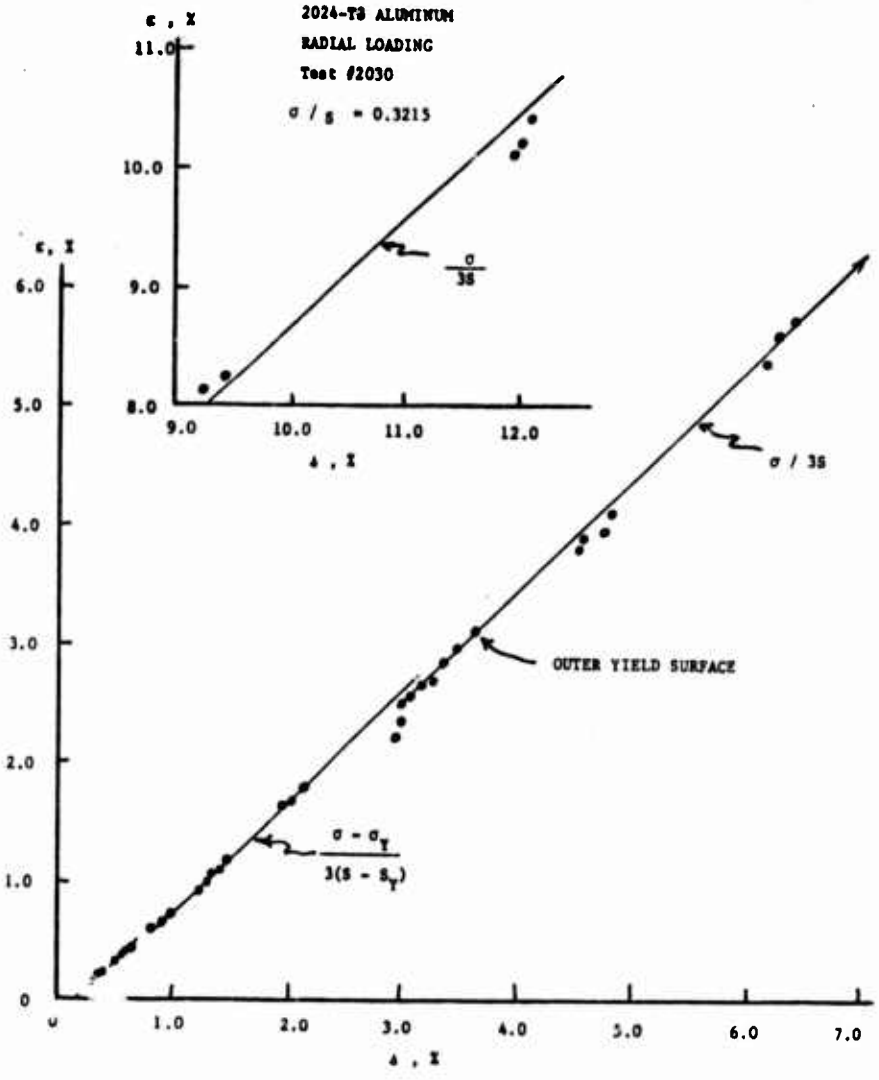
2024-T3 ALUMINUM
RADIAL LOADING
Test #2030
σ / s = 0.3215
ε , %
11.0
10.0
9.0
8.0
9.0
10.0
11.0
12.0
Δ , %
σ / 3s
ε, %
6.0
5.0
4.0
3.0
2.0
1.0
0
1.0
2.0
3.0
4.0
5.0
6.0
7.0
Δ , %
σ / 3s
OUTER YIELD SURFACE
σ - σ_Y / 3(s - s_Y)

Fig. 23 (c)

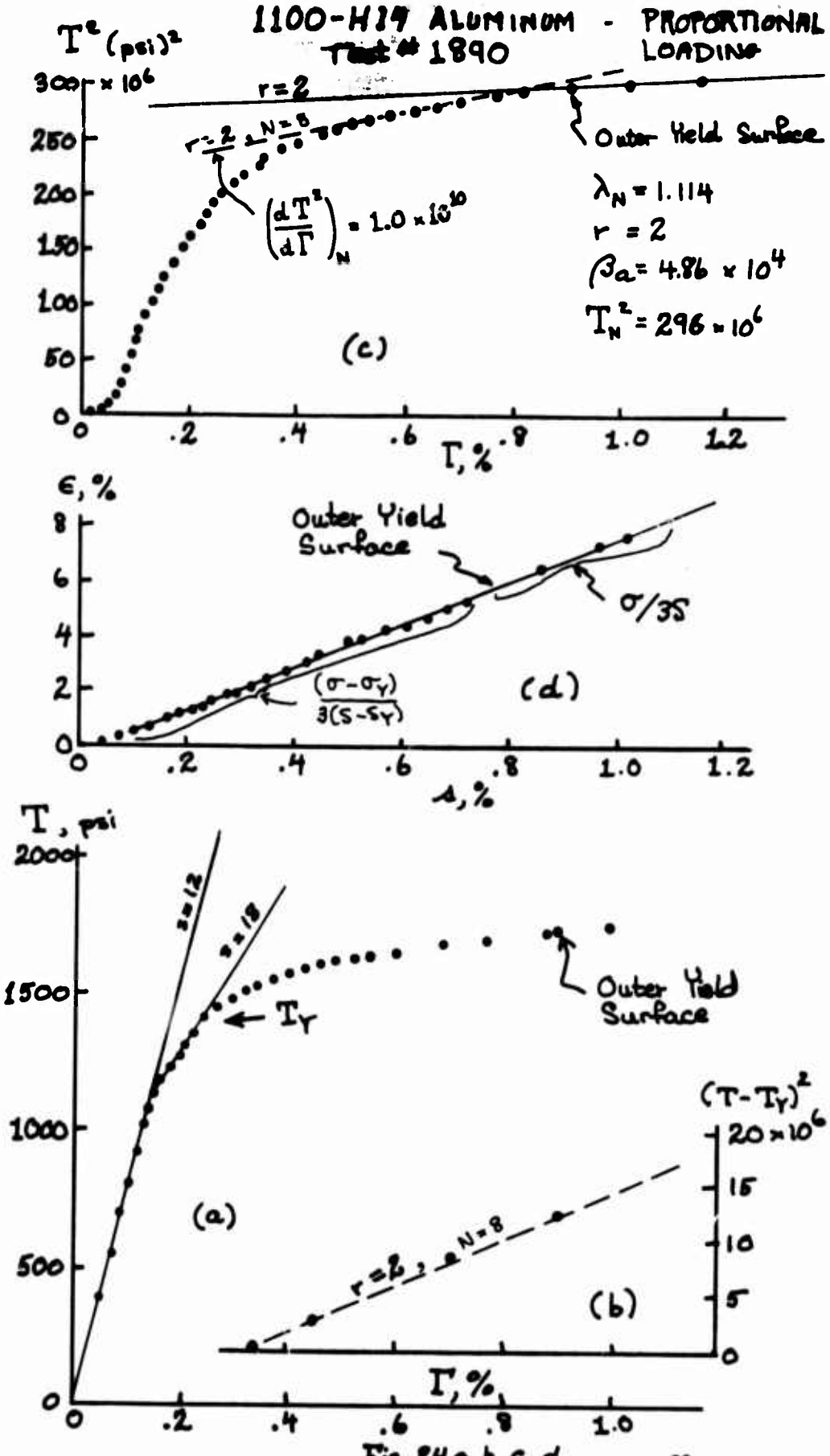
1100-H14 ALUMINUM - PROPORTIONAL LOADING
Test # 1890
$T^2$ (psi)$^2$
$\times 10^6$
r = 2
r = 2, N = 8
Outer Yield Surface
$\left(\frac{dT^2}{d\Gamma}\right)_N = 1.0 \times 10^{10}$
$\lambda_N = 1.114$
r = 2
$\beta_a = 4.86 \times 10^4$
$T_N^2 = 296 \times 10^6$
(c)
$\Gamma$, %
$\epsilon$, %
Outer Yield Surface
$\sigma/35$
$\frac{(\sigma-\sigma_Y)}{3(S-S_Y)}$
(d)
s, %
T, psi
r = 12
r = 18
$T_Y$
Outer Yield Surface
$(T-T_Y)^2$
$20 \times 10^6$
(a)
r = 6, N = 8
(b)
$\Gamma$, %

Fig. 24 a, b, c, d

Non-Proportional Loading

By far the most important and interesting experiments in this series are those for non-proportional, or non-radial, loading. It is only from such experiments that one may ascertain whether or not the general constitutive equations are incremental. Furthermore, as will be shown below, from such loading paths an interesting independent check can be made as to the existence of the two regions of deformation, and on the determination of $\lambda_N$.

The first and most important feature in that respect is the discovery that throughout the intermediate elastic-plastic region, whatever be the loading path, provided $dT$ is $\geq 0$, the location at which the inner yield surface is crossed governs the equation for the loading surface, Eq. (25). Once the outer yield surface is reached, the deformation continues without any reference to the location at which the inner yield surface was traversed.

Many different loading paths have been studied for fully annealed aluminum and copper. As of this writing, the loading paths for metal alloys for which I have thus far been able to carry out experiments consist, first of all, in loading in simple tension to some prescribed value which is then held constant while the loading continues to failure in torsion alone. Secondly, in a similar test, the first loading is in torsion, followed by tension alone. In a third type of test the initial loading is proportional to some prescribed ratio until, at a predetermined generalized stress, the test continues in either tension alone or torsion alone.

The most interesting of these tests are those for which the change in the loading path occurs in the intermediate region, for then it is possible to observe the abrupt change in the slope of the incremental strain vector upon crossing the outer yield surface.

Before discussing experiments for non-proportional loading paths in the metal alloys, I shall describe one such test for a fully annealed metal. It is from experiments of this type on annealed copper, and for strains above 1% in annealed aluminum that the incremental equations (14) were shown to be applicable, with the parabolic

generalized statement of Eq. (11) requiring the integration along the strain path, Eq. (4). The specimen was a thin-walled tube of ETP copper, annealed for 1 hour at 1100°F, and furnace cooled to produce a solid which long has been studied extensively.

For the fully annealed metal, for which $\lambda_N = 1.000$, the intermediate region is either non-existent or negligible. In test #2033 of Fig. 25 a,b,c,d,e, the specimen first was elongated in simple tension to a strain of approximately 3% at a stress of 14500 psi. The tension then was stopped and the test continued in torsion. The constant stress rate was 91 psi/min until the axial strain $\epsilon$ had reached 13% and the shear strain s, 22½% .

In Fig. 25a is a $T^2$ vs $\Gamma$ plot of the results, where $\Gamma$ is integrated along the strain path. We note that the initial parabola of $r = 4$, commonly observed in this solid, undergoes a transition to $r = 3$ at $N = 18$. After the cessation of tension at the point indicated in the figure, there is a rapid increase in strain until the transition strain of $N = 13$, whereupon there is a return to the $r = 4$ parabola of the initial deformation. We see that subsequent second-order transitions occur at $N = 10$ and $N = 8$; the test ends at $N = 6$.

The solid lines are the calculated values of the known parabola coefficients in copper. From Eq. (8), $\mu(0) = 5110$ kg/mm$^2$, $B_o = 0.0052$, $T_m = 1358°K$, and $T$ is the room temperature. Since $\sigma_y = \sigma_z = 0$ in Eqs. (14), if the theory applies for this test, the incremental strain vector, which is normal to the yield surface, should be given by Eq. (16).

That this is indeed the situation is shown in Fig. 25b in which the arrows represent the predicted slope for the known values of $\sigma$ and S; they are seen to be in precise accord with observation right to the end of the test at very large strain. That deformation type constitutive equations, such as those for proportional loading paths, Eqs. (15), are not applicable is shown by the large non-agreement of the thin dashed lines in Fig. 25b which were calculated by assuming that type of deformation.

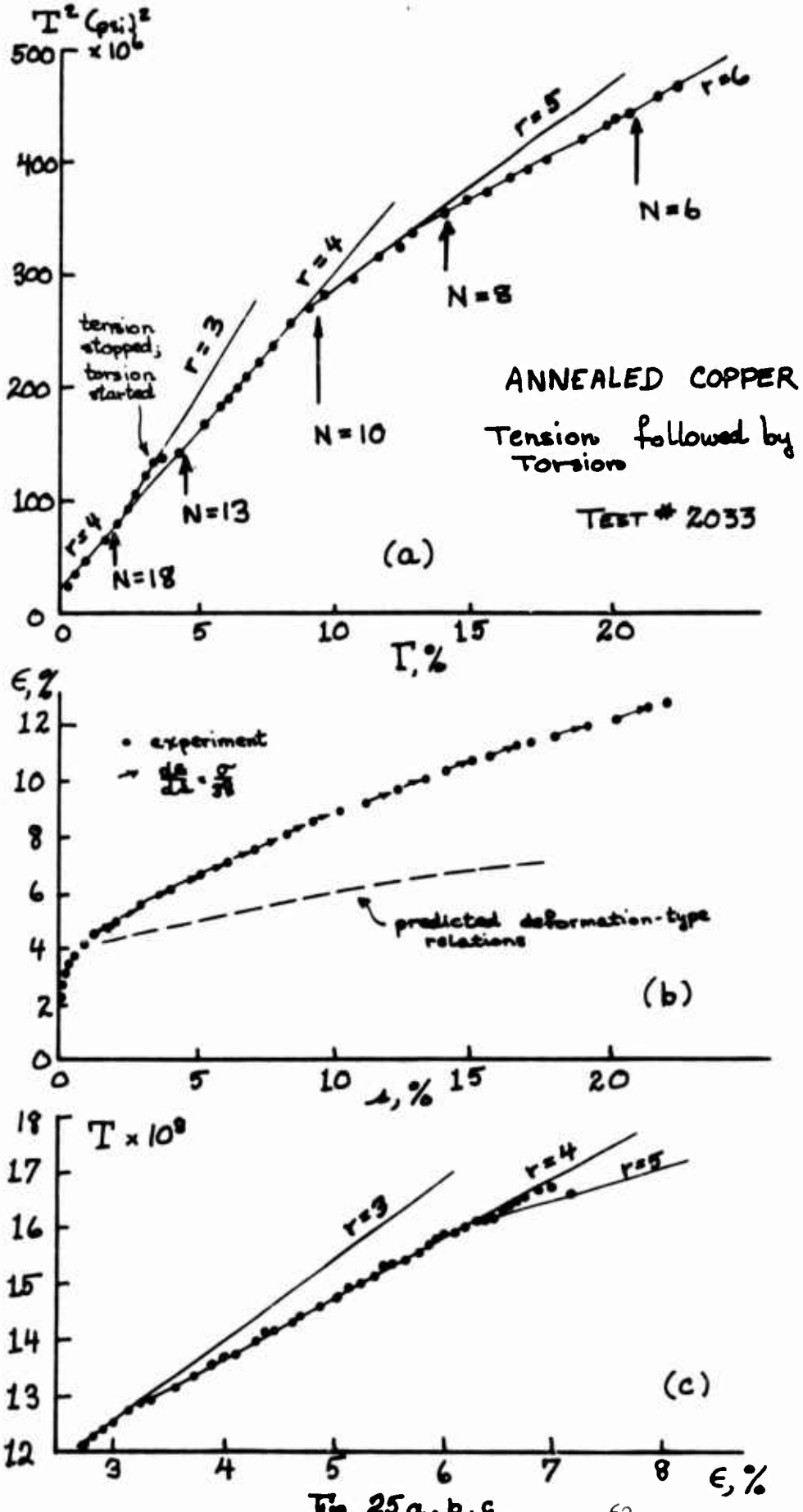
$T^2(\sigma_{ij})^2 \times 10^6$
500
400
300
200
100
0
r=5
r=6
N=6
r=4
N=8
tension stopped; torsion started
r=3
N=10
N=13
r=4
N=18
ANNEALED COPPER
Tension followed by Torsion
TEST # 2033
(a)
0
5
10
15
20
Γ, %
ε, %
12
10
8
6
4
2
0
experiment
predicted deformation-type relations
(b)
0
5
10
15
20
s, %
18
17
16
15
14
13
12
$T \times 10^9$
r=3
r=4
r=5
(c)
3
4
5
6
7
8
ε, %

Fig. 25 a, b, c

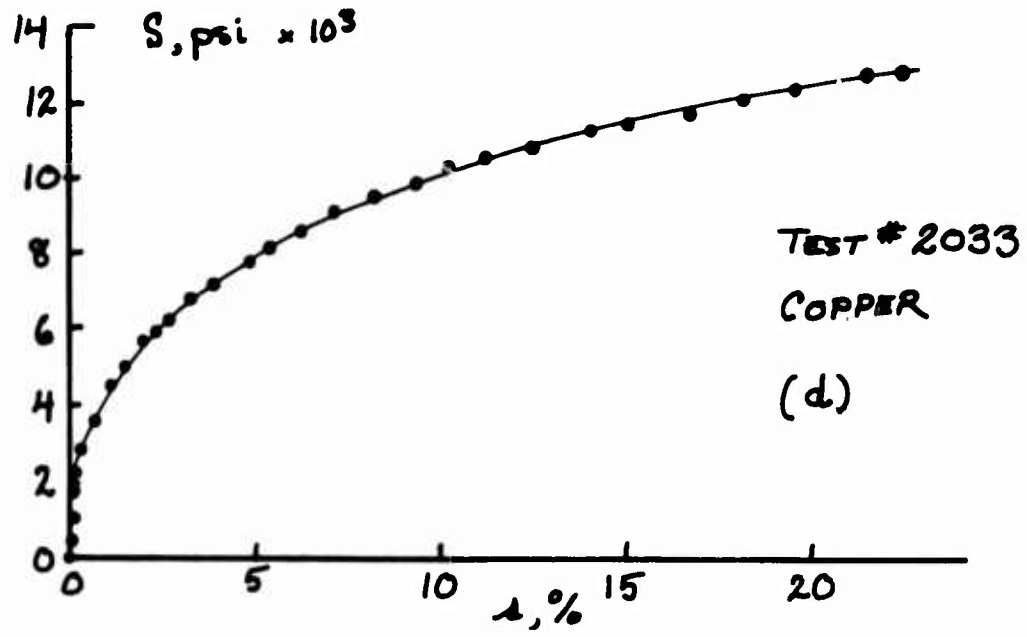
S, psi x 10³
14
12
10
8
6
4
2
0
0
5
10
15
20
ε, %
TEST # 2033
COPPER
(d)

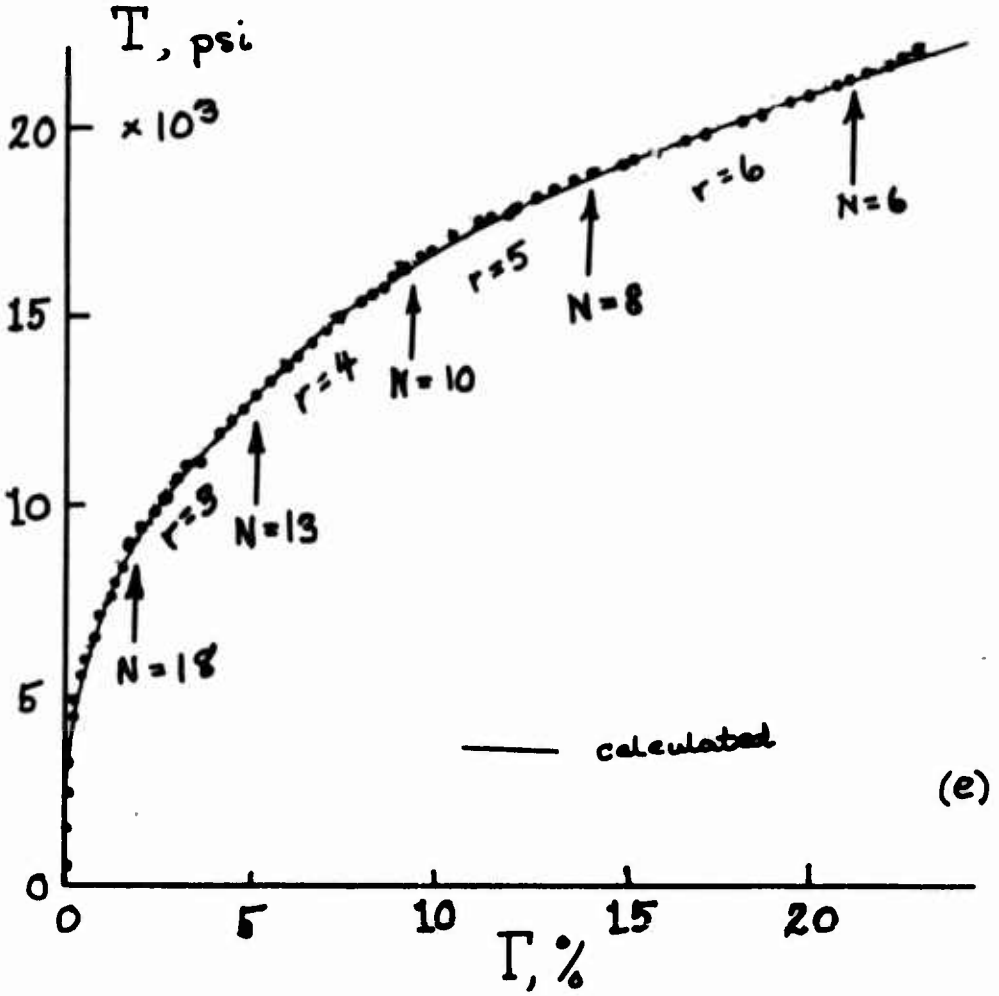
Γ, psi
x 10³
20
15
10
5
0
0
5
10
15
20
Γ, %
N=18
r=3
N=13
r=4
N=10
r=5
N=8
r=6
N=6
calculated
(e)

Fig. 25 d, e

As a further check upon the applicability of incremental constitutive equations we note from the definition of T in Eq. (3) that dT is given by Eq. (45) when $\sigma_y = \sigma_z = 0$.

$$dT = \frac{2/3\ \sigma d\sigma + a S dS}{T} \tag{45}$$

During the second interval of loading, for which $d\sigma = 0$ and $\sigma = \sigma_0$ is constant, we note from Eq. (14) for $\sigma_y = 0$ that $dT/d\epsilon$ has the constant slope of Eq. (46).

$$\frac{dT}{d\epsilon} = \frac{3\bar{K}^3 \beta_s^2}{4\sigma_0} \tag{46}$$

Plotting T against $\epsilon$, as is shown in Fig. 25c, one obtains the predicted constant slopes (solid lines) for each deformation mode. In Fig. 25d is a plot of S against s determined from integrating Eqs. (14) during the region of torsion. The comparison between prediction and experimental data in the region of each of the deformation mode indices r reveals a close accord.

Finally, in Fig. 25e is shown a T vs $\Gamma$ plot of this test; the agreement between prediction (solid lines) and experimental data for this non-proportional loading path is precise to a very large deformation.

That this is but one of many different types of non-proportional loading paths, including the alternation from tension alone to torsion alone several times during the test for which similar results have been obtained, establishes that the proposed theory indeed is applicable for the fully annealed metal.

To illustrate that these results also extend to the metal alloys for which $\lambda_N$ is not equal to unity, data are given from

a few experiments in which tension alone is followed by torsion alone, or torsion alone is followed by tension alone. The important point in these experiments, beyond their general agreement with the constitutive statements provided above, is whether or not the abrupt change in the loading path occurs in the intermediate elastic-plastic region, or in the totally plastic region.

If in the latter, then in an $\epsilon$ vs s plot the incremental strain vector has slopes determined in the same manner as those for the fully annealed metal for the known values of $\sigma$ and S . If the abrupt change occurs in the intermediate region, the incremental strain vector is not normal to the yield surface for such loading paths; the vector is given by Eq. (34) rather than by Eq. (35) where either $\sigma_Y$ or $S_Y$ is zero, depending upon the initial loading. For that situation a comparison of Eqs. (34) and (35) reveals that an abrupt change in the slope of the incremental strain vector can be anticipated when the outer yield surface is reached at $\Gamma_c$ .

That this is indeed the situation is shown in Fig. 26b in the $\epsilon$ vs s plot of a test on a 6061-T6 aluminum alloy tube for which the initial loading path was torsion alone. The T vs $\Gamma$ plot for this test is shown in Fig. 26a.

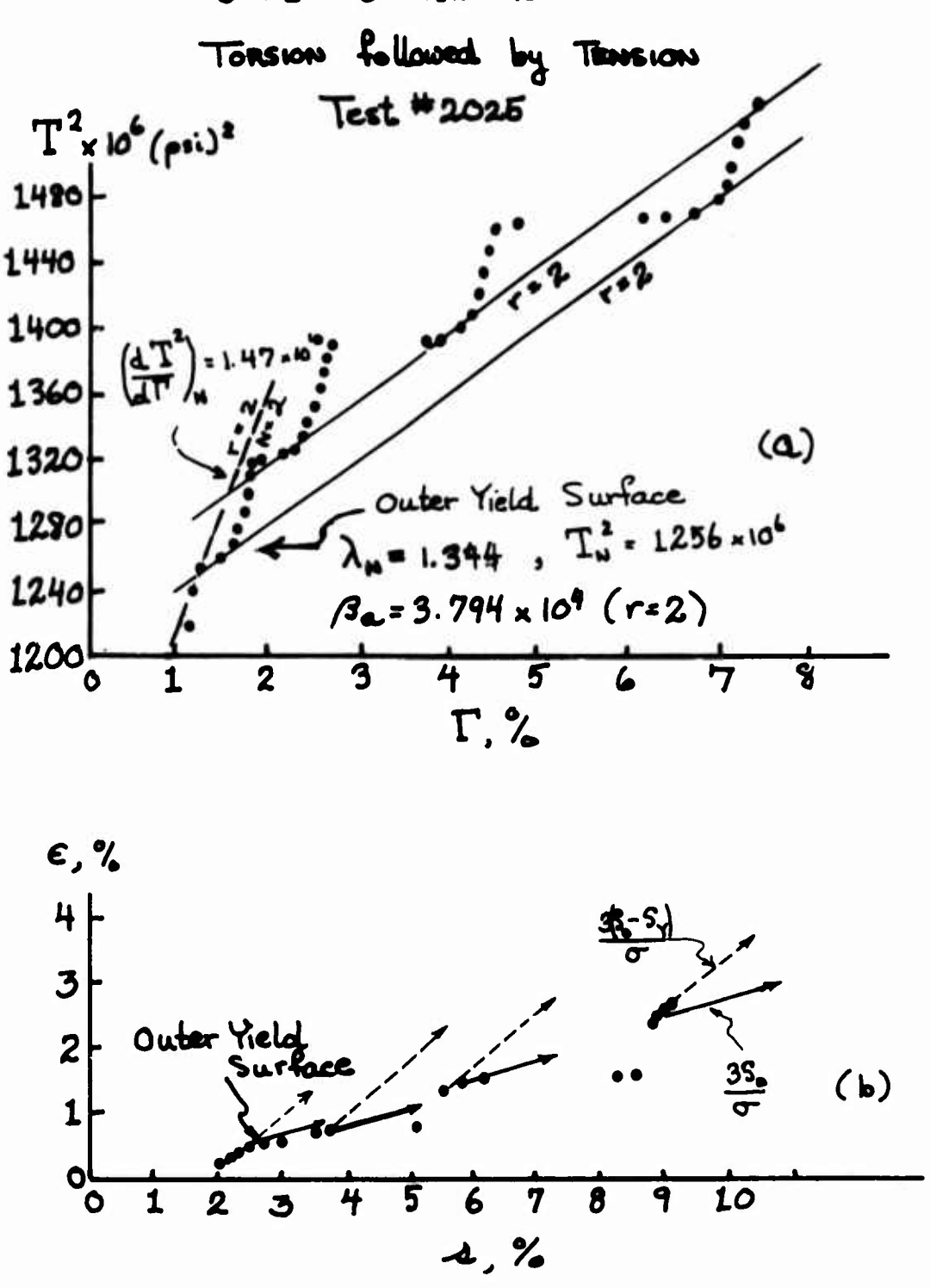
6061-T6 Aluminum
Torsion followed by Tension
Test #2025
$T^2 \times 10^6$ (psi)$^2$
1480
1440
1400
1360
1320
1280
1240
1200
0 1 2 3 4 5 6 7 8
Γ, %
$\left(\frac{dT^2}{d\Gamma}\right)_N = 1.47 \times 10^6$
r=2
r=2
(a)
Outer Yield Surface
$\lambda_N = 1.344$ , $T_N^2 = 1.256 \times 10^6$
$\beta_a = 3.794 \times 10^9$ (r=2)
ε, %
4
3
2
1
0
0 1 2 3 4 5 6 7 8 9 10
Outer Yield Surface
$\frac{3\bar{S}-S_y}{\sigma}$
$\frac{3S_0}{\sigma}$
(b)
s, %

Fig. 26 a,b

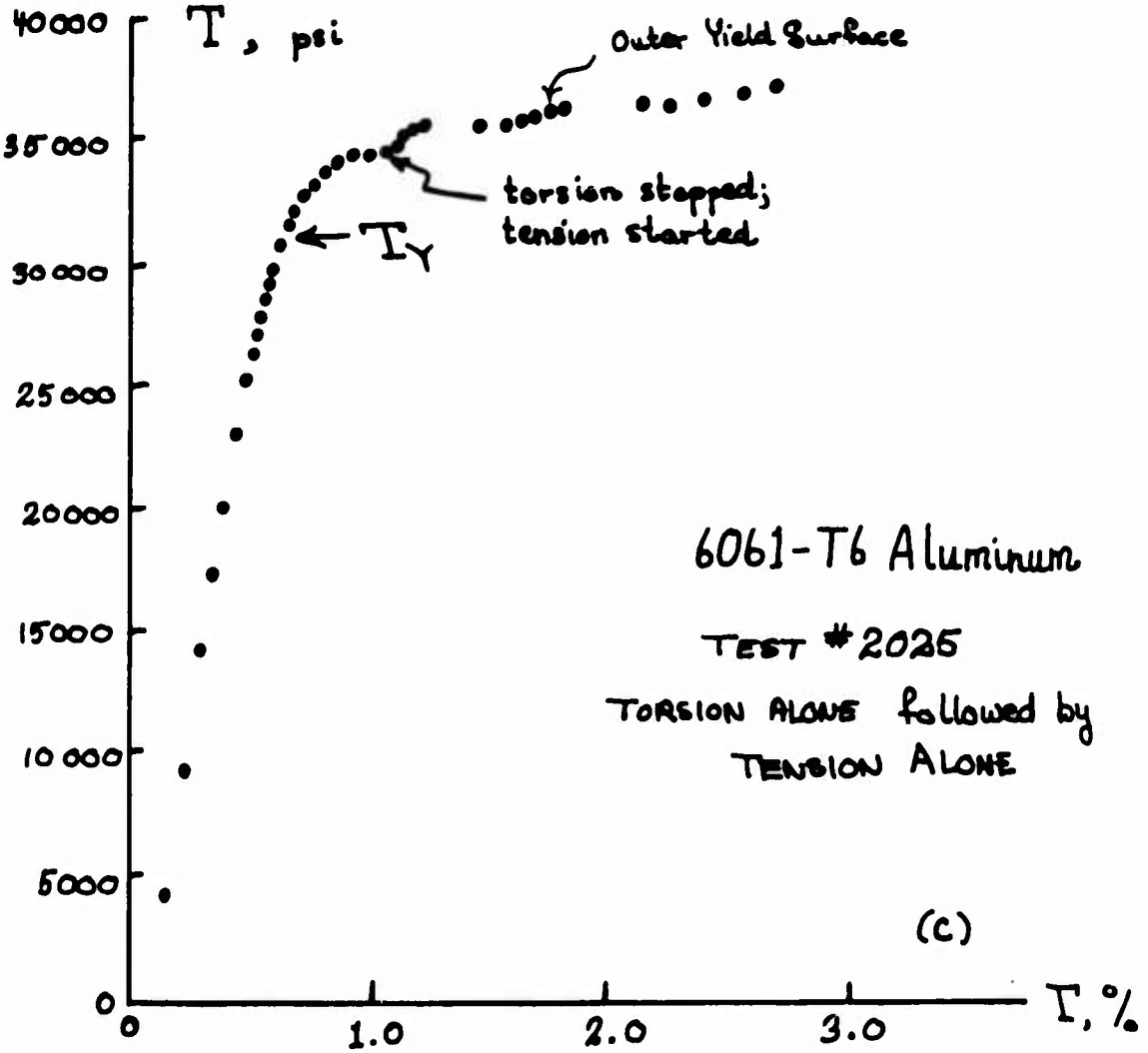
T, psi
Outer Yield Surface
torsion stopped; tension started
$T_Y$
40000
35000
30000
25000
20000
15000
10000
5000
0
0
1.0
2.0
3.0
Γ, %
6061-T6 Aluminum
TEST #2025
TORSION ALONE followed by TENSION ALONE
(c)

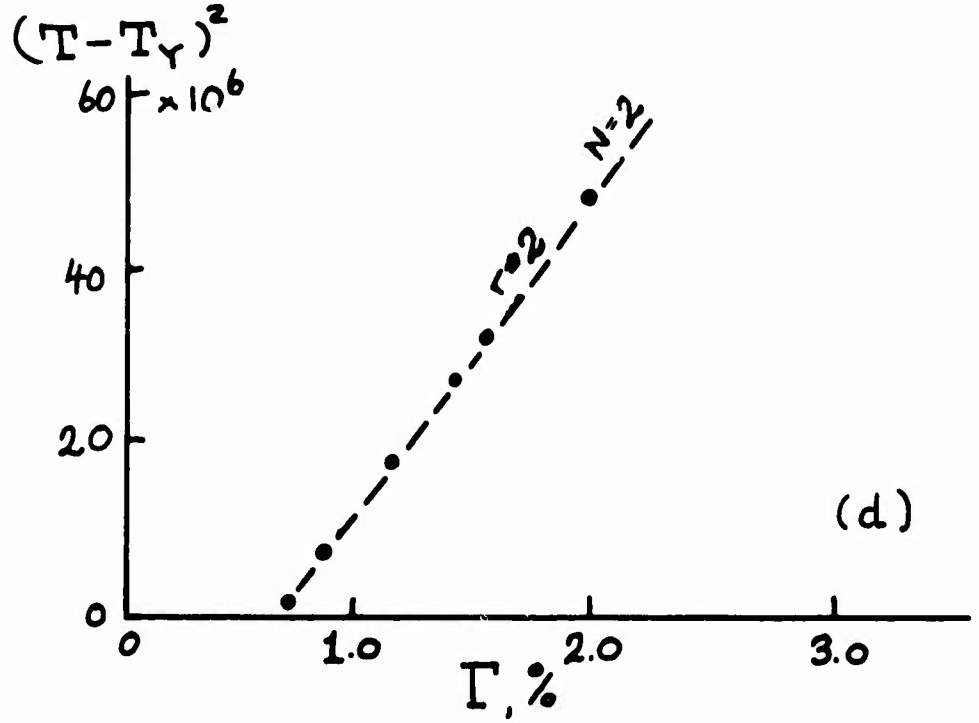
$(T-T_Y)^2$
$\times 10^6$
60
40
20
0
N=2
$\Gamma^{N=2}$
0
1.0
2.0
3.0
Γ, %
(d)

Fig. 26 c, d

The dashed line arrows are the slopes for the strain increment vector calculated from Eq. (34) for the intermediate elastic-plastic region, and the solid line arrows are those for the totally plastic region calculated from Eq. (35). We see that there is in fact an abrupt change in slope corresponding to predicted values which occur at an $s$ and an $\epsilon$ from which one may ascertain a value for $\lambda_N$ independent of which of the types of calculation has been employed above. A value thus calculated at the indicated position where a change of slope occurs, is $\lambda_N = 1.344$ ; this is 3% below the predicted value of $\lambda_N = 1.385$, i.e., for $N = 2$, $r = 2$ , invariably obtained for all types of tests for this metal alloy, whether on a tube, a rod, or a plate.

In Fig. 26a is the $T^2$ vs $\Gamma$ plot. The location of the outer yield surface for this value of $\lambda_N$ is shown as the slope for the predicted $r = 2$ parabola and the slope from Eq. (29) at the end of the intermediate elastic-plastic region.

It is characteristic of these experiments that from the outer yield surface on, large Savart-Masson (Portevin - le Chatelier) steps are observed. As with the fully annealed metal these steps represent a departure from, and a return to, the predicted parabola. I have chosen test #2025 of Fig. 26 to illustrate the extreme height of the steps which occasionally can be seen. An inspection of Fig. 26a reveals that such large steps are not as readily apparent in a $T$ vs $\Gamma$ plot as they are in a $T^2$ vs $\Gamma$ plot.

Finally, I included a $(T - T_Y)^2$ vs $\Gamma$ plot to illustrate that in the intermediate elastic-plastic region, Eq. (25) is applicable for the same $r = 2$ parabola.

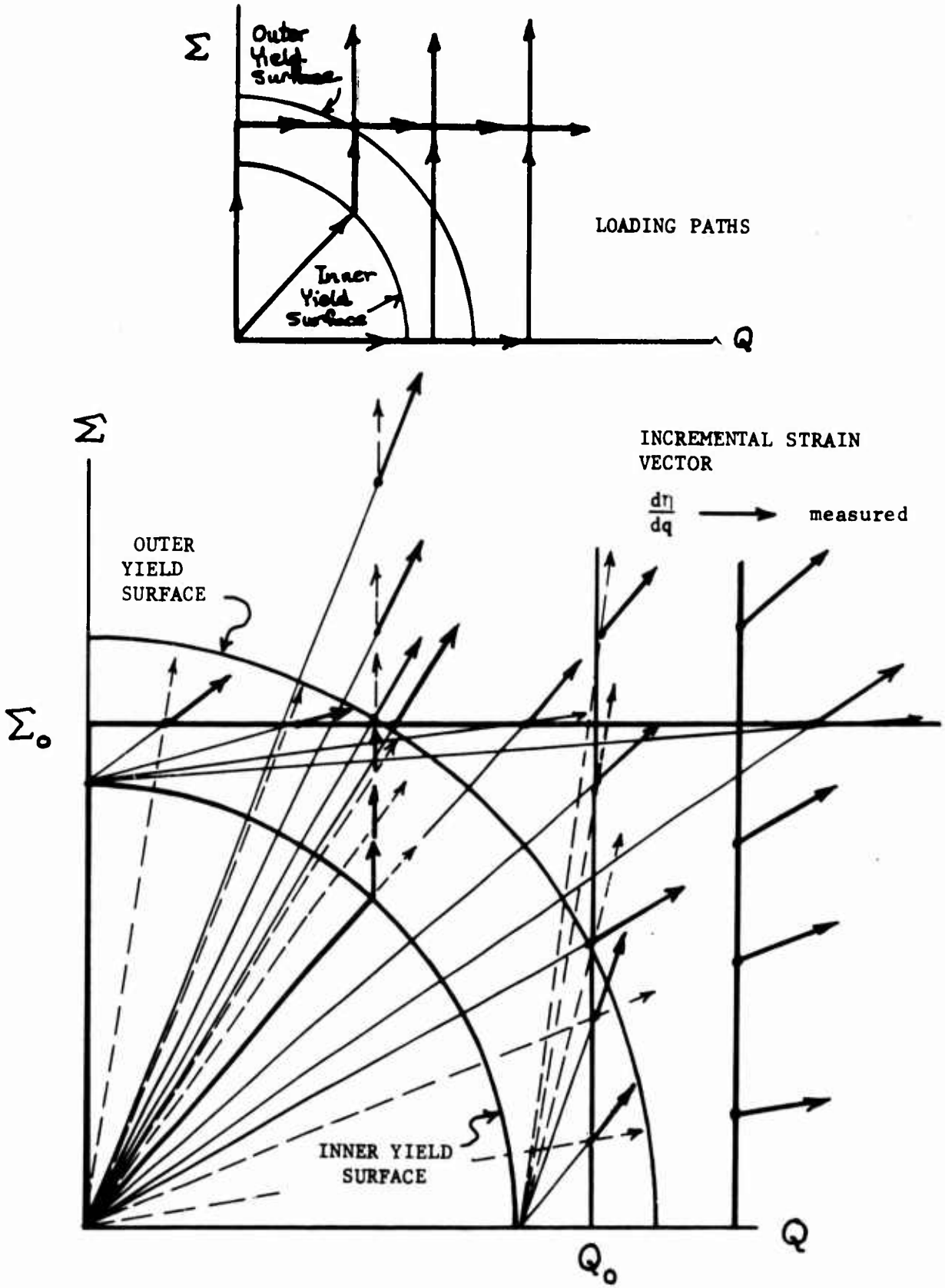
Σ
Outer Yield Surface
LOADING PATHS
Inner Yield Surface
Q
Σ
INCREMENTAL STRAIN VECTOR
dη/dq
measured
OUTER YIELD SURFACE
Σ₀
INNER YIELD SURFACE
Q
Q₀

Fig. 27

In Fig. 27, I have shown a schematic diagram which permits a graphical determination of the incremental strain vector for various loading paths, and illustrates the nature of this newly discovered phenomenon for the incremental strain vector. It further illustrates the sources of the previous confusion regarding partially annealed metals for which the inner and outer yield surfaces are not too different. Small differences in the preloading, hence, altered the conclusions reached with respect to yield surface criteria when it was thought that only a single yield surface existed.

For simplicity in this schematic figure I have introduced $\Sigma = \sqrt{\frac{2}{3}}\,\sigma$ and $Q = \sqrt{2}\,S$ so that the paths of constant generalized stress become circular. Also introducing $\eta = \sqrt{\frac{3}{2}}\,\epsilon$ and $q = s/\sqrt{2}$ we see that Eq. (34) becomes Eq. (47) for the intermediate elastic-plastic region, and Eq. (35) becomes Eq. (48) for the incremental strain vector in the totally plastic region.

$$\frac{d\eta}{dq} = \frac{E - E_Y}{Q - Q_Y} \tag{47}$$

$$\frac{d\eta}{dq} = \frac{E}{Q} \tag{48}$$

The heavy arrows of Fig. 27 correspond to the slope of the incremental strain vector in either region. The dashed arrows correspond to the alternate prediction. The boundary between the two, designated as O.Y.S. in the figure, in each of the examples which follow coincides with that obtained from the measurement of $T_N$ and $\beta_a$ in a $T^2$ vs $\Gamma$ plot from Eq. (27) and Eq. (28) as given above.

In Fig. 28 is an $\epsilon$ vs $s$ plot and the corresponding slopes of the torsion alone, followed by tension alone, in 1100-H14 aluminum tested as-received. The value of $\lambda_N = 1.110$ determined from the change in slope, is in close accord with the calculated $\lambda_N = 1.114$ for $N = 8$, $r = 2$.

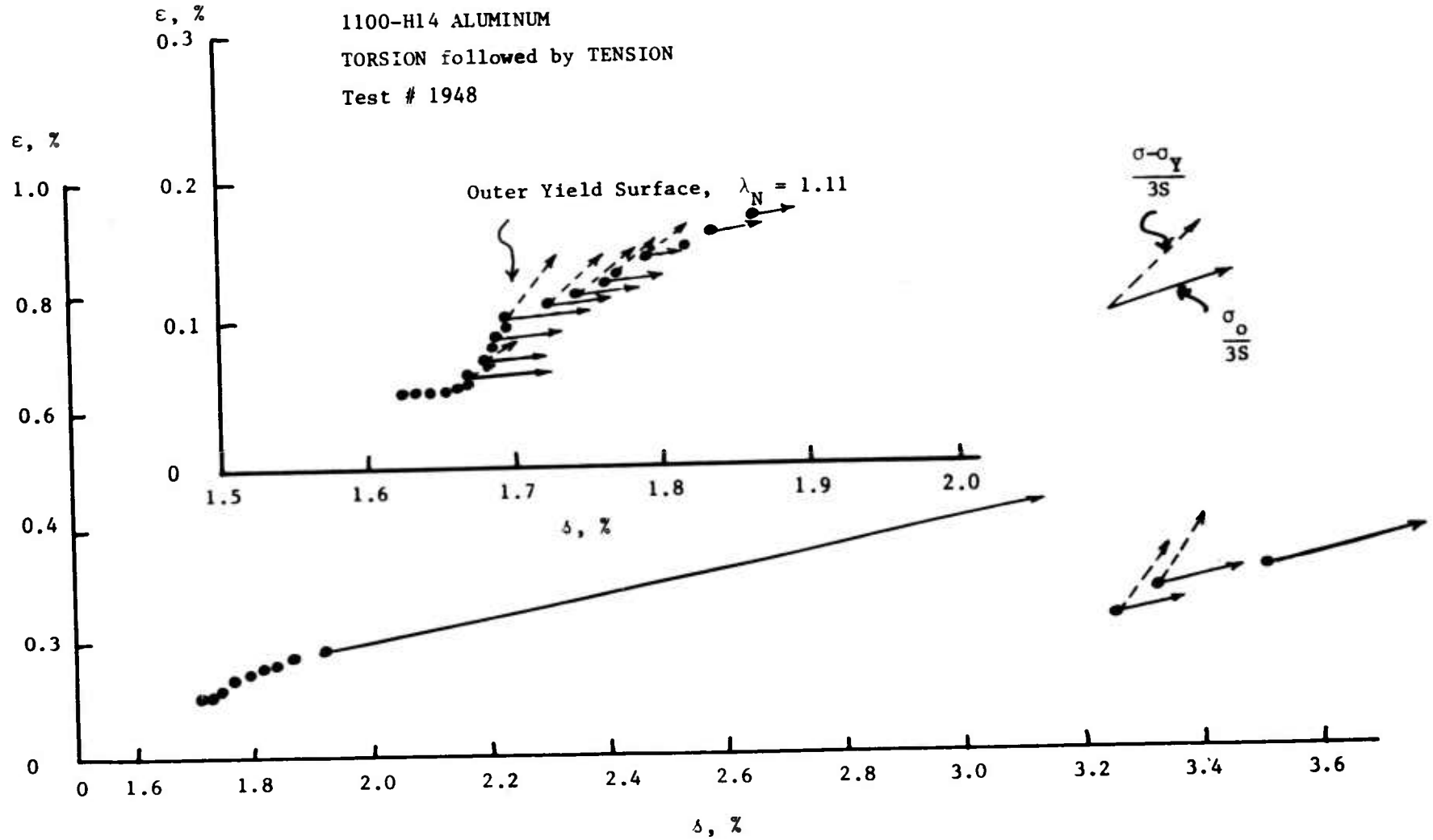
1100-H14 ALUMINUM
TORSION followed by TENSION
Test # 1948
ε, %
0.3
0.2
0.1
0
1.5
1.6
1.7
1.8
1.9
2.0
δ, %
Outer Yield Surface, $\lambda_N = 1.11$
$\frac{\sigma-\sigma_Y}{3S}$
$\frac{\sigma_o}{3S}$
ε, %
1.0
0.8
0.6
0.4
0.3
0
0
1.6
1.8
2.0
2.2
2.4
2.6
2.8
3.0
3.2
3.4
3.6
δ, %

Fig. 28

In Fig. 29 are the results of a test for tension alone, followed by torsion alone, for the same metal alloy; $\lambda_N = 1.116$

In Fig. 30 is the $\epsilon$ vs $s$ plot of a test, again in this same metal alloy, in which the change from initial torsion loading to only tension loading occurred beyond the outer yield surface. A comparison of the two slopes reveals that the incremental strain vector is solely that for the totally plastic region.

In Fig. 31a is the $\epsilon$ vs $s$ plot of a test in 2024-T3 aluminum alloy. The initial deformation was radial, with a constant loading rate, $\dot{\sigma}/\dot{s}$, of 2.90 to the position indicated in the intermediate region, where the torsion component was stopped and the test proceeded solely in tension.

In this instance, too, as may be seen in the $T$ vs $\Gamma$ plot in Fig. 31b, large Savart-Masson steps appear when there is a sharp change in the loading path. The value of $\lambda_N = 1.575$, calculated from the measured $T_N$ and $\rho_a$ for this test, is in precise agreement with the predicted $\lambda_N = 1.577$ for $N = 0$, $r = 2$. Also shown in Fig. 31b is a $(T - T_Y)^2$ vs $\Gamma$ plot which demonstrates that for the same $N = 0$, $r = 2$, Eq. (25) applies in the intermediate elastic-plastic region.

That large Savart-Masson steps do not necessarily accompany an abrupt change in loading path may be seen in the $T^2$ vs $\Gamma$ plot of Fig. 32a where from measured $T_N$ and $\rho_a$, $\lambda_N = 1.115$ is the same as that obtained with the proportional loading of the 1100-H14 metal alloy for which $\lambda_N = 1.114$ for $N = 8$, $r = 2$. This was a test for torsion alone followed by tension alone; the change of path occurred during the intermediate region. The predicted abrupt change in slope on reaching the outer yield surface may be seen in the $\epsilon$ vs $s$ plot of this test, shown in Fig. 32b

Fig 29

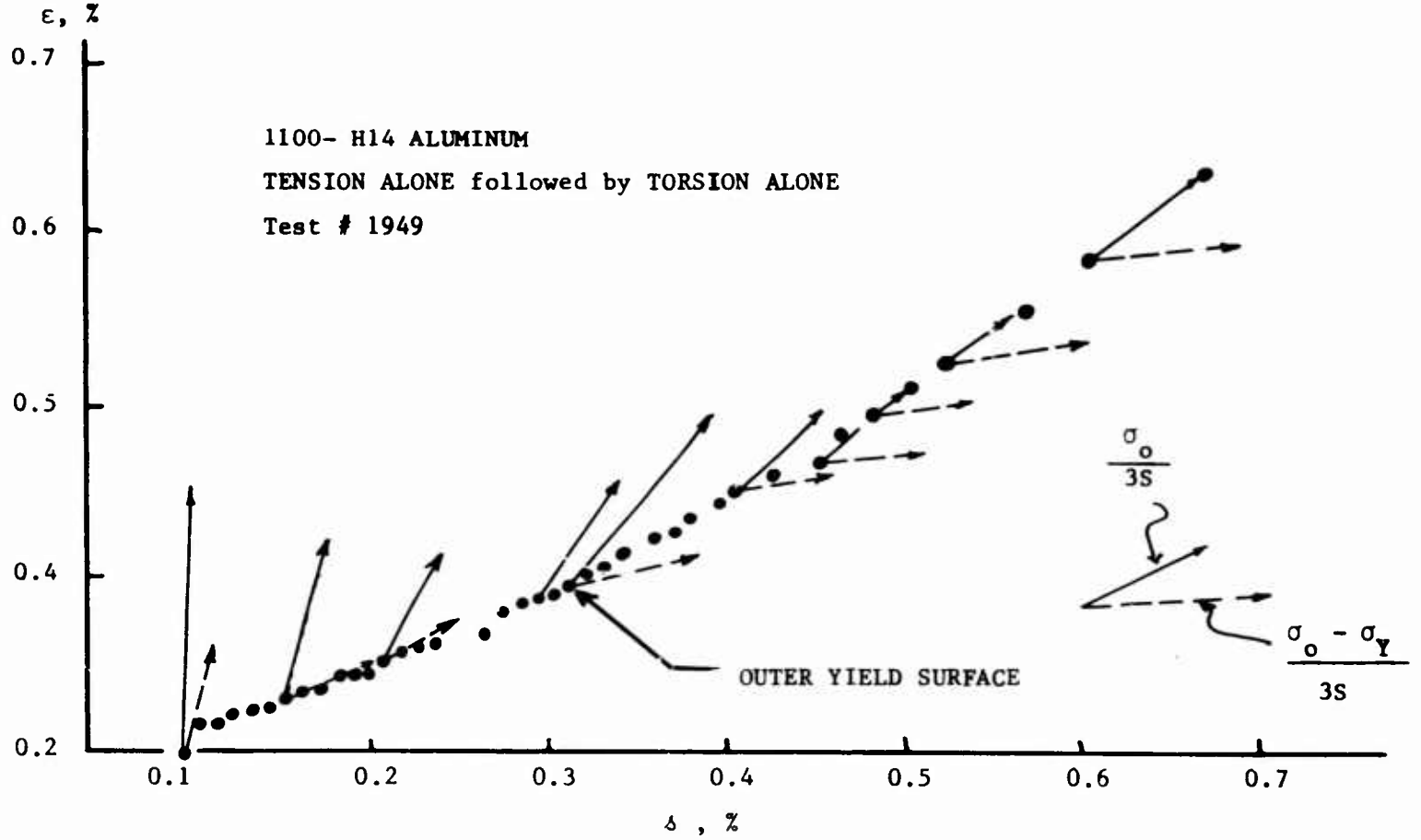
ε, %
0.7
0.6
0.5
0.4
0.2
1100- H14 ALUMINUM
TENSION ALONE followed by TORSION ALONE
Test # 1949
$\frac{\sigma_o}{3S}$
$\frac{\sigma_o - \sigma_Y}{3S}$
OUTER YIELD SURFACE
0.1
0.2
0.3
0.4
0.5
0.6
0.7
δ , %

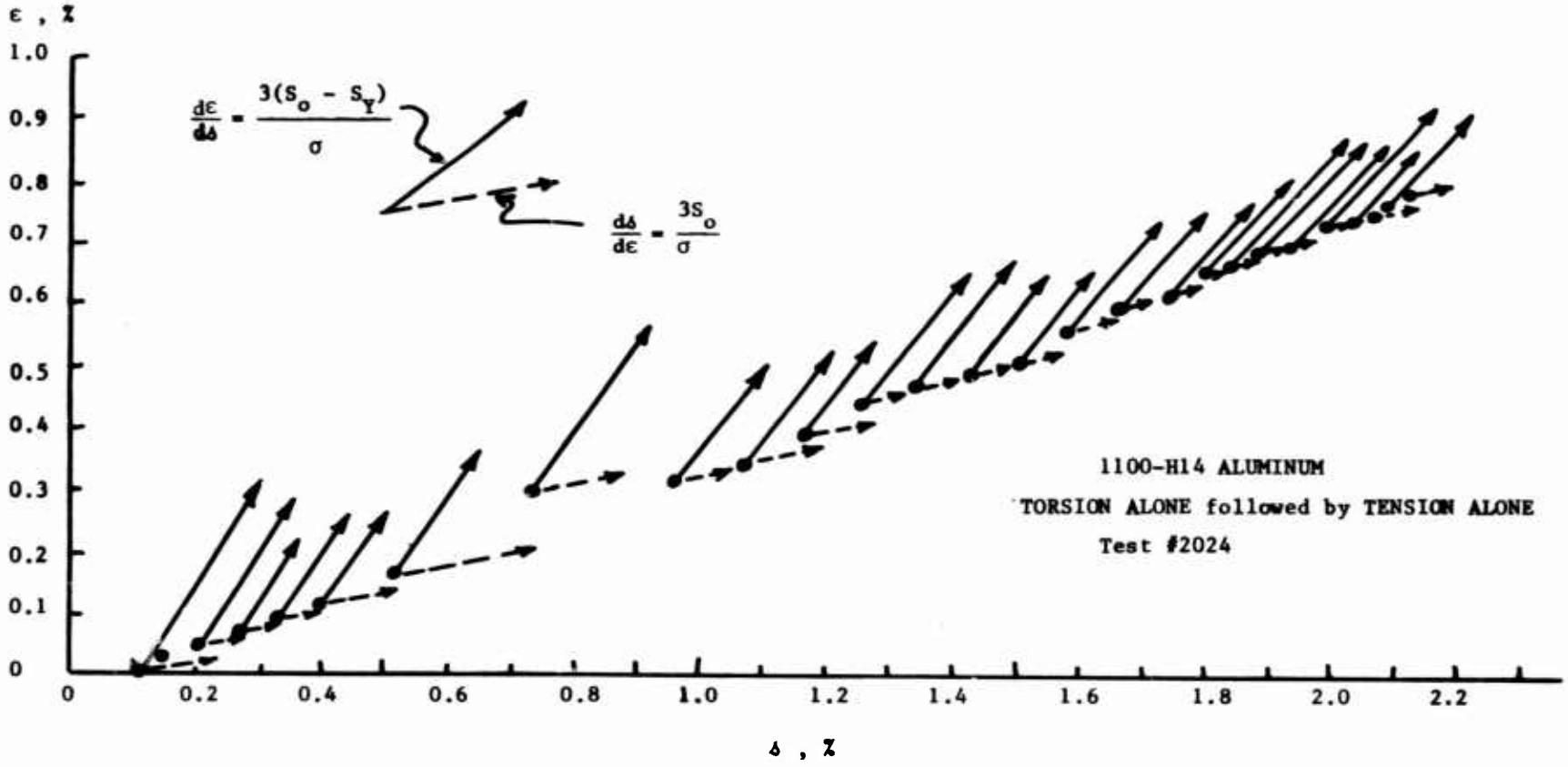
ε , %
1.0
0.9
0.8
0.7
0.6
0.5
0.4
0.3
0.2
0.1
0
$\frac{d\varepsilon}{d\delta} = \frac{3(S_o - S_Y)}{\sigma}$
$\frac{d\delta}{d\varepsilon} = \frac{3S_o}{\sigma}$
1100-H14 ALUMINUM
TORSION ALONE followed by TENSION ALONE
Test #2024
0
0.2
0.4
0.6
0.8
1.0
1.2
1.4
1.6
1.8
2.0
2.2
δ , %

Fig 30

Fig. 31 (a)

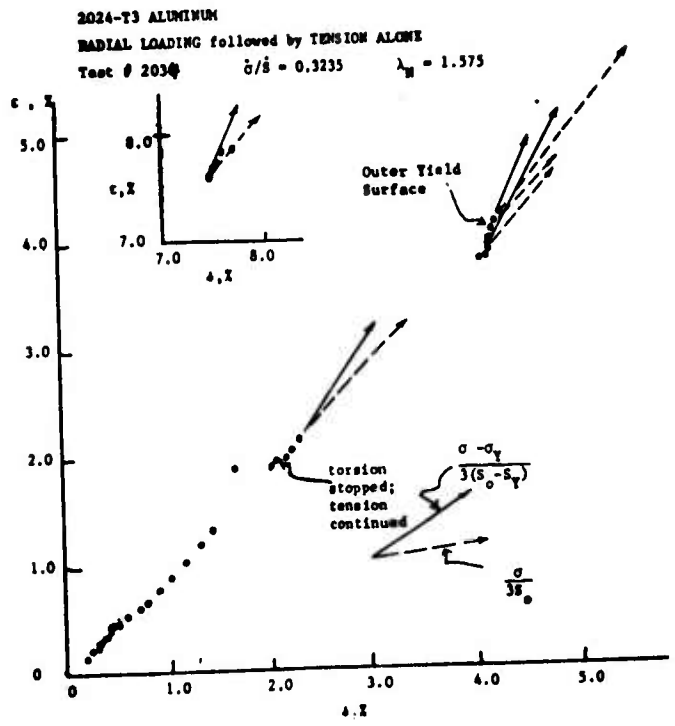


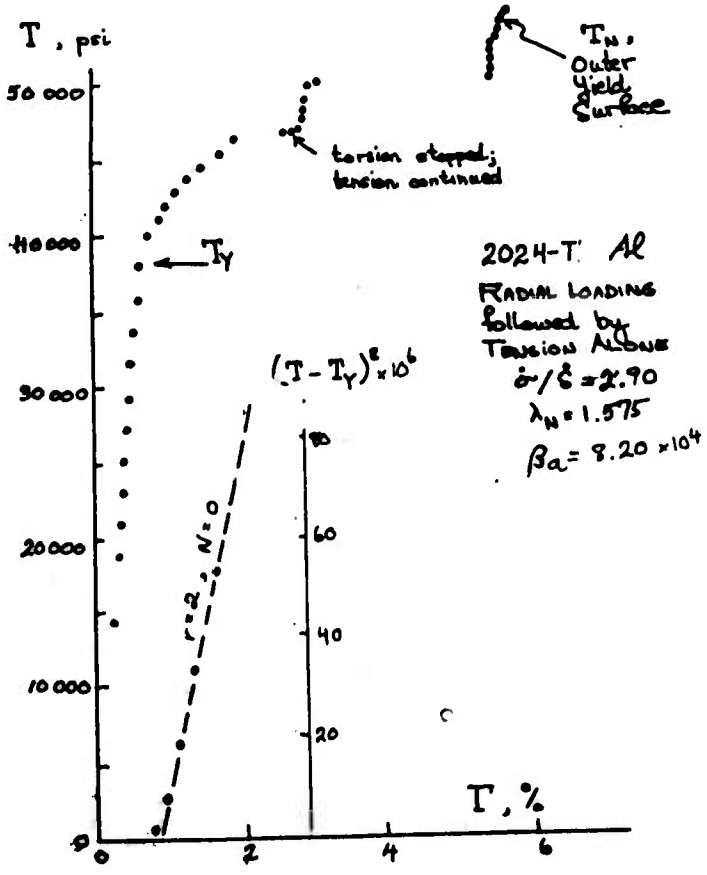


Fig. 31 (b)

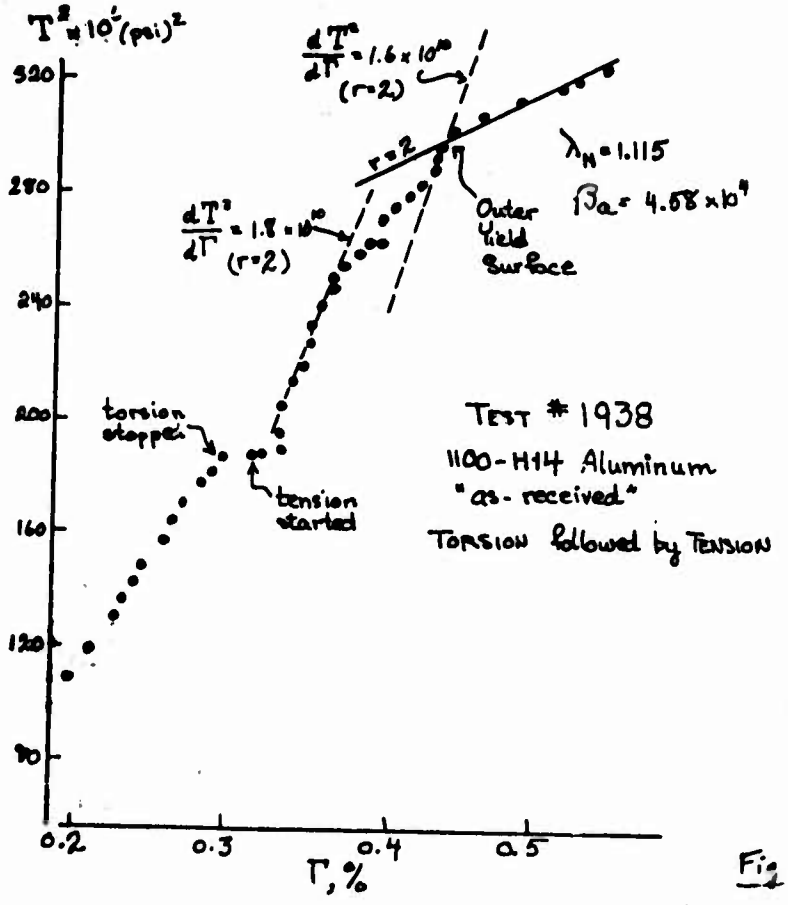


Fig 32 (a)

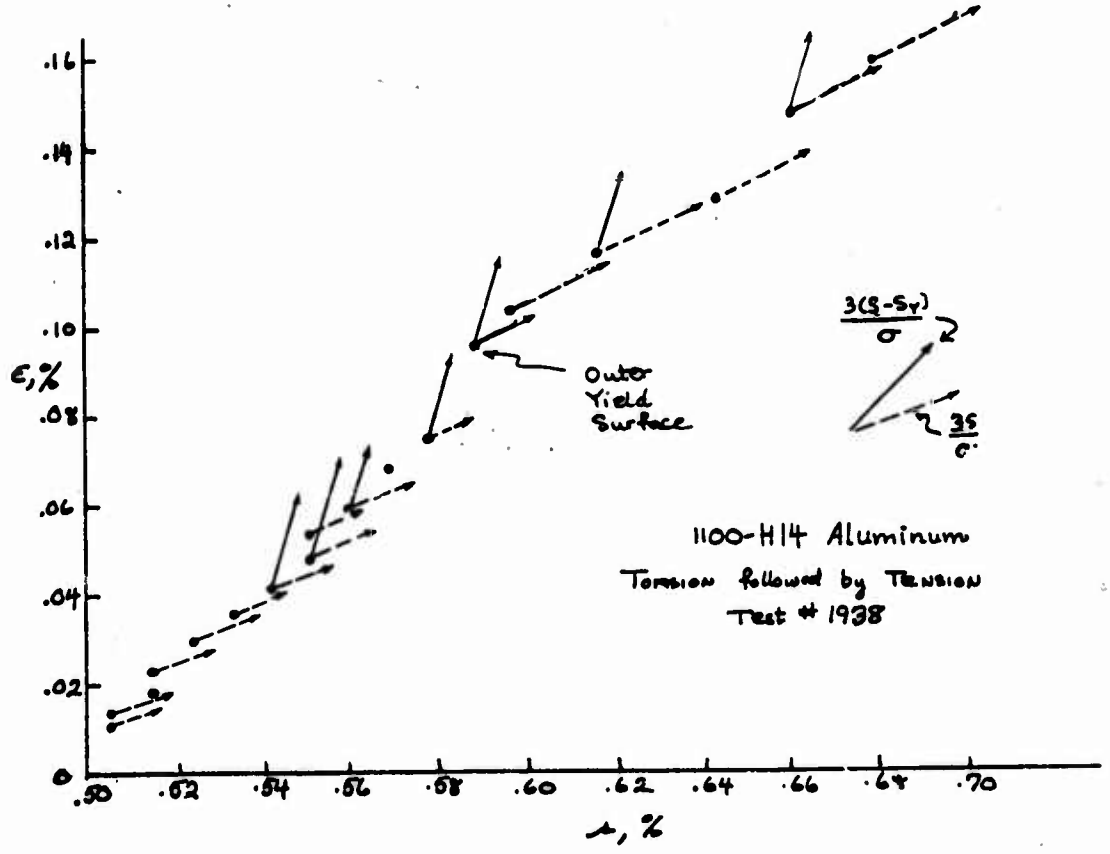




Fig 32 (b)

The series of illustrations given above for proportional and for non-proportional loading of structural metal alloys amply demonstrates that this new generalized theory of large plastic deformation indeed is applicable to the structural metal alloys. We now may consider whether or not for these alloys, as for the fully annealed metals, the same formulation also is extendible to dynamic plasticity.

## Dynamic Plasticity

An overwhelming proportion of experimental research in this laboratory since the first incremental wave experiments in 1949 has been concerned with the study of the dynamic plasticity of the fully annealed metals. In fact, it was from those studies of high strain rates in microsecond intervals of time that the parabolic response function and second-order transition structure originally were discovered.

The types of experiments are many. The most important of the series, one which has been unique to this laboratory for over twenty years, is the use of 30,000 or more lines per inch cylindrical diffraction gratings for the direct study of strain and surface angle during the propagation of the plastic wave. The plastic wave is introduced by means of the symmetrical free-flight axial impact of identical specimens. Among the many parameters which are varied in these experiments are the impact velocity, the ambient temperature, the position along the specimen, the time in which the specimens remain in contact, i.e., the time of contact, $t_o$ ; the detail of unloading waves; the coefficient of restitution, etc.

From these experiments it has been established that, for all of the fully annealed metals studied, the generalized response functions outline above for quasi-static loading are applicable. During wave propagation at higher strain rates, second-order transitions are not observed until the maximum strain plateau has

been reached. However, second-order transitions do occur during loading for quasi-static tests. Thus when measured dynamic and quasi-static response functions are compared, the difference in material stability properties at a critical strain is often incorrectly ascribed to viscosity. In some fully annealed metals, such as high purity aluminum and annealed copper, for which the first second-order transition occurs at large strain, the quasi-static and dynamic response functions are identical.

A similar series of experiments were undertaken for the metal alloys of interest here. Because of the mammoth experimental program involved, as well as the increased difficulties of applying these techniques to high-stressed structural metals, the program of research on the dynamic plasticity of the metal alloys is by no means complete. Except for a few preliminary tests in other metal alloys, the main focus of attention has been upon the study of 6061-T6 and 1100-H14 aluminum alloys. However, the work has proceeded sufficiently far not only to demonstrate that the general theory outlined above does indeed supply response functions from finite amplitude wave propagation in these solids, but also to reveal that an "eruptive" plastic deformation occurs when the maximum particle velocity is high enough to reach the outer yield surface.

As I have described in many papers, in the monograph The Physics of Large Deformation of Crystalline Solids, and in the Handbuch der Physik treatise, in order to determine the response function governing finite amplitude wave propagation one must not assume a priori either the applicable non-linear wave theory or the response functions one wishes to determine. Strain-time profiles must be determined during wave propagation at a minimum of three positions, from which traverse times measured at different levels of strain show whether or not the propagation velocities are constant.

A second set of experiments provide a check upon the constancy of wave speeds. Velocity-time profiles are obtained

either by the optical displacement technique developed several years ago in this laboratory for that purpose, or by magnetic induction. If both wave speeds are constant, as was found in all the fully annealed metals, then the functional relation between velocity and strain assumed in the Taylor-von Karman theory of non-linear waves is given. From this relation between velocity and strain one may obtain the response function governing wave propagation.

Two other cross-checks on the applicability of the theory are available. Because of the possibility that small viscosity may not be detectable when wave speeds are compared, it is essential in the final analysis to perform a large number of tests at many impact velocities.

Another check on the applicability of the theory which is very sensitive to the presence or the non-presence of viscosity, is the comparison of maximum strains and maximum particle velocities. The latter are observed over a large range of values to ascertain that the functional relationship between strain and particle velocity obtained from the wave speed studies are in accord.

Finally, as I have shown[8] from measurements of surface angle during the passage of the wave, it is possible to ascertain by direct measurement whether or not the propagating wave is in fact one dimensional. For the metal alloys there has been insufficient time to complete this series of cross-checks. However, here we are interested in knowing from experiment whether or not specifically known response functions apply for one-dimensional wave propagation in the intermediate elastic-plastic region, Eq. (36), and in the totally plastic region, Eq. (37).

From a series of ten diffraction grating measurements in "as-received" hard 1100-H14 aluminum, wave speeds were obtained. These wave speeds were determined from the traverse times at different levels of strain from diffraction gratings located at 1", 1½", 2", and 3½" from the impact face, on the stationary member of two identical specimens in free-flight symmetrical impact.

In the Taylor - von Karman theory the wave speeds which are constant for each level of strain are given by the tangent modulus of the response function, i.e., $c_p = \sqrt{d\sigma/d\epsilon / \rho}$ . Differentiating Eq. (36) we find for the wave speeds in the intermediate elastic-plastic region, Eq. (49).

$$c_p = \sqrt{\frac{d\sigma/d\epsilon}{\rho}} = \sqrt{\frac{\beta_2}{2\rho(\epsilon - \epsilon_Y)^{1/2}}} \qquad (49)$$

Differentiating Eq. (37) for the totally plastic region, we obtain Eq. (50).

$$c_p = \sqrt{\frac{d\sigma/d\epsilon}{\rho}} = \sqrt{\frac{\beta_2}{2\rho(\epsilon - \epsilon_c + \frac{\epsilon_N}{\lambda_N})^{1/2}}} \qquad (50)$$

In Fig. 33 is shown a plot of $c_p$ vs $\epsilon$ for 1100-H14 aluminum. The dashed line is the $c_p$ vs $\epsilon$ in the intermediate region calculated from Eq. (49) which, except for strains in the immediate vicinity of the linear region, are in fair accord with observation. The solid lines are the wave speeds for the totally plastic region determined from Eq. (50), for an outer yield surface occurring at $\epsilon_c = 0.035$ . As will be shown below, the $\epsilon_Y$ for Eq. (36) is determined from dynamic measurement.

From this initial series of measurements one may anticipate that the observations and conclusions from the studies of the dynamic plasticity of the fully annealed metal may be extrapolated to the structural metal alloy, as was true for quasi-static loading.

The Taylor - von Karman theory provides the interrelation between particle velocity and strain, Eq. (51).

$$v = \int c_p \, d\epsilon \qquad (51)$$

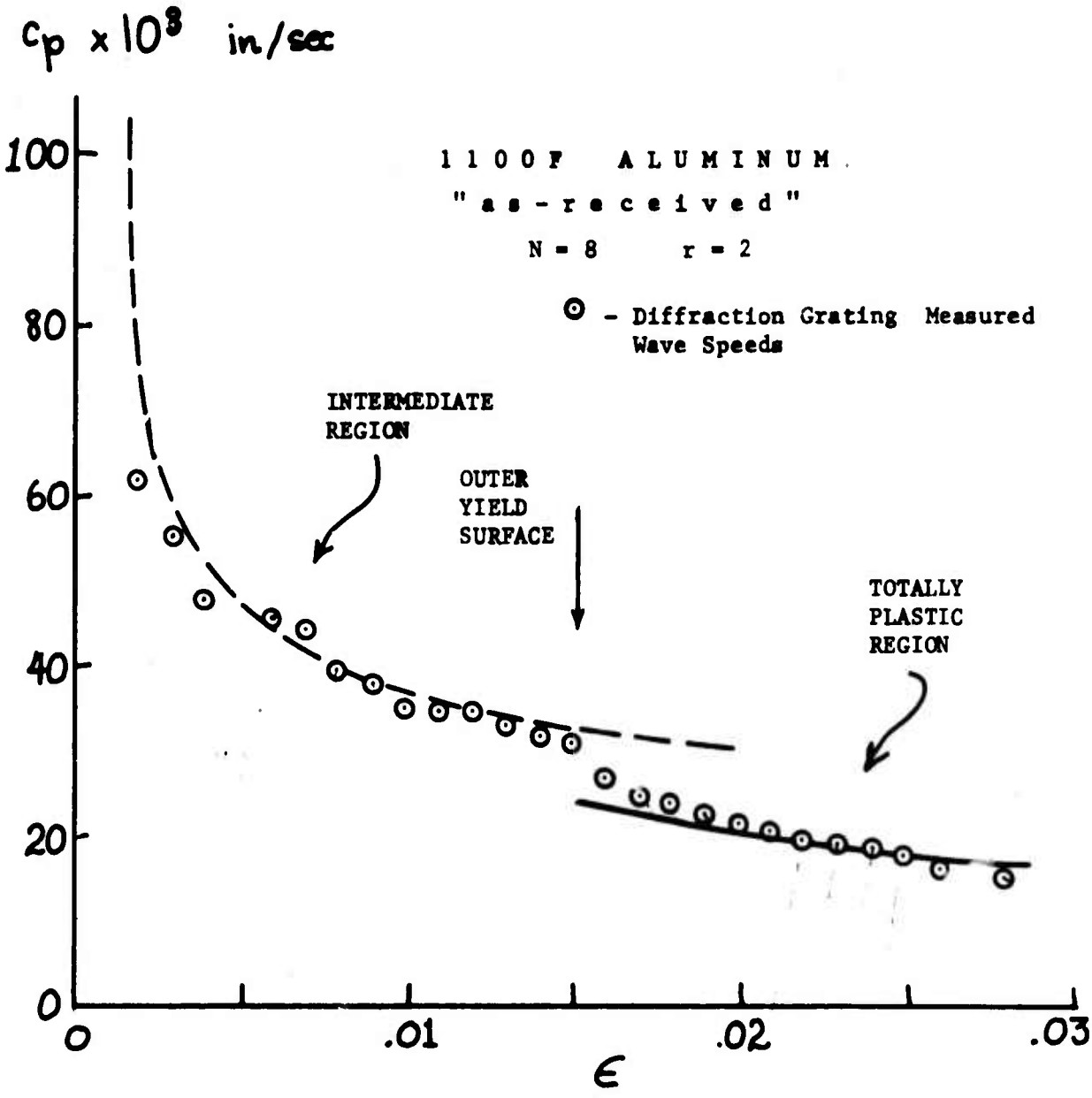
$c_p \times 10^8$ in/sec
1100F ALUMINUM
"as-received"
N = 8 r = 2
⊙ - Diffraction Grating Measured Wave Speeds
INTERMEDIATE REGION
OUTER YIELD SURFACE
TOTALLY PLASTIC REGION
100
80
60
40
20
0
0
.01
.02
.03
$\epsilon$

Fig. 33

Inasmuch as the series of experiments on velocity-time profiles has not been completed, I am showing here, in Fig. 34, the relation between the known, i.e., the measured maximum particle velocity, and the measured maximum strain. From $\epsilon_o$ of Fig. 33, from $\sigma_Y$ and $\epsilon_Y$ as determined below, Eqs. (36) and (38) provided a value of $\lambda_N = 1.128$, slightly higher than $\lambda_N = 1.114$ for $N = 8$.

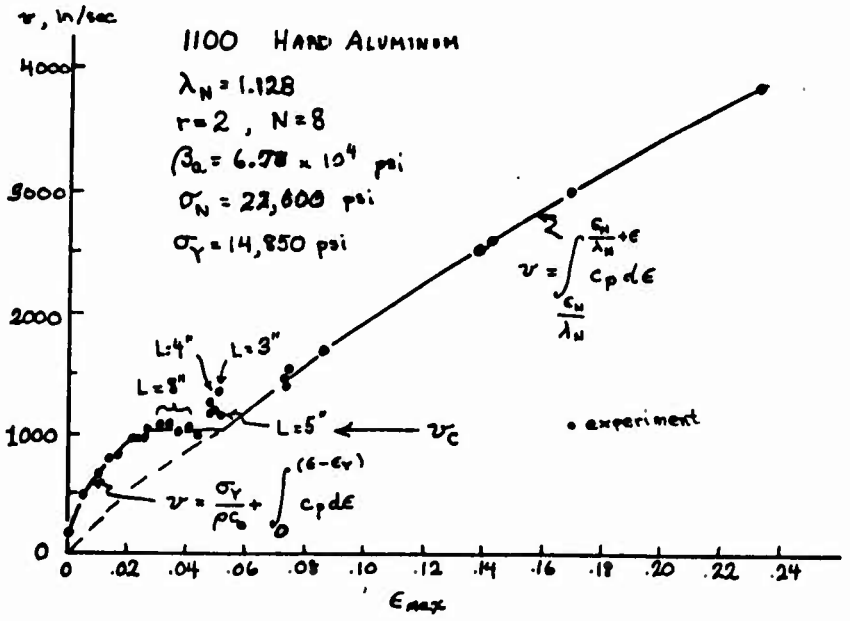


Fig. 34

For the intermediate region, the calculated velocity-strain relation is given by Eq. (52) which includes the contribution from the linear region.

$$v = \int c_p \, d\epsilon = \frac{\sigma_Y}{\rho c_o} + \sqrt{\frac{8}{9}\,\frac{\beta_2}{\rho}}\,(\epsilon - \epsilon_Y)^{3/4} \qquad (52)$$

$$\epsilon \leq \epsilon_c$$

We see that to a velocity of approximately 1000 in/sec, prediction and observation are indeed in correlation. At the strain in the vicinity of 2%, slightly beyond the dynamically determined outer yield surface, a marked change in behavior is observed. This corresponds to a velocity, $v_o$, at the strain $\epsilon_c$ at the outer yield surface, Eq. (53). (See schematic diagram, Fig. 1.)

$$v_c = \frac{\sigma_Y}{\rho c_o} + \sqrt{\frac{8}{9}\,\frac{\beta_2}{\rho}}\,(\epsilon_c - \epsilon_Y)^{3/4} \qquad (53)$$

For all the calculations given here for 1100-H14 aluminum I have used $\lambda_N = 1.128$ and $\beta_a = \lambda_N^{3/2}\beta = 6.7 \times 10^4$ psi; or, $N = 8$, $r = 2$. When $v > v_o$ the behavior is decidedly different from what would be anticipated if one were to continue to integrate the slopes into the totally plastic region. This is an important new discovery based solely in observation, namely, that when $v > v_o$ the maximum strain is determined without reference to either the linear elastic component or that of the intermediate region, Eq. (52).

As I have shown (see reference 8, section 4.30, pp. 646-649) for the fully annealed metal, during plastic wave propagation there is a complete relaxation of the linear elastic portion. For the structural metal alloys, as is seen from impact experiments in 1100-H14 aluminum and 6061-T6 aluminum, when the impact velocity exceeds that of the outer yield surface <u>both</u> the linear region <u>and</u> the intermediate elastic-plastic region cease to appear. All the energy is contained in the totally plastic region. The maximum strain is not given by Eq. (53), but by Eq. (54).

$$v = \sqrt{\frac{9\beta_a}{9\rho}}\left[\left(\epsilon + \frac{\epsilon_N}{\lambda_N}\right)^{3/4} - \left(\frac{\epsilon_N}{\lambda_N}\right)^{3/4}\right] \qquad (54)$$

The maximum plastic strain so calculated exceeds that for $v_c$ when $v$ is only slightly greater than $v_o$ and, depending upon the metal alloy, produces maximum strains from 3 to 8 times greater than would be anticipated if the linear and the intermediate regions had not been completely eliminated.

This "eruptive" plastic deformation obviously is important in the impact of structures, since, in general, even for the high strength metal alloys, the critical velocity $v_o$ is relatively low.

An interesting consequence is that when $v > v_o$, particularly for $N = 0$ or $2$, such as for 7075-T6, 2024-T3, 6061-T6, and 5083-H131 aluminum alloys, and for HF-1, 1095 and maraging steels, the slopes of the response function in the totally plastic region differ only slightly over a range of 10% deformation. If $v$ is sufficiently high to produce, say, 10% maximum strain with $v > v_c$ we may introduce with very small error, the approximations of Eqs. (55) and (56).

$$v = c_{pNa}\,\epsilon/\lambda_N \quad \text{where} \quad c_{pNa} = \sqrt{\frac{\beta_a}{2\rho\left(\frac{\epsilon_N}{\lambda_N}\right)^{1/2}}} \qquad (55)$$

$$v = c_{pN}\,\epsilon \quad \text{where} \quad c_{pN} = \sqrt{\frac{\beta}{2\rho\epsilon_N^{1/2}}} \qquad (56)$$

i.e., $c_{pNa} = \lambda_N c_{pN}$.

For example, in Fig. 34, at an impact velocity of 8000 in/sec (in symmetrical impact a maximum particle velocity of 4000 in/sec), we obtain a maximum strain of .235 from Eq. (54) and a predicted $\epsilon_{max}$ of .221 from the approximation of Eq. (55), a difference of less than 6%. If an estimated average slope at a strain .1 above $\epsilon_N$ is used in Eq. (55), the predicted strain from Eq. (55) is .231, a difference of less than 2% from the complete calculation.

This approximation for $v \geq v_o$ simplifies calculations in structural design problems with high velocity loading.

The calculations for the intermediate region, Eqs. (49) and (52), require that $\sigma_Y$ be known. The first method of determining this value was to examine the initial portion of the strain-time data. From such an analysis of several tests at different impact velocities the value of $\epsilon_Y = 0.00153$ was obtained, which for a modulus $E = 10.2 \times 10^6$ gives at the elastic limit a stress of $\sigma_Y = 15{,}600$ psi.

A more sensitive measure of the end of the linear region has been obtained from an experimental study of the time of contact. In my Handbuch der Physik treatise I traced the study of impact on elastic bars in what I have referred to as the "Boltzmann experiment" from Ludwig Boltzmann's first such measurements in 1881, to those in the present. The Boltzmann experiment consists in the axial impact of identical rods hung in bifilar suspension. The reason for a half century of intensive experimental study of the subject was that Boltzmann, and later Voigt and others, found that for the finite length rods considered, the one-dimensional bar theory of Saint-Venant was not in accord with experiment. One of the parameters extensively studied by many of the participants in the three-quarters of a century controversy on this matter was the time of contact, $t_c$, or the measurement of the length of time the two specimens remain contiguous.

I have included a plot from the experimental results of Sears in 1926 on the duration of impact vs impact velocity, in which it may be seen that even in linear elasticity there is a rapid increase in the time of contact as the impact velocity decreases. (Fig. 35).

On the other hand, during plastic deformation, as I have shown in earlier papers,[2,27] the time of contact increases with increasing impact velocity in the plastic region. A series of experiments were performed in which the duration of contact in the symmetrical impact was determined optically. The impact velocities ranged from values known to be in the linear elastic region to relatively high values which produced plastic deformation. These data are shown as circles in Fig. 36.

SEARS (1912)

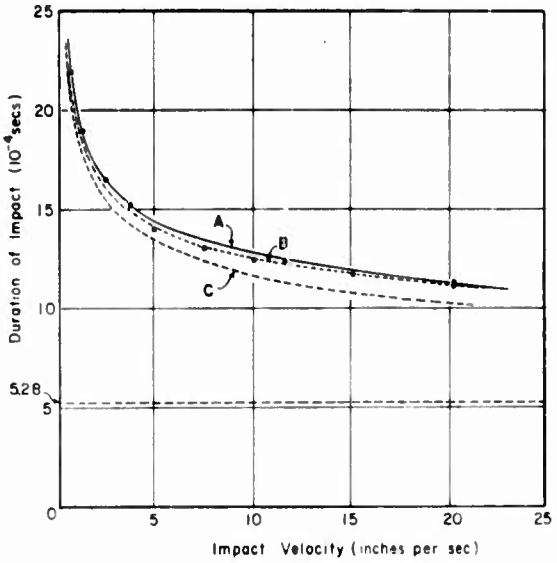


Fig. 35

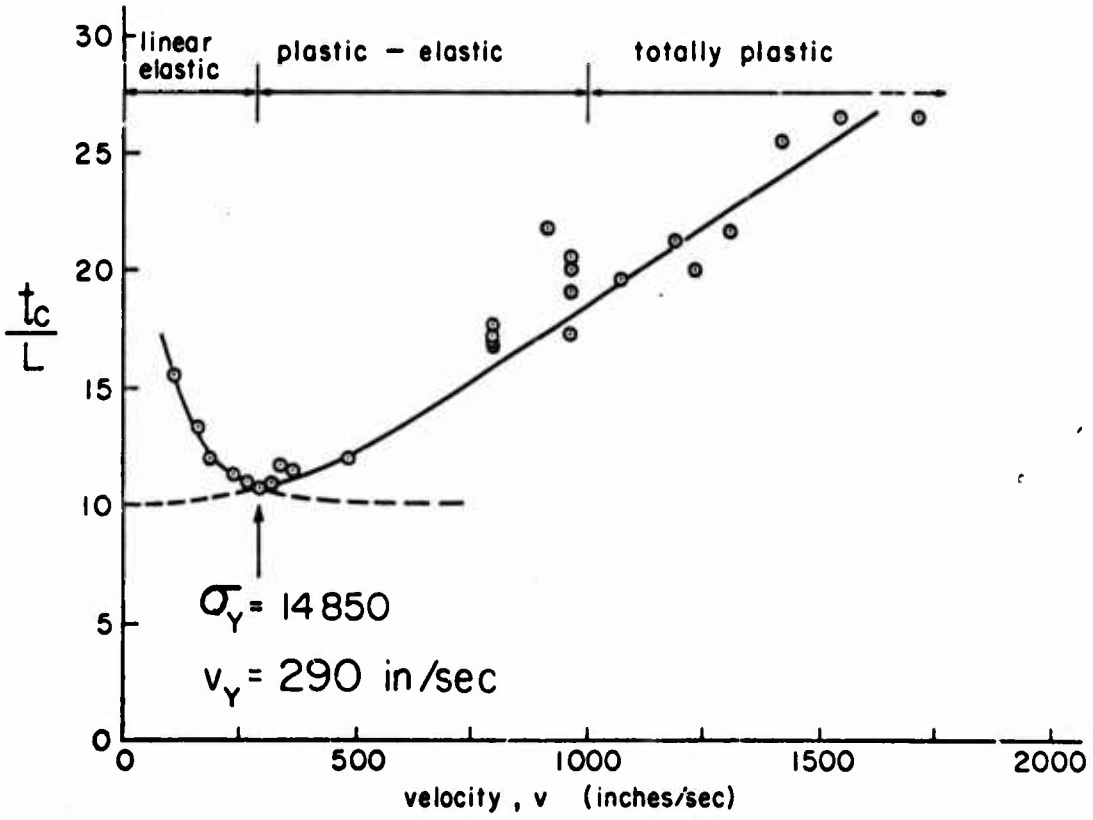


Fig. 36

At a velocity of $v = 2\ 90$ in/sec there is a change from the linear elastic data of Sears (see Fig. 35); the linear region ends (dashed line) and the increasing time of contact of the plastic region begins (solid line). This velocity of $v = 290$ in/sec corresponds to an elastic limit $\sigma_Y = 14{,}850$ psi and a strain $\epsilon_Y = 0.00146$. This is somewhat below the less accurate value, $\epsilon_Y = 0.00153$, obtained from the examination of the initial portion of wave profiles determined from diffraction gratings.

The time of contact data are fairly simply determined, as are the data on the coefficient of restitution, i.e., $e = -\left(\frac{\text{relative velocity after impact}}{\text{relative velocity before impact}}\right)$. The method of obtaining data on the coefficient of restitution has been described in several papers[2,24,27] and consists in allowing a thin uniform light field on one side of a specimen to be interrupted by the colliding specimen. As the hitter specimen approaches the stationary specimen, there is a decrease in light; the calibrated slope of the decrease gives the relative velocity before impact. During impact no light is emitted, and after impact the increase in light on separation of the specimens provides the relative velocity. Monitoring the light with a photomultiplier tube in a properly calibrated experiment, one obtains the result shown in Fig. 37.

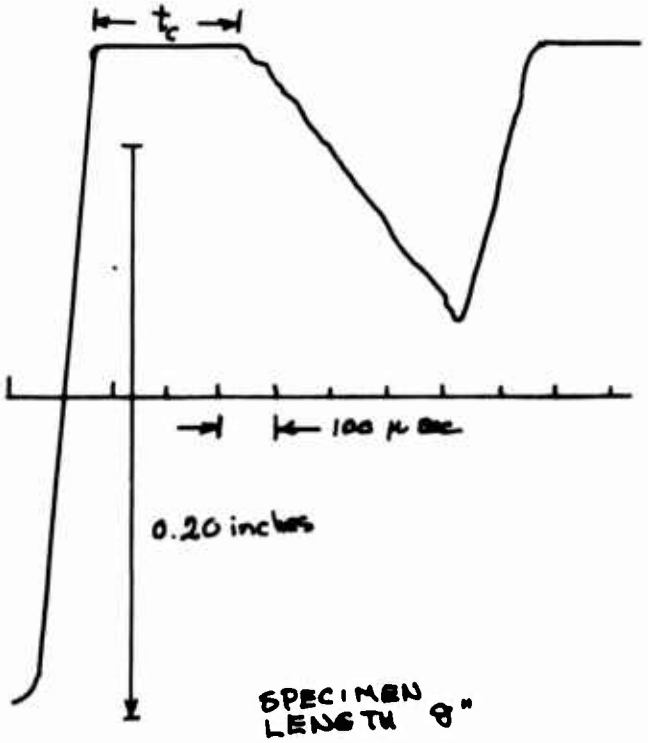


 Fig 37

The coefficient of restitution also is determined by the use of paired contact wires and electronic counters, one pair on the hitter specimen just prior to contact and the other pair on the struck specimen just after impact. The solid line in Fig. 38 is the early calculation for $e$ which, as is shown, may be extended to determine the coefficient of restitution of a hardened metal alloy. In those same papers I showed purely empirically that it also was possible to calculate the time of contact for the fully annealed metal at all impact velocities. In 1970 in a lengthy computer calculation with N. Cristescu[26] this empirical prediction was found to be consistent with my earlier prediction, Eq. (59).

$$t_c = \frac{L}{C_p\left(\frac{\sigma_{max}}{2}\right)} + \frac{L}{C_o} \qquad \text{where L = length of specimen} \qquad (59)$$

For the metal alloy, however, the behavior of the specimens at the time of contact does not correlate with Eq. (59), at least for maximum particle velocities below 2000 in/sec in 1100-H14 aluminum, as an inspection of Fig. 39 reveals.

In Fig. 39 the measured time of contact for the fully annealed metal is compared with that for the metal alloy. The solid line for the former is the prediction from Eq. (59). The fully annealed metal was 1100 aluminum annealed for two hours at 1100°F and furnace cooled, while the metal alloy was the same solid, aluminum, tested in the as-received condition.

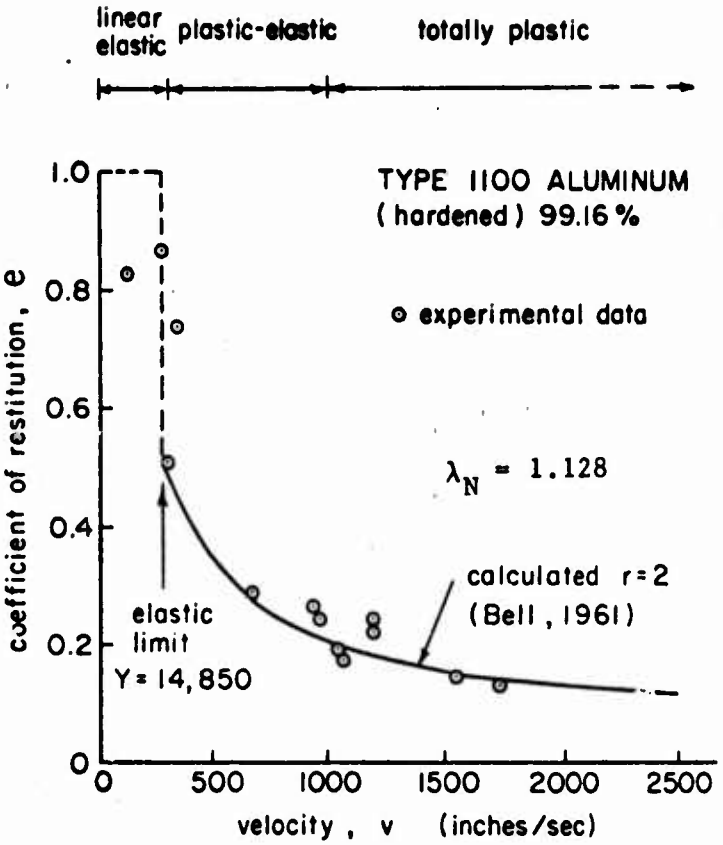
linear elastic
plastic-elastic
totally plastic
TYPE 1100 ALUMINUM
(hardened) 99.16 %
⊙ experimental data
$\lambda_N$ = 1.128
calculated r=2
(Bell, 1961)
elastic limit
Y = 14,850
coefficient of restitution, e
velocity, v (inches/sec)
1.0
0.8
0.6
0.4
0.2
0
0
500
1000
1500
2000
2500

Fig 38

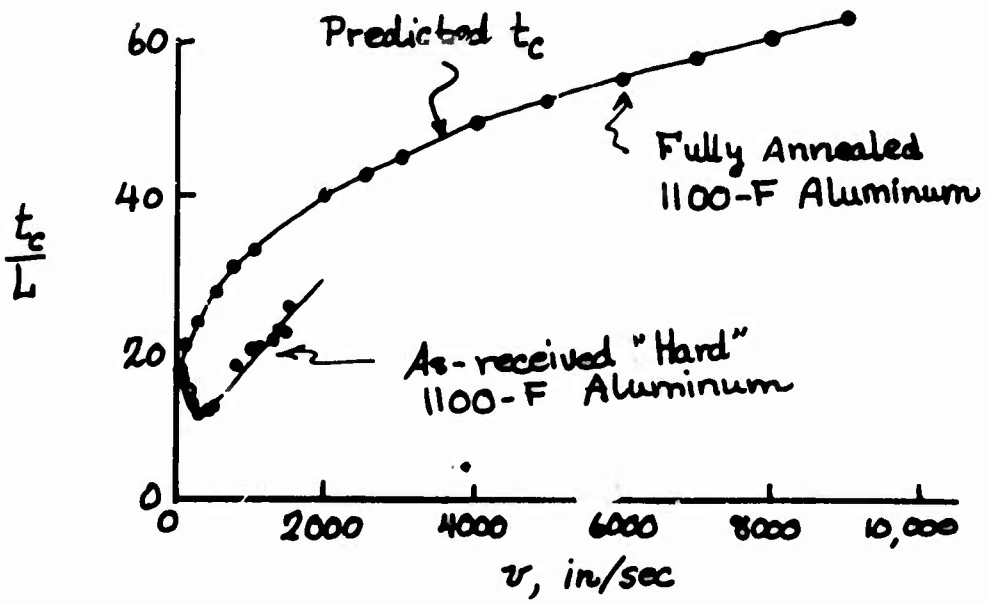
Predicted $t_c$
Fully Annealed
1100-F Aluminum
As-received "Hard"
1100-F Aluminum
$\frac{t_c}{L}$
60
40
20
0
0
2000
4000
6000
8000
10,000
v, in/sec

Fig. 39

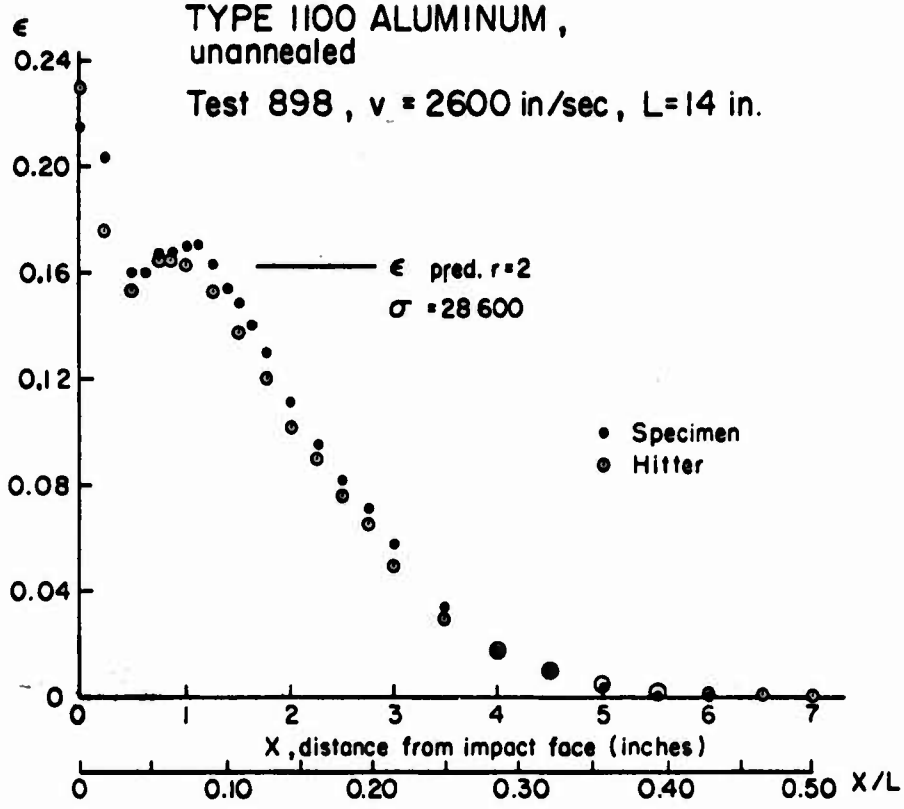
TYPE 1100 ALUMINUM,
unannealed
Test 898, v = 2600 in/sec, L=14 in.
ε
0.24
0.20
0.16
0.12
0.08
0.04
0
ε pred. r=2
σ =28 600
Specimen
Hitter
0 1 2 3 4 5 6 7
X, distance from impact face (inches)
0 0.10 0.20 0.30 0.40 0.50 X/L

Fig 40

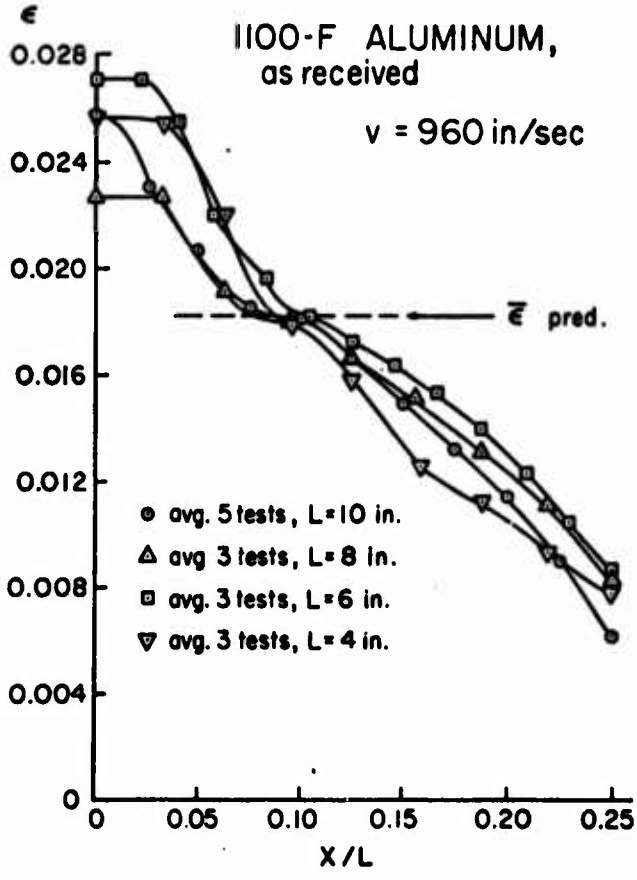
ε
1100-F ALUMINUM,
as received
v = 960 in/sec
0.028
0.024
0.020
0.016
0.012
0.008
0.004
0
ε̄ pred.
avg. 5 tests, L=10 in.
avg 3 tests, L=8 in.
avg. 3 tests, L=6 in.
avg. 3 tests, L=4 in.
0 0.05 0.10 0.15 0.20 0.25
X/L

Fig 41

That the unloading problem indeed is complicated in the metal alloy may be seen from a comparison of the measured permanent deformation of specimens of the same length subjected to different impact velocities. In Fig. 40 is shown the permanent strain distribution determined for a specimen in symmetrical impact, having a maximum particle velocity of 2600 in/sec . Before and after measurements were made of the diameters and the lengths of the specimens. Assuming that the axial strain is twice the radial strain, as is shown in the diffraction grating measurements of surface angle referred to above, and as is implied in Eq. (1), the maximum strain for this impact velocity is, in fact, that which is measured in the immediate vicinity of the impact face.

In Fig. 41 is shown the permanent strain distribution for specimens of 1100-H14 hard aluminum. The penetration of the plastic deformation is as X/L for specimens of different lengths having the same impact velocity. This observation is consistent with the result obtained from diffraction grating measurements, namely that viscoplasticity effects are negligible in this metal alloy. It demonstrates, too, that for the hardened metal, as had been found earlier for the fully annealed metal, the unloading phenomenon from free end reflection is also as X/L, i.e., non-viscous.

Approximately fifteen years ago, for the fully annealed metals, I made an extensive study of the energy balance during, and at the end of impact. As was shown at the time, a correlation of better than 2% could be obtained.[2,24,25]

A more interesting illustration, historically and practically, and but one example among many which I have found for work hardened metal alloys employing the theory of plasticity described above, is the following. Two 1100 F, as-received hard bars in free flight, with a symmetrical impact at a maximum particle velocity v of 1350 in/sec (i.e., $v_H$ = 2700 in/sec), gave a maximum strain of 6% near the impact face, a distribution of final permanent strain as shown in Fig. 42, and a pre-impact kinetic energy of 3560 in.lbs.

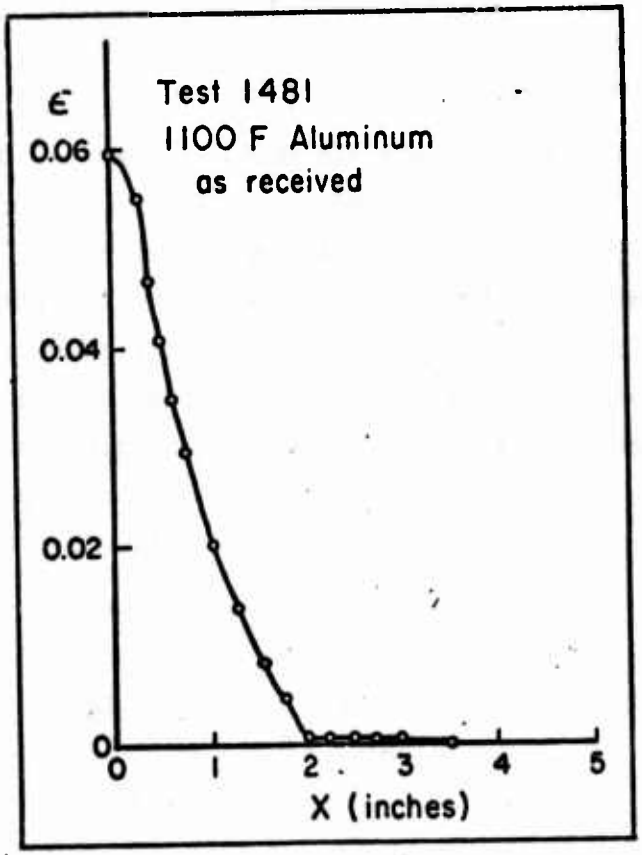


Fig. 42

Integration of Eq. (36) provided a measure of the energy of deformation until the strain reached its value at the outer yield surface, i.e., at 1.5% plastic strain; and integration of Eq. (37) in the same manner provided such a measure for the totally plastic

deformation from the outer yield surface to the maximum strain of 6%. The diameter of the bars was 0.990 inches and the initial length was 5.0 inches. From the data of Fig. 43 and the above integration, the distribution of the energy of post-impact deformation of Fig. 44 was determined.

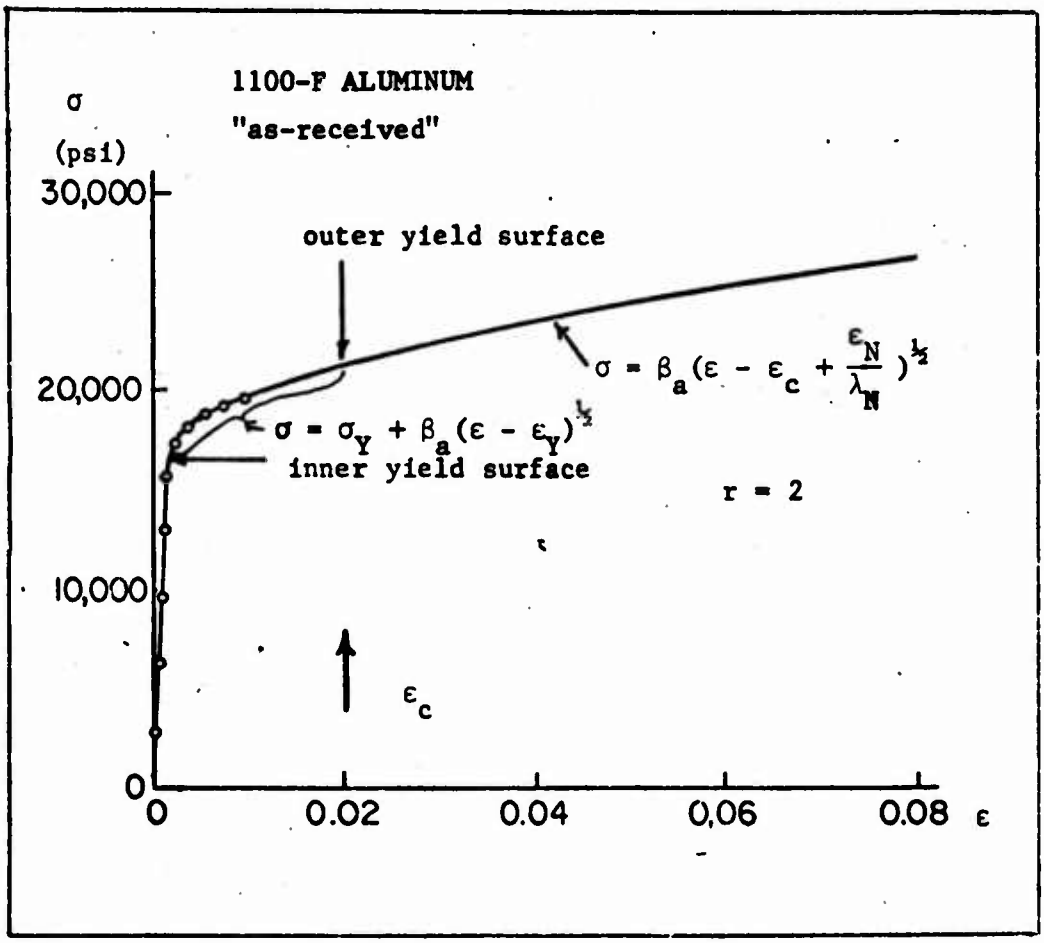


Fig. 43

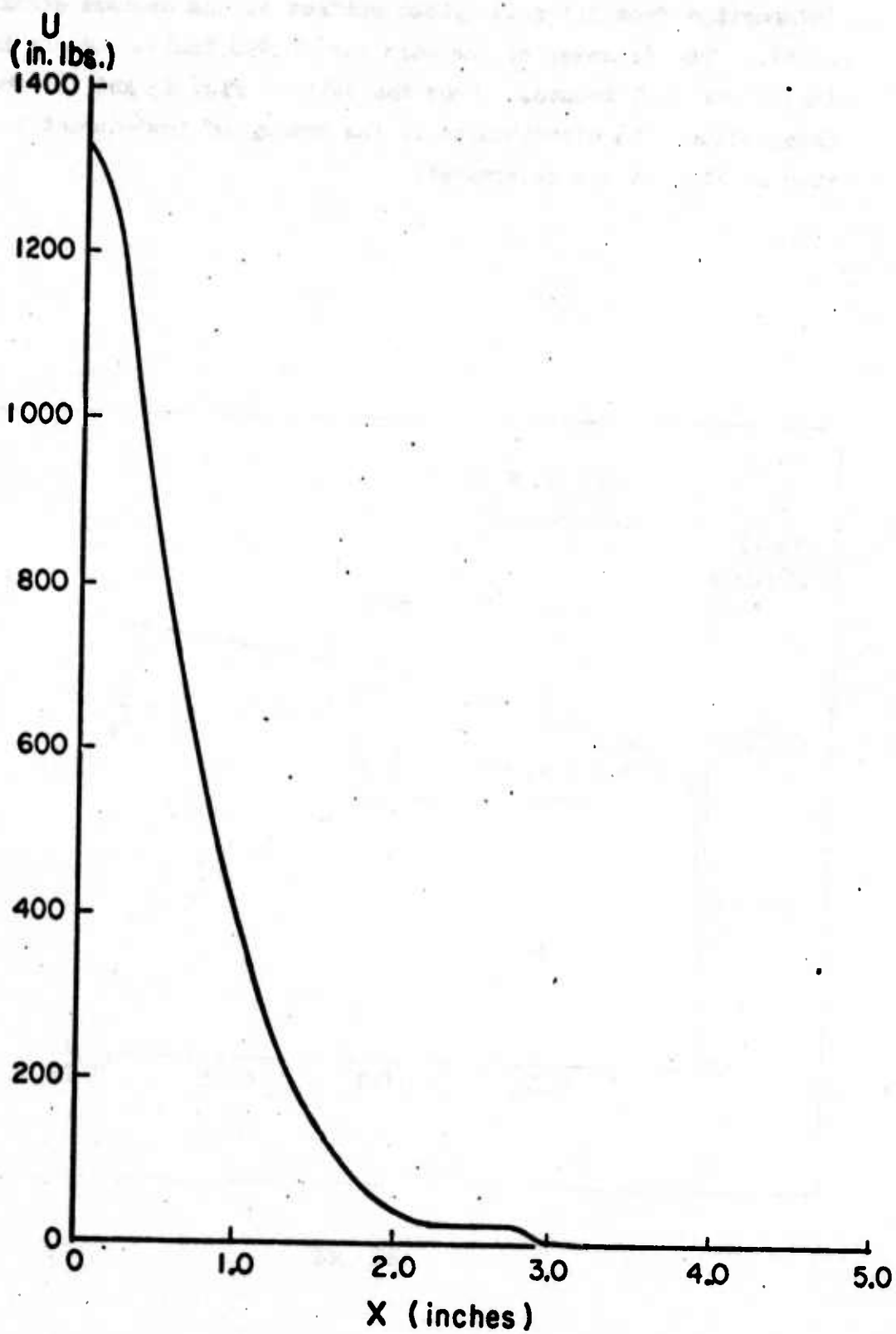


Fig. 44

Summing this deformation energy provided a value of 848 in.lbs. in each specimen for a total permanent deformation energy of 1696 in.lbs. A measured coefficient of restitution of e = 0.17 was obtained from electrically monitoring the velocity of the projectile just prior to impact and the velocity of the struck specimen just after impact. This measurement was independently cross-checked for both specimens from the optical measurement of the time of contact, $t_o$ . The final velocity of the projectile was 1120 in/sec and of the struck bar 1580 in/sec, giving final total kinetic energies of 614 in.lbs. and 1220 in.lbs., respectively.

Summing the post-impact energies, we find a total energy of 3530 in.lbs., which may be compared with the pre-impact total kinetic energy given above, 3560 in.lbs., a difference of less than 1%.

This resolution of a 19th century aspiration in dynamic plasticity is of historical interest in emphasizing the difficulties of realizing such a dream before it was possible to have mid-20th century developments in the experiment and theory of dispersive waves of finite amplitude.

Fourteen years ago I showed[24,27] from experiment that the Lee theory[28] of unloading waves described the unloading process for the fully annealed metal. That the same theory is applicable to the structural metal alloy is indicated by the illustration which follows.

For the Lee theory, the reflected unloading wave moving at linear elastic wave speeds is absorbed on encountering the slower moving plastic wave. In Lee's Eq. (60) for the fully annealed metal, $\sigma_B$ designates the stress before intersection; $\sigma_A$ is the stress after the intersection; Y is the elastic limit; $\rho$ is the mass density; $c_o$ is the elastic wave speed; and $v_B$ is the particle velocity for the plastic component just prior to intersection of the two wave fronts.

$$\sigma_A - \sigma_B = \frac{2Y - [\rho c_o v_B - \sigma_B]}{2} \qquad (60)$$

For the structural metal alloy, Eq. (60) becomes Eq. (61).

$$\sigma_A - \sigma_B = Y - \tfrac{1}{2}\left(\lambda_N \rho c_o v_B - \sigma_B\right) \qquad (61)$$

For complete absorption, $2Y = \left(\lambda_N \rho c_o v_B - \sigma_B\right)$.

No computer calculations using the Lee theory have as yet been made for the structural metal alloys such as the investigation of fully annealed aluminum by Cristescu and Bell.[23] However, we note that for 1100F "as-received" aluminum with $Y = 14850$ psi, $\lambda_N = 1.128$, $\beta_a = 6.7 \times 10^4$ psi, and $\sigma_N = 22600$ psi as given above, Eq.(61) provides for $\sigma_A = \sigma_B$, i.e., complete absorption, a velocity for the totally plastic region of $v_B = 1016$ in/sec and $\sigma_B = 28{,}934$ psi. This corresponds to a strain in Fig. 45 of 0.052 at the end of the horizontal plateau. A calculation at the end of the intermediate region reveals that complete absorption has not yet occurred. Thus, for all impact velocities below $v_c$, as may be seen in Fig. 45, the partially absorbed unloading wave reaches the impact face at a time of $2L/c_o$. In the totally plastic region the unloading is delayed by the complete absorption of the initial reflected elastic wave front.

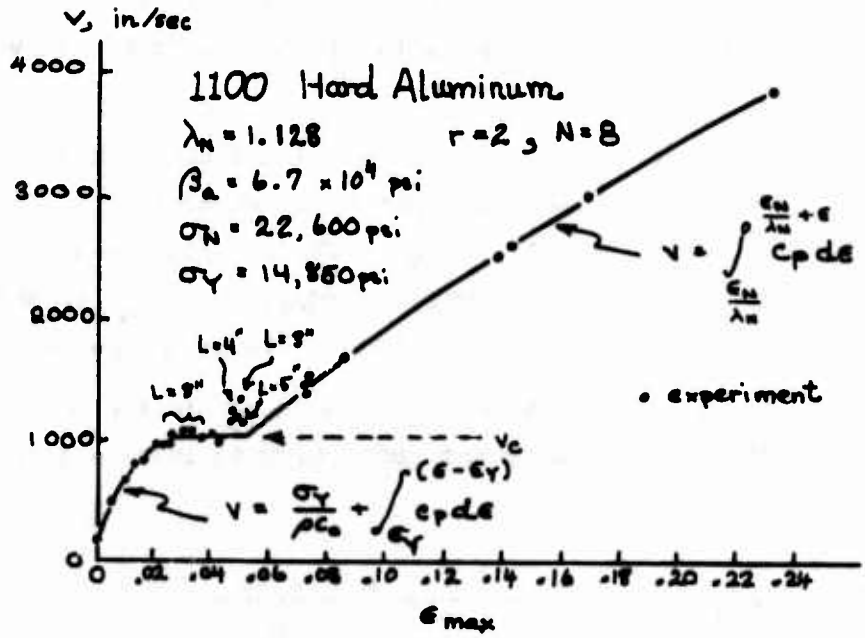


Fig. 45

The problem of estimating the absorption of energy becomes more complicated when the impacted structure is in contact with other metals which either remain elastic or, when plastic, are of some material for which the parabola coefficients are different on either side of the interface contact.

In such a case, the plastic wave in a very complex non-linear manner is reflected as additional loading back into the oncoming original wave. The total amount of plastic deformation is increased, as are the duration of loading and, through higher total stresses and plastic strains, the probability of dynamic buckling and the accompanying large distortion of the member. Unloading will not occur until the transmitted wave in the adjacent member, whether plastic or elastic, encounters a free surface or surfaces, and reflects a component of the unloading wave across the interface.

In a series of measurements of various types performed several years ago, which I have not found time to publish, the details of this type of behavior are outlined. Although this sort of study has not yet been extended to the work-hardened metals, it seems quite probable that such a projection is feasible.

If the struck specimen is not a cylinder of equal diameter throughout its length, but has a section of larger or smaller diameter occurring at some distance along its length, the problem again is complicated beyond the simple situation. If the second section is smaller, the reflected wave unloads the plastic wave in the first section and produces much larger plastic deformation in the second. However, with the reverse situation, the reflected wave provides additional loading in the initial section.

Several years ago I examined this latter situation experimentally in connection with a series of measurements on dynamic plastic buckling, which also are to be published in the near future. The diameters of specimens of solid cylinders were changed, but the impact velocity was kept constant. As the diameters decreased, the distance from the impact face at which buckling occurred also decreased. This behavior could be observed by means of diffraction grating measurements during the propagation of the waves, and also by

observing the deformed specimens after impact. When I studied specimens which had the same total length but had an increase in diameter at some position approximately midway along the specimen, the distance along the specimen at which buckling began was unaltered yet the magnitude of the angular distorsion observed both during impact and after impact was greatly increased.

A comparison of post-impact results is shown in Fig. 46 for three experiments in annealed aluminum. The specimens were 0.483 inches in diameter and 16 inches long, and the projectile velocity was $v_H$ = 1600 in/sec. In Fig. 46, the calculated point of dynamic buckling is shown by dashed lines.

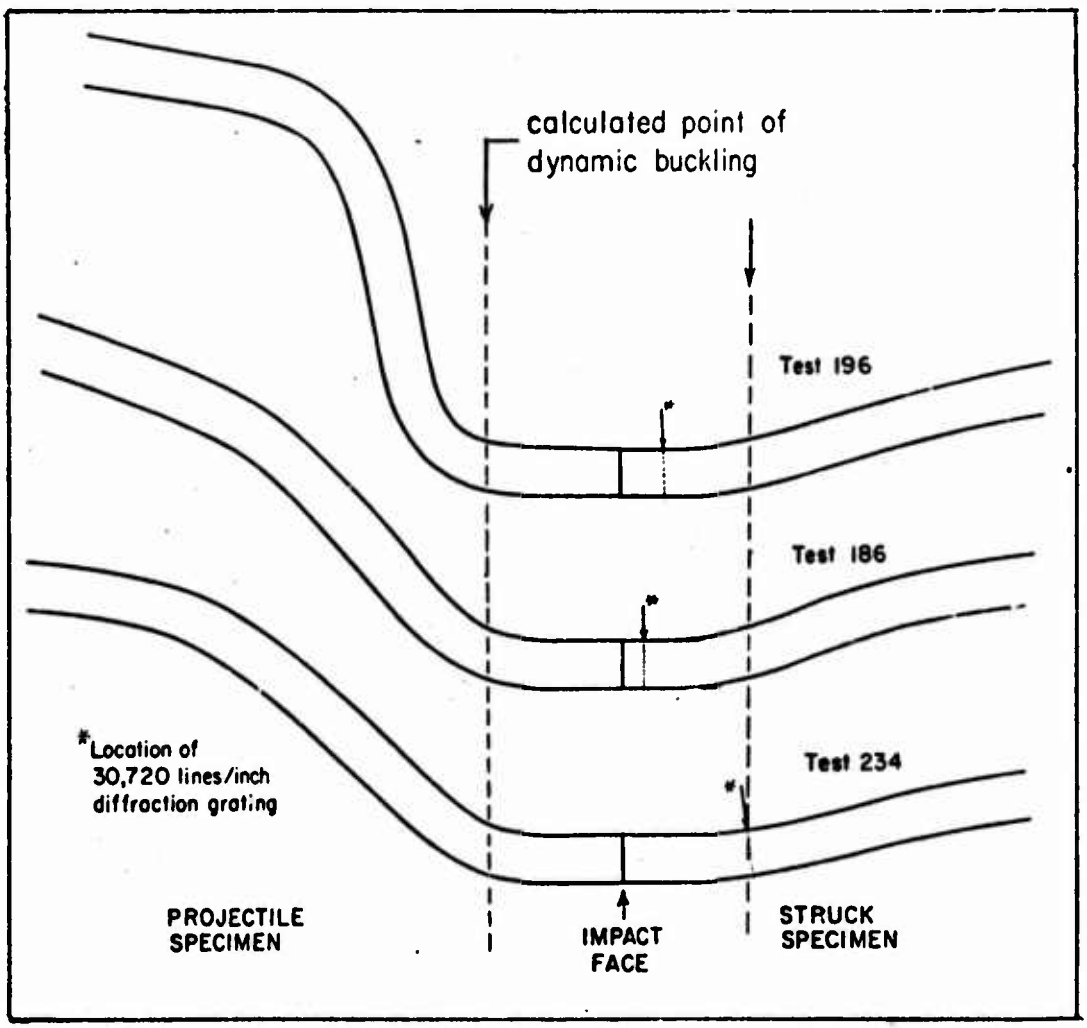


Fig. 46

I found that the distance from the impact face at which such buckling began was determinable from the introduction of the Engesser tangent modulus into the Euler buckling formula for fixed ends in each specimen. In this instance $d\sigma/d\epsilon = \rho c_p^2$. The tangent modulus is considered in terms of the wave speed, $c_p$, of the maximum stress from the parabolic response function I earlier had found to govern the dynamic plastic behavior. Experimental results in 0.483 inch, 0.842 inch, and 1.000 inch diameter aluminum specimens were used to predict accurately the point of the beginning of the small buckling observed in specimens of annealed copper 1.000 inches in diameter, 20 inches long. In these calculations the length of the specimen is important because the amount of observed angular distortion depends upon the duration of impact, or the time of contact, which in turn depends upon the unloading waves and thus the length of the specimen.

The place where such buckling begins depends only upon the impact velocity or the maximum stress and its corresponding dynamic tangent modulus as given by the appropriate parabolic response function. The two experiments which have been performed with an awareness of this background in the fully annealed solid are insufficient to warrant declaring that the dynamic buckling of structural metals in the as-received condition is equally amenable to such an analysis, but the experiments are consistent with the anticipation that this indeed will be the case.

## Summary

In the above it has been shown from an analysis of approximately 200 quasi-static and impact tests on 16 metal alloys that a new, unified theory of plasticity is capable of defining the details of large deformation for arbitrary loading paths in the two-dimensional domain. For simple compression it is extendible to the high strain rates of plastic wave propagation. The new theory is based on the discovery of a distribution of

stable material states for the metal alloy, intimately related to the second-order transition structure I discovered many years ago and applied to the continuing deformation of the single crystal and the fully annealed polycrystal.

A further discovery in this work is that there exist two regions of deformation: the intermediate and the totally plastic regions bounded by an outer yield surface. Detailed constitutive statements are provided for both regions so that strain, irrespective of whether or not the arbitrary loading path is proportional or non-proportional among the stress components, may be given accurately from zero strain to ultimate stress.

Furthermore, in dynamic plasticity when the impact velocity is sufficiently high so that the deformation reaches the outer yield surface, I have discovered that there is an "eruptive" plastic deformation for which maximum strains may be from three to eight times higher than anticipated from the measurement of slopes of the response function in the linear elastic and in the intermediate elastic-plastic regions.

The parabola coefficients contain the temperature dependence and material dependence in the same manner as had been shown earlier for the fully annealed metals for which a class of 27 metals were seen to have unified response functions, i.e., given known parameters such as the melting point and the shear modulus at the zero point, one may be predicted from the other.

The uniform stress distributions employed in the experiments discussed here have provided the constitutive equations for the engineering analysis of structural problems. In such problems when stress and strain are distributed in the solid, and the zones corresponding to the inner and the outer yield surfaces are present since the entire solid does not arrive at theoretical values simultaneously, the non-linear problems in applied mechanics will,

of course, depend upon the successful application of these results to computer analyses.

Now that an experimentally based general theory of plasticity provides a set of reliable constitutive equations for important structural metal alloys, the main problems lie in the field of applied mechanics in terms of proper computer analyses of problems in distributed stress which contains regions bounded by two yield surfaces and two regions of plastic deformation. Both the regions of plastic deformation, and their boundary at the outer yield surface, now are well understood.

## References


1. James F. Bell, "Study of Initial Conditions in Constant Velocity Impact," Journal of Applied Physics, Vol. 31, No. 12, pp. 2188-2195, (1960).

2. James F. Bell, "Experimental Study of the Interrelation between the Theory of Dislocations in Polycrystalline Media and Finite Amplitude Wave Propagation in Solids," Journal of Applied Physics, Vol. 32, No. 10, pp. 1982-1993, (1961).

3. James F. Bell,"Experiments on Large Amplitude Waves in Finite Elastic Strain," Proceedings, IUTAM Symposium on Second-Order Effects in Elasticity, Plasticity, and Fluid Dynamics, Haifa, Israel, pp. 173-186. (1962) (Oxford-Paris-NY: Pergamon Press:1964)

4. James F. Bell and John H. Suckling, "The Dynamic Overstress and the Hydrodynamic Transition Velocity in the Symmetrical Free-Flight Plastic Impact of Annealed Aluminum," Proceedings, 4th U. S. National Congress of Applied Mechanics, pp. 877-883, (1962).

5. James F. Bell, "The Initiation of Finite Amplitude Waves in Annealed Metals," Proceedings, IUTAM Symposium on Stress Waves in Anelastic Solids, Brown University, Providence, Rhode Island, pp. 166-182. (1943) (Berlin-Göttingen-Heidelberg: Springer,1964)

6. Hahngue Moon, "An Experimental Study of the Outer Yield Surface and of the Incremental Response Function in the Totally Plastic Region for Annealed Polycrystalline Aluminum," Ph.D dissertation The Johns Hopkins University, Baltimore, Maryland (1973)

7. James F. Bell, The Physics of Large Deformation of Crystalline Solids. Springer Tracts in Natural Philosophy, Vol. 14. Berlin-Heidelberg-New York: Springer (1968).

8. James F. Bell, "The Experimental Foundations of Solid Mechanics," Handbuch der Physik, Vol. VIa/1 . Springer-Verlag, Berlin-Heidelberg-New York, (1973).

9. Evan A. Davis, "Increase of Stress with Permanent Strain and Stress-Strain Relations in the Plastic State for Copper under Combined Stresses," Journal of Applied Mechanics, Vol. 10, A-187 to A-196 (December, 1943).

10. Evan A. Davis, "Yielding and Fracture of Medium-Carbon Steel under Combined Stress," Journal of Applied Mechanics (Transactions of the American Society of Mechanical Engineers) Vol. 12, No. 1, A-13 to A-24 (March, 1945)

11. Sir Geoffrey Ingram Taylor, "Plastic Strain in Metals," Journal of the Institute of Metals, Vol. 62, pp. 307-324 (1938); (Also in The Scientific Papers of...Taylor, Vol. I, paper No. 27, pp. 424-438.(1958)

12. Sir Geoffrey Ingram Taylor, "Analysis of Plastic Strain in a Cubic Crystal," Stephen Timoshenko 60th Anniversary Volume, pp. 218-224. NY: Macmillan (1938)
(Also in collected papers of Taylor, paper No. 28, pp. 439-445)

13. Sir Geoffrey Ingram Taylor, "Strains in Crystalline Aggregates," Proceedings of the Colloquium on Deformation and Flow of Solids, pp. 3-12, Madrid, Spain (1955). (Springer: 1956). (Also in collected papers of Taylor, paper No. 41, pp. 586-593).

14. Sir Geoffrey Ingram Taylor, The Scientific Papers of Sir Geoffrey Ingram Taylor, Vol. I: Mechanics of Solids, edited by George K. Batchelor, at the University Press, Cambridge, England (1958).

15. J. F. W. Bishop and Rodney Hill, "A Theoretical Derivation of the Plastic Properties of Polycrystalline Face-Centred Metals," Philosophical Magazine, Vol 42, pp. 1298-1307 (1951).

16. J. F. W. Bishop and Rodney Hill, "A Theory of Plastic Distortion of a Polycrystalline Aggregate under Combined Stresses," Philosophical Magazine, Vol. 42, pp. 414-427 (1951).

17. Thomas H. Dawson, "The Plastic Deformation of Crystalline Aggregates," Ph.D dissertation, The Johns Hopkins University, Baltimore, Maryland (1968). (and see: Thomas H. Dawson, "The Mechanics of Crystalline Aggregate Deformation," International Journal Mech. Sci., Vol. 12, pp. 197-204 (1970).

18. James F. Bell and W. Meade Werner, "Applicability of the Taylor Theory of the Polycrystalline Aggregate to Finite Amplitude Wave Propagation in Annealed Copper," Journal of Applied Physics, Vol. 33, No. 8, pp. 2416-2425 (1962).

19. James F. Bell, "Single Temperature-Dependent Stress-Strain Law for the Dynamic Plastic Deformation of Annealed Face-Centered Cubic Metals," Journal of Applied Physics, Vol. 34, No. 1, pp. 134-141 (January, 1963).

20. James F. Bell, "A Generalized Large Deformation Behaviour for Face-Centred Cubic Solids—High Purity Copper," Philosophical Magazine, Vol. 10, No. 103, pp. 107-126 (1964).

21. James F. Bell, "Generalized Large Deformation Behaviour for Face-Centred Cubic Solids: Nickel, Aluminum, Gold, Silver, and Lead," Philosophical Magazine, Vol. 11, No. 114, pp. 1135-1156 (1965).

22. D. L. Holt, S. G. Babcock, S. J. Green, and C. J. Maiden, "The Strain-Rate Dependence of the Flow Stress in Some Aluminum Alloys," Transactions Quarterly, Vol. 60, No. 2, pp. 152-159 (June, 1967).

23. T. Nicholas and J. D. Campbell, Experimental Mechanics, Vol. 12, No. 10, pp. 441-447 (1972).

24. James F. Bell, "An Experimental Study of the Unloading Phenomenon in Constant Velocity Impact," Journal of the Mechanics and Physics of Solids, Vol. 9, pp. 1-15 (1961)

25. James F. Bell, "Technological Perspectives from Two Decades of Fundamental Research in Dynamic Plasticity," U. S. Army Ballistic Research Laboratory Contract Report No. 184, Oct 74.

26. Nicolae Cristescu and James F. Bell, "On Unloading in the Symmetrical Impact of Two Aluminum Bars," Battelle Memorial Institute Symposium (October, 1969); Proceedings, Columbus, Ohio, pp. 397-421 (1970).

27. James F. Bell, "Further Experimental Study of the Unloading Phenomenon in Constant Velocity Impact," Journal of the Mechanics and Physics of Solids, Vol. 9, pp. 261-278 (1961).

28. E. H. Lee, "A Boundary Value Problem in the Theory of Plastic Wave Propagation," Quarterly of Applied Mathematics, Vol. 10, No. 4, pp. 335-346 (1953).

DISTRIBUTION LIST

| No. of Copies | Organization |
|---|---|
| 2 | Commander<br>Defense Documentation Center<br>ATTN: DDC-TCA<br>Cameron Station<br>Alexandria, VA 22314 |
| 1 | Director<br>Defense Advanced Research Projects Agency<br>ATTN: Tech Info<br>1400 Wilson Boulevard<br>Arlington, VA 22209 |
| 2 | Commander<br>US Army Materiel Command<br>ATTN: AMCDMA/Mr. N. Klein<br>Mr. J. Bender<br>5001 Eisenhower Avenue<br>Alexandria, VA 22333 |
| 1 | Commander<br>US Army Materiel Command<br>ATTN: AMCRD/BG H. A. Griffith<br>5001 Eisenhower Avenue<br>Alexandria, VA 22333 |
| 1 | Commander<br>US Army Materiel Command<br>ATTN: AMCRD-T<br>5001 Eisenhower Avenue<br>Alexandria, VA 22333 |
| 1 | Commander<br>US Army Materiel Command<br>ATTN: AMCRD-R<br>5001 Eisenhower Avenue<br>Alexandria, VA 22333 |
| 1 | Commander<br>US Army Materiel Command<br>ATTN: AMCRD-WN-RE/<br>Mr. Corrigan<br>5001 Eisenhower Avenue<br>Alexandria, VA 22333 |
| 1 | Commander<br>US Army Aviation Systems Command<br>ATTN: AMSAV-E<br>12th and Spruce Streets<br>St. Louis, MO 63166 |
| 1 | Director<br>US Army Air Mobility Research and Development Laboratory<br>Ames Research Center<br>Moffett Field, CA 94035 |
| 2 | Commander<br>US Army Electronics Command<br>ATTN: AMSEL-RD<br>AMSEL-HL-CT/S. Crossman<br>Fort Monmouth, NJ 07703 |
| 2 | Commander<br>US Army Missile Command<br>ATTN: AMSMI-R<br>AMSMI-RBL<br>Redstone Arsenal, AL 35809 |
| 1 | Commander<br>US Army Tank Automotive Command<br>ATTN: AMSTA-RHFL<br>Warren, MI 48090 |
| 2 | Commander<br>US Army Mobility Equipment Research & Development Center<br>ATTN: Tech Docu Cen, Bldg. 315<br>AMSME-RZT<br>Fort Belvoir, VA 22060 |
| 1 | Commander<br>US Army Armament Command<br>Rock Island, IL 61202 |
| 1 | Commander<br>US Army Electronic Proving Ground<br>ATTN: Tech Lib<br>Fort Huachuca, AZ 85613 |

DISTRIBUTION LIST

| No. of Copies | Organization |
|---|---|
| 1 | Commander<br>US Army Watervliet Arsenal<br>ATTN: Dr. F. Schneider<br>Watervliet, NY 12189 |
| 1 | Commander<br>US Army Harry Diamond Labs<br>ATTN: AMXDO-TI<br>2800 Powder Mill Road<br>Adelphi, MD 20783 |
| 5 | Commander<br>US Army Materials and Mechanics Research Center<br>ATTN: AMXMR-ATL<br>AMXMR-T/J. Bluhm<br>AMXMR-XH/J. Dignum<br>AMXMR-XO/E. Hagge<br>AMXMR-XP/Dr. J. Burke<br>Watertown, MA 02172 |
| 1 | Commander<br>US Army Natick Laboratories<br>ATTN: AMXRE/Dr. D. Sieling<br>Natick, MA 01762 |
| 1 | Deputy Assistant Secretary of the Army (R&D)<br>Department of the Army<br>Washington, DC 20310 |
| 1 | HQDA (DAMA-ARP-P/Dr. Watson)<br>Washington, DC 20310 |
| 1 | HQDA (DAMA-MS)<br>Washington, DC 20310 |
| 1 | Commander<br>US Army Research Office<br>P.O. Box 12211<br>Research Triangle Park, NC 27709 |
| 1 | Commander<br>US Army Ballistic Missile Defense Systems Command<br>ATTN: SENSC/Mr. Davidson<br>P.O. Box 1500<br>Huntsville, AL 35804 |
| 1 | Director<br>US Army Ballistic Missile Defense Systems Office<br>1320 Wilson Boulevard<br>Arlington, VA 22209 |
| 1 | Director<br>US Army Advanced BMD Technology Center<br>ATTN: CRDABH-5/Mr. W. Loomis<br>P.O. Box 1500<br>Huntsville, AL 35809 |
| 1 | Commander<br>US Army War College<br>ATTN: Lib<br>Carlisle Barracks, PA 17013 |
| 1 | Commander<br>US Army Command and General Staff College<br>ATTN: Archives<br>Fort Leavenworth, KS 66027 |
| 1 | Mathematics Research Center<br>US Army<br>University of Wisconsin<br>Madison, WI 53706 |
| 3 | Commander<br>US Naval Air Systems Command<br>ATTN: AIR-604<br>Washington, DC 20360 |

DISTRIBUTION LIST

| No. of Copies | Organization |
|---|---|
| 3 | Commander<br>US Naval Ordnance Systems Command<br>ATTN: ORD-0632<br>ORD-035<br>ORD-5524<br>Washington, DC 20360 |
| 1 | Office of Naval Research<br>Department of the Navy<br>ATTN: Code 402<br>Washington, DC 20360 |
| 1 | Commander<br>US Naval Surface Weapons Center<br>ATTN: Code Gr-9/Dr. W. Soper<br>Dahlgren, VA 22448 |
| 1 | Commander and Director<br>US Naval Electronics Lab<br>ATTN: Lib<br>San Diego, CA 92152 |
| 3 | Director<br>US Naval Research Laboratory<br>ATTN: Code 5270/<br>Mr. F. MacDonald<br>Code 2020/Tech Lib<br>Code 7786/J. Baker<br>Washington, DC 20360 |
| 1 | AFATL (DLR)<br>Eglin AFB, FL 32542 |
| 1 | AFATL (DLRD)<br>Eglin AFB, FL 32542 |
| 1 | AFATL (DLRV)<br>Eglin AFB, FL 32542 |
| 1 | RADC (EMTLD, Lib)<br>Griffiss AFB, NY 13440 |
| 1 | AUL (3T-AUL-6-118)<br>Maxwell AFB, AL 36112 |
| 1 | AFML (Mr. J. Halpin)<br>Wright-Patterson AFB, OH 45433 |
| 1 | Director<br>Environmental Science Service Administration<br>US Department of Commerce<br>Boulder, CO 80302 |
| 1 | Director<br>Jet Propulsion Laboratory<br>ATTN: Lib (TDS)<br>4800 Oak Grove Drive<br>Pasadena, CA 91103 |
| 1 | Director<br>National Aeronautics and Space Administration<br>Manned Spacecraft Center<br>ATTN: Lib<br>Houston, TX 77058 |
| 1 | Bechtel Power Corporation<br>ATTN: Dr. Akhtar Khan<br>P.O. Box 607<br>15740 Shady Grove Road<br>Gaithersburg, MD 20760 |
| 1 | Dupont Experimental Labs<br>ATTN: Mr. J. Lupton<br>Wilmington, DE 19801 |
| 2 | President<br>General Research Corporation<br>ATTN: Lib<br>Arlington, VA 22209 |
| 7 | Sandia Laboratories<br>ATTN: Mr. L. Davison<br>Div 5163<br>Dr. C. Harness<br>H. J. Sutherland<br>Code 5133<br>Code 1721<br>Dr. P. Chen<br>Albuquerque, NM 87115 |

DISTRIBUTION LIST

| No. of Copies | Organization |
|---|---|
| 1 | Troydyne Corporation<br>Research & Engineering Dept.<br>ATTN: Dr. W. F. Hartman<br>39 Industrial Avenue<br>Teterboro, NJ 07608 |
| 6 | Brown University<br>Division of Engineering<br>ATTN: Prof. R. Clifton<br>Prof. H. Kolsky<br>Prof. A. Pipkin<br>Prof. P. Symonds<br>Prof. J. Martin<br>Dr. P. Duffy<br>Providence, RI 02192 |
| 4 | California Institute of Technology<br>Division of Engineering and Applied Science<br>ATTN: Dr. J. Milowitz<br>Dr. E. Sternberg<br>Dr. J. Knowles<br>Dr. T. Coguhey<br>Pasadena, CA 91102 |
| 6 | Carnegie Mellon University<br>Department of Mathematics<br>ATTN: Dr. D. Owen<br>Dr. M. E. Gurtin<br>Dr. B. Coleman<br>Dr. W. Williams<br>Dr. W. Noll<br>Dr. J. L. Sedlow<br>Pittsburg, PA 15213 |
| 2 | Catholic University of America<br>School of Engineering and Architecture<br>ATTN: Prof. A. Durelli<br>Prof. J. McCoy<br>Washington, DC 20017 |
| 5 | Cornell University<br>Department of Theoretical Applied Machanics<br>ATTN: Prof. E. Cranch<br>Prof. G. Ludford<br>Prof. D. Robinson<br>Prof. W. Sachse<br>Prof. Y-H Pao<br>Ithaca, NY 14850 |
| 2 | Harvard University<br>Division of Engineering and Applied Physics<br>ATTN: Dr. G. Carrier<br>Dr. B. Budiansky<br>Cambridge, MA 02138 |
| 2 | Iowa State University<br>Engineering Research Lab<br>ATTN: Dr. G. Nariboli<br>Dr. A. Sedov<br>Ames, IA 50010 |
| 9 | The Johns Hopkins University<br>ATTN: Dr. J. Ericksen<br>Dr. J. Bell<br>Dr. R. Green<br>Dr. C. Truesdell<br>Dr. R. Pond<br>Mr. F. Moeckel<br>Mr. J. Randall<br>Mr. R. Khanwalkar<br>Instit. of Coop. Rsch.;<br>ATTN: Mr. S. Houck<br>34th and Charles Streets<br>Baltimore, MD 21218 |
| 3 | Lehigh University<br>Center for the Application of Mathematics<br>ATTN: Dr. E. Varley<br>Dr. R. Rivlin<br>Prof. M. Mortell<br>Bethlehem, PA 18015 |

DISTRIBUTION LIST

| No. of Copies | Organization |
|---|---|
| 1 | Massachusetts Institute of Technology<br>ATTN: Dr. R. Probstein<br>77 Massachusetts Avenue<br>Cambridge, MA 02139 |
| 1 | Michigan State University<br>College of Engineering<br>ATTN: Prof. W. Sharpe<br>East Lansing, MI 48823 |
| 1 | New York University<br>Department of Mathematics<br>ATTN: Dr. J. Keller<br>University Heights<br>New York, NY 10053 |
| 1 | North Carolina State University<br>Dept of Engr Mech<br>ATTN: Dr. W. Bingham<br>P.O. Box 5071<br>Raleigh, NC 27607 |
| 2 | Pennsylvania State University<br>Engr Mech Dept<br>ATTN: Prof. Juanzemis<br>Prof. N. Davids<br>University Park, PA 16802 |
| 2 | Forrestal Research Center<br>Aeronautical Engineering Lab<br>Princeton University<br>ATTN: Dr. S. Lam<br>Dr. A. Eringen<br>Princeton, NJ 05840 |
| 2 | Purdue University<br>Institute for Mathematical Sciences<br>ATTN: Dr. E. Cumberbatch<br>Dr. M. Stanisic<br>Lafayette, IN 47907 |
| 2 | Rensselaer Polytechnic Institute<br>Dept of Mech Engr, Aeronautical Engineering, and Mechanics<br>ATTN: Prof. E. Krempl<br>Dr. H. Moon<br>Troy, NJ 12181 |
| 2 | Rice University<br>ATTN: Dr. R. Bowen<br>Dr. C. C. Wang<br>P.O. Box 1892<br>Houston, TX 77001 |
| 1 | Southern Methodist University<br>Solid Mechanics Division<br>ATTN: Prof. H. Watson<br>Dallas, TX 75221 |
| 2 | Southwest Research Institute<br>Dept of Mech Sciences<br>ATTN: Dr. U. Lindholm<br>Dr. W. Baker<br>8500 Culebra Road<br>San Antonio, TX 78228 |
| 1 | Stanford Research Institute<br>Poulter Laboratory<br>333 Ravenswood Avenue<br>Menlo Park, CA 94025 |
| 1 | Stanford University<br>ATTN: Dr. E. H. Lee<br>Stanford, CA 94305 |
| 1 | Tulane University<br>Dept of Mech Engr<br>ATTN: Dr. S. Cowin<br>New Orleans, LA 70112 |
| 1 | University of Alabama<br>AME Department<br>ATTN: Prof. A. E. Calden<br>University, Alabama 35486 |

DISTRIBUTION LIST

| No. of Copies | Organization |
|---|---|
| 2 | University of California<br>ATTN: Dr. M. Carroll<br>Dr. P. Naghdi<br>Berkeley, CA 94704 |
| 1 | University of California<br>Dept of Aerospace and Mechanical Engineering Sciences<br>ATTN: Dr. Y. C. Fung<br>P.O. Box 109<br>La Jolla, CA 92037 |
| 5 | University of California<br>Lawrence Livermore Laboratory<br>H Division<br>ATTN: Dr. Mark L. Wilkens<br>Dr. Chuck Henry<br>Dr. W. Isbell<br>Dr. Douglas Norris<br>Dr. Mathias Van Thiu<br>Livermore, CA 94550 |
| 1 | University of California<br>Department of Mechanics<br>ATTN: Dr. R. Stern<br>504 Hilgard Avenue<br>Los Angeles, CA 90024 |
| 1 | University of Delaware<br>Dept of Mech Engr<br>ATTN: Prof. J. Vinson<br>Newark, DE 19711 |
| 3 | University of Florida<br>Dept of Engr Science and Mech<br>ATTN: Dr. C. A. Sciammarilla<br>Dr. L. Malvern<br>Dr. E. Walsh<br>Gainesville, FL 32601 |
| 2 | University of Houston<br>Dept of Mech Engr<br>ATTN: Dr. T. Wheeler<br>Dr. R. Nachlinger<br>Houston, TX 77004 |
| 3 | University of Illinois<br>Dept of Theoretical and Applied Mechanics<br>ATTN: Dr. D. Carlson<br>Dr. D. Drucker<br>Dr. R. Shields<br>Urbana, IL 61801 |
| 2 | University of Illinois at Chicago Circle<br>College of Engineering<br>Dept of Materials Engineering<br>ATTN: Prof. A. Schulta<br>D. T. C. T. Ting<br>P.O. Box 4348<br>Chicago, IL 60680 |
| 1 | University of Iowa<br>ATTN: Dr. K. Valanis<br>Iowa City, IA 50010 |
| 4 | University of Kentucky<br>Dept of Engr Mech<br>ATTN: Dr. M. Beatty<br>Prof. O. Dillon, Jr.<br>Prof. P. Gillis<br>Dr. D. Leigh<br>Lexington, KY 40506 |
| 2 | The University of Maryland<br>Dept of Mech Engr<br>ATTN: Prof. J. Yang<br>Dr. J. Dally<br>College Park, MD 20742 |
| 1 | University of Minnesota<br>Dept of Engr Mech<br>ATTN: Dr. R. Fosdick<br>Minneapolis, MN 55455 |
| 1 | University of Notre Dame<br>Dept of Metallurgical Engineering and Materials Sciences<br>ATTN: Dr. N. Fiore<br>Notre Dame, IN 46556 |

DISTRIBUTION LIST

| No. of Copies | Organization |
|---|---|
| 1 | University of Pennsylvania<br>Towne School of Civil and<br>Mechanical Engineering<br>ATTN: Prof. Z. Hashin<br>Philadelphia, PA 19105 |
| 4 | University of Texas<br>Dept of Engr Mech<br>ATTN: Prof. H. Calvit<br>Dr. M. Stern<br>Dr. M. Bedford<br>Prof. Ripperger<br>Austin, TX 78712 |
| 1 | University of Washington<br>Dept of Mech Engr<br>ATTN: Prof. J. Chalupnik<br>Seattle, WA 98105 |
| 3 | Yale University<br>ATTN: Dr. B. Chu<br>Dr. E. Onat<br>Dr. A. Phillips<br>400 Temple Street<br>New Haven, CT 96520 |

Aberdeen Proving Ground

Marine Coprs Ln Ofc
Dir, USAMSAA